A VISUAL INVESTIGATION OF THE WALL REGION IN TURBULENT FLOW

DISSERTATION

Presented in Partial Fulfillment of the Requirements for the Degree Doctor of Philosophy in the Graduate School of The Ohio State University

By

Edward Robert Corino, B.Sc. Ch. E., M.Sc.

* * * * * *

The Ohio State University
1965

Approved by

Adviser
Department of Chemical Engineering

ACKNOWLEDGMENTS

I wish to express my sincere thanks to my adviser, Dr. R. S. Brodkey, for his direction and advice during all stages of this study. His deep personal interest and enthusiasm provided much needed encouragement during difficult times. I would also like to express my gratitude for the general environment he established for study and research, and for providing substantial financial assistance from a National Science Foundation grant (G-14807) which supported this study.

I want to thank Dr. J. H. Koffolt, Chairman of the Department of Chemical Engineering for his continued interest during my stay in the department and for providing financial assistance in the form of assistantship and fellowship.

The Dow Chemical Company most graciously and promptly provided the trichloroethylene used in this work whenever the request was made of them.

There is no way to adequately acknowledge the contributions and efforts of my wife, Marlene, who was patient and understanding and an endless spring of encouragement and optimism. Moreover, her enthusiastic concurrence in the graduate education program undertaken is deeply appreciated.

Finally, I wish to acknowledge my parents for providing the environment which pointed me in this direction, and particularly my father who did not live to read this.

CONTENTS

CONTENTS--continued

ILLUSTRATIONS

ILLUSTRATIONS--continued

TABLES

NOMENCLATURE

A	slope of E vs $\bar{U}_x$ curve
D	molecular diffusivity
E	volts (output of hot film probe)
$E_i(n)$	Lagrangian energy distribution function
I	RMS meter reading (milliamp)
K	instantaneous local mass transfer coefficient
$\bar{K}$	local mean mass transfer coefficient
N_{Re}	Reynolds number based on average velocity-pipe flow
N_{Re_x}	Reynolds number based on X distance-flat plate flow
N_{Sc}	Schmidt number
N_{Pr}	Prandtl number
N_{α}	either N_{Sc} or N_{Pr}
P	pressure
$(P_r)_{\gamma}$	production of turbulent energy
R	pipe radius
$\bar{U}_{avg.}$	average flow velocity
$\bar{U}_i$	local mean average velocity, i^{th} component
U_i	instantaneous velocity, i^{th} component, $U_i = \bar{U}_i + u_i$
W_{μ}	direct viscous dissipation
a	$36\mu/2(\rho p+\rho_f)d^2$
b	actual ejection velocity
c	negative of carriage velocity

d	particle diameter
e	apparent length of particle travel
f	function factor coefficient
g	apparent ejection velocity
$i.j,k$	subscript index for component
k	fluctuating mass transfer coefficient
r	radial position
t	time
u^+	$\frac{u_i}{u^*}$
u^*	$(\tau_w\, gc/\rho)^{1/2}$
u_i	instantaneous turbulent velocity fluctuation
u'_i	root mean square value of u_i
v_{pi}	Lagrangian particle velocity, i^{th} component
v_{fi}	Lagrangian velocity of fluid, i^{th} component
x	axial coordinate in polar coordinate system
y	coordinate normal to flat plate in rectangular coordinate
y^+	$\frac{(R-r)u^*}{\nu}$
α	apparent ejection angle
β_i	calibration value for RMS meter
Γ_{fL}	Lagrangian integral scale of turbulence
ϵ	eddy diffusivity
θ	angular coordinate in polar coordinates time in surface renewal theories
λ	parameter for streak spacing

λ^+ correlation coefficient for stretch spacing

μ molecular viscosity coefficient

ν kinematic viscosity

ρ_P particle density

ρ_f or ρ fluid density

σ reduced volume

τ shear stress (τ_w for wall)

INTRODUCTION

The importance of the region near a solid boundary on fluid motions has been acknowledged since Prandtl (44) proposed the boundary layer hypothesis. In its most general context, the boundary layer is that fluid near a boundary where the viscous effects become important and strongly influence the fluid motions. At large distances from the boundary, the inertial effects completely dominate the flow, the viscous effects are negligible. The boundary layer concept is valid for both laminar and turbulent flow, although in the latter case the presence of turbulence creates additional complexities. The laminar boundary layer has yielded to mathematical attack and presents no great problem. The turbulent boundary layer, much as turbulent shear flow in general, has not been successfully treated by rigorous mathematical approaches. The difficulty, of course, arises from the presence in the equations of motion of non-linear terms which give rise to an infinite set of equations. For special cases, or where a knowledge of the velocity field permits simplification of the equations, some solutions are possible. To treat most cases, however, the general approach has been to abandon the rigorous mathematics and employ empirical and phenomenological techniques. While many of these results

successfully predict mean flow characteristics or effects, they cannot reveal any new information about turbulent characteristics or time-dependent occurrences. In this category are the well-known "Prandtl mixing length" (45) and "Von Kármán similarity" (69) hypotheses. These, just as the others which followed, attempted to establish a relation between the Reynolds stresses and the mean motions of the velocity field so that the effects of the turbulent fluctuations could be treated in much the same manner as manner as molecular transport mechanisms. The necessity of accounting for the disappearance of the turbulence fluctuations at the solid wall led to the arbitrary division of the boundary layer into three regions, the turbulent core, the transition or buffer region, and the sublayer region. The latter was formerly called the laminar sublayer because the fluid motions within it were held to be completely laminar. Later this was shown to be untrue, and the term sublayer or viscous sublayer was substituted. In the discussion to follow, the combined sublayer and transition region will be called the wall region. More recently other authors have proposed velocity distribution relations which do not require this arbitrary division. One of the most successful is Pai's (42) equation for the mean velocity profile.

Some authors, Munk (38), Townsend (64), Einstein and Li (8), and Sternberg (59), have proposed other empirical or semi-theoretical models or relations to explain the turbulent

characteristics of boundary layer flows. None have been overly successful.

Although its nature is not fully known, the wall region is sufficiently well characterized to indicate its extreme importance in the control of transport phenomena and the generation and maintenance of turbulence. Considering the first effect, the relatively small amount of mixing within the sublayer compared to that of the core causes the transport in this region to proceed primarily by molecular mechanisms, and consequently, it occurs more slowly here than elsewhere. A large number of articles have appeared which attempt to predict the rates of transport by assigning various characteristics to this region, and developing models or relations from these assumptions. Many of the familiar analogies between momentum and heat and mass transfer use such an approach. In a number of cases, notably, Von Kármán (10), Summerfield (60), Taylor (61), and Deissler and Eian (7), these approaches have been unsuccessful if the N_{Sc} or $N_{Pr} \neq 1$. These approaches all had the common failing of not permitting any mixing to occur in the sublayer. Similar treatments by Lin, Putnam, and Moulton (34) and Deissler (6), which did assume some mixing in the sublayer, were more successful even at high N_{Sc} and N_{Pr} values. Another group approached the problem by assuming models after the fashion of the Higbie (19), Danckwerts (5) surface renewal theory, and deriving relations for transfer rates from these models.

Among the more successful are Harriott (18), Hanratty (16), and Toor and Marchello (36,63).

All these treatments have one thing in common. They all begin by assuming a particular character for the wall region. From these assumptions, equations for mass transfer rates or coefficients are developed. These equations usually contain one or more parameters which must be evaluated from experimental data. Upon evaluating the parameters in this fashion, nearly all the models can be made to predict, over a limited range of N_{Sc} values, the proper dependency of the transfer coefficient on N_{Sc} as given by experimental data. Outside this N_{Sc} range the predicted dependency is usually incorrect. Although there is quite a variety in the character of the assumed models, the fact that many can be made to agree with the same experimental data demonstrates the insensitivity of the results to the assumptions. This insensitivity precludes any possibility of deciding which of the successful models most accurately depicts the true nature of the wall region or the transport mechanism on the basis of their success in predicting transfer rates or "concentration" profiles. Moreover, because the experimental results reflect averaged or integral values, they cannot define the instantaneous or fluctuating character of the region. Quite the contrary is true. The nature of the wall region must be known before the proper model can be selected.

The importance of the wall region in the generation and maintenance of turbulence has been experimentally demonstrated. Since the kinetic energy of turbulence is continuously dissipated to heat through viscous effects, a continuous supply of new turbulence must be created within the flow if the quasi-steady state character of turbulent boundary layer flow is to be maintained. The source of the energy is the mean flow, but as yet the mechanism of transfer is unknown. The investigations by Laufer (31) for pipe flow, and Klebanoff (26) and Townsend (65) for flow over a flat plate, clearly demonstrated that the generation of turbulence is a maximum within the wall region, and that the dissipation also is a maximum there. In addition, Laufer (31) and Townsend (66) each determined the distribution with respect to the wall of the conversion of mean flow energy to turbulence. In both cases the maximum occurred in the wall region. These measurements were made with hot wire anemometers and have revealed a great deal about the properties of turbulent flow. They showed that velocity fluctuations exist within the sublayer. They have not, however, succeeded in describing why turbulence generation is a maximum in the wall region or how it occurs. One difficulty of hot wire measurements is in interpreting the signal in terms of a physical picture of the fluid motions.

There are more direct observations of the nature of the wall region. Fage and Townsend (10) observed distinct

departures from laminar flow within the sublayer, but revealed little else. More recently Runstadler (50) used dye injection and visual-photographic techniques to make a detailed investigation of the boundary layer over a flat plate. His study revealed that the wall region possessed a distinct structure and a definite, non-regular time-dependent motion.

The above discussion was presented to demonstrate the importance of the wall region and to emphasize the need for greater knowledge of its character. The lack of knowledge concerning this region is due in part to the difficulties of obtaining accurate measurements and observations within it. This is a result of the extremely small dimensions involved. For example, in a 2-inch pipe for liquids, i.e., trichloroethylene, at $N_{Re} = 50,000$ the entire sublayer region $y^+ \doteq 5$, is contained in 0.004 inches. Any probe or injection device introduced into the region will have dimension of the order of magnitude of the region. In addition, for liquids, the necessity of providing physical strength to the probes causes them to be larger than those used in gases. What is required is a method of investigation which can reveal the character of the wall region and yet does not require the introduction of any measuring device into the flow. A qualitative physical picture of the structure of the flow coupled with quantitative measurements would be very valuable.

This present study was undertaken to develop a technique which would permit an investigation of the wall region but which would not require the introduction of any device into it. This technique is then used in an intensive study of the fluid motions. The objective of the study is to characterize the nature of the wall region in turbulent pipe flow and to determine from this physical picture the manner in which the wall region causes the effects attributed to it. In addition, this knowledge should permit the selection of the transport model, if any, which is in best agreement with the actual nature of the region. If no model agrees, suggestions for a new one can be proposed.

Specifically, the investigation entails a visual-photographic study of the wall region in fully turbulent pipe flow. The technique developed employs colloidal sized particles suspended in the fluid as tracers, and requires no injection or the introduction of any measuring device into the flow. High speed (650-1000 frames/second) motion pictures of the magnified wall region are taken as the camera is transported downstream with the flow. This is the first time that such pictures of the wall region in turbulent pipe flow have been obtained. In a circular pipe, this region would not normally be visible because of the light refraction at the pipe wall. This problem was eliminated by using in the flow system a liquid that had the same refractive index as the glass pipe, and surrounding the pipe with a viewing

cell of the same fluid. The motion pictures are analyzed to obtain a detailed physical description, supported by quantitative measurements, of the nature of the fluid motions in the wall region. These results are combined with the general knowledge of turbulent flow to produce an hypothesis which describes the fluid behavior in this region, and explains its significance in the generation and maintenance of turbulence. In addition, the effect of the character of the wall region on transport phenomena is explored, and suggestions for a new model to predict transfer rates are presented.

The main body of this work is divided into two parts. in Part 1 the experimental technique that has been developed and the equipment used are presented and discussed. Although the underlying principles of the technique, and in fact the basic technique, have been known for many years, a considerable amount of development was necessary to provide the capabilities required for this investigation.

In Part 2 the experimental results are presented and the hypothesis proposed. These are discussed and compared with pertinent data available in the literature.

In addition to this written text, there is a motion picture film available which shows the important features

of the wall region which are discussed in this work.[1] In fact, since many of the characteristics of the wall region show a definite time dependency and involve relative motions of various kinds, they are more readily observed in these motion pictures than in still photographs.

[1]This is a silent, black and white, 16 mm. motion picture. A loan copy is available on request to Motion Picture Division, The Ohio State University, 1885 Neil Avenue, Columbus, Ohio 43210. Request "A Visual Investigation of the Wall Region in Turbulent Flow," Chemical Engineering. There is a handling charge of approximately $3.00.

EQUIPMENT AND EXPERIMENTAL PROCEDURES

General description

In this section a general description of the equipment and experimental procedures will be presented. The details of the different pieces of equipment and procedures will be discussed later.

The equipment may be divided into two parts; the flow system and the photo-optical system. The flow system consisted of a 150 gallon tank (A)[1] from which the test fluid was pumped by a centrifugal pump (B) through the various control valves (C) to the test section. The test section was a 10 foot length of 2" I.D. Pyrex glass pipe (D) which was enclosed in a viewing cell (E). This section was preceded by a straight length made up of 20 feet (2-10 foot sections) of 2" I.D. glass pipe (F), and 4 feet of 2" schedule 40 steel pipe. These pipe sections were supported by steel braces which were bolted to the concrete floor. The end of the test section was connected to 6 feet of steel pipe which was joined to the return pipe. This section of pipe contained the orifice meter (G) used to meter the high rates of flow. A rotameter (H) was used to meter the low rates of

[1]Letters refer to marked parts in Figure 1.

flow. The piping system, including the test section, thus comprised a closed loop. In the section of pipe downstream of the test section a filter (I) was located which could remove all solids larger than 5 microns. One of the thermocouples (J) used to continously record the fluid temperature was also located in this section. To eliminate possible end effects, only the central part of the 10 foot test section was used.

Trichloroethylene was selected as the test fluid primarily because its refractive index closely approximated the refractive index of the glass. The viewing cell was also filled with trichloroethylene for the same reason. With the glass pipe completely covered with liquid of the same refractive index as the glass, the problems of refraction were eliminated, and the wall region could be examined. In order to mark the fluid elements so that the motions would be visible, very fine particles of "Seemag"[1] magnesium oxide were suspended in the liquid. These particles had an average diameter of 0.6 microns. The particle concentration was dense enough so that a large number of particles appeared within the field of view simultaneously, but sufficiently dilute so that particle-particle interaction almost never occurred. The test fluid appeared perfectly clear and colorless in normal light, and only under dark field illumination were the particles visible. Then they appeared as bright

[1]Commercial product of FMC Corporation.

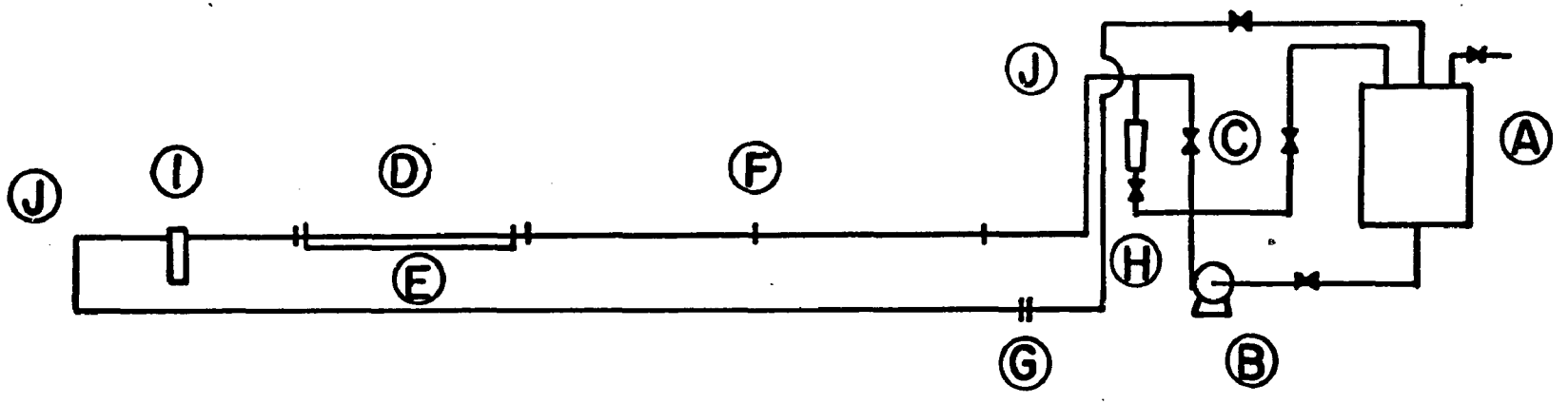

Figure I. Schematic of Flow System

points of light against a dark background. This is a result of the well-known Tyndall effect. It should be emphasized that these particles were suspended in the fluid at all times and no injection was required during a run.

The photo-optical system consisted of all the lighting, photographic, and optical equipment needed to record the particle motions on film. Since the particle motions were very rapid, a high speed motion picture camera (A)[1] was used at filming speeds of 650 to 1000 frames per second. These correspond to shutter speeds of 0.0005 to 0.00033 seconds. The lens system of the camera was adapted to produce images of the area of interest of 4.3X and 2X magnification. These magnified images greatly enhanced the ability of the system to define the fluid motions within the very narrow wall region. Because of the high filming speeds, the magnification, and the dark field illumination, a very intense light source was required. An ultra-high pressure D.C. mercury arc lamp (B) was used, and the beam was focused by means of a spherical mirror through slits into the field of view. The elimination of the refraction problem caused by the curved pipe wall was mentioned under the discussion of the test fluid. The use of a mercury arc lamp and not a monochromatic light source prevented the complete elimination of any effect of refraction, but the small effect which remained was used

---

[1]Letter refers to marked parts of Figure 2.

to good advantage as a means of locating the inside pipe wall in the photographs.

For reasons which will be discussed more fully later, it was found to be a distinct advantage to have the capability of moving the entire photo-optical system downstream with the flow during photography. This naturally required that the field of view be kept in focus during the movement, and also that no mechanical vibrations which might affect the photo-optical system be present. To accomplish this an 8-foot lathe bed (C) was aligned with the pipe and bolted to the concrete floor. The lathe carriage (D) which is designed to slide along the ground steel ways was fitted with a heavy steel frame (E) which supported the camera (A) and light source (B). This carriage was driven down the lathe bed at closely controlled constant speeds by an hydraulic piston. In this manner the entire recording system could be moved with the flow, and at any pre-selected speed. This meant that any local mean axial velocity in the wall region could be matched by the carriage velocity, and, therefore, that a particular segment of fluid could be kept in view as the fluid motions developed.

The experimental runs were conducted in the following fashion. The flow conditions or Reynolds number desired was established by adjusting the control valves in the flow system. The area of view and axial position within the test section were selected, and the photo-optical system aligned

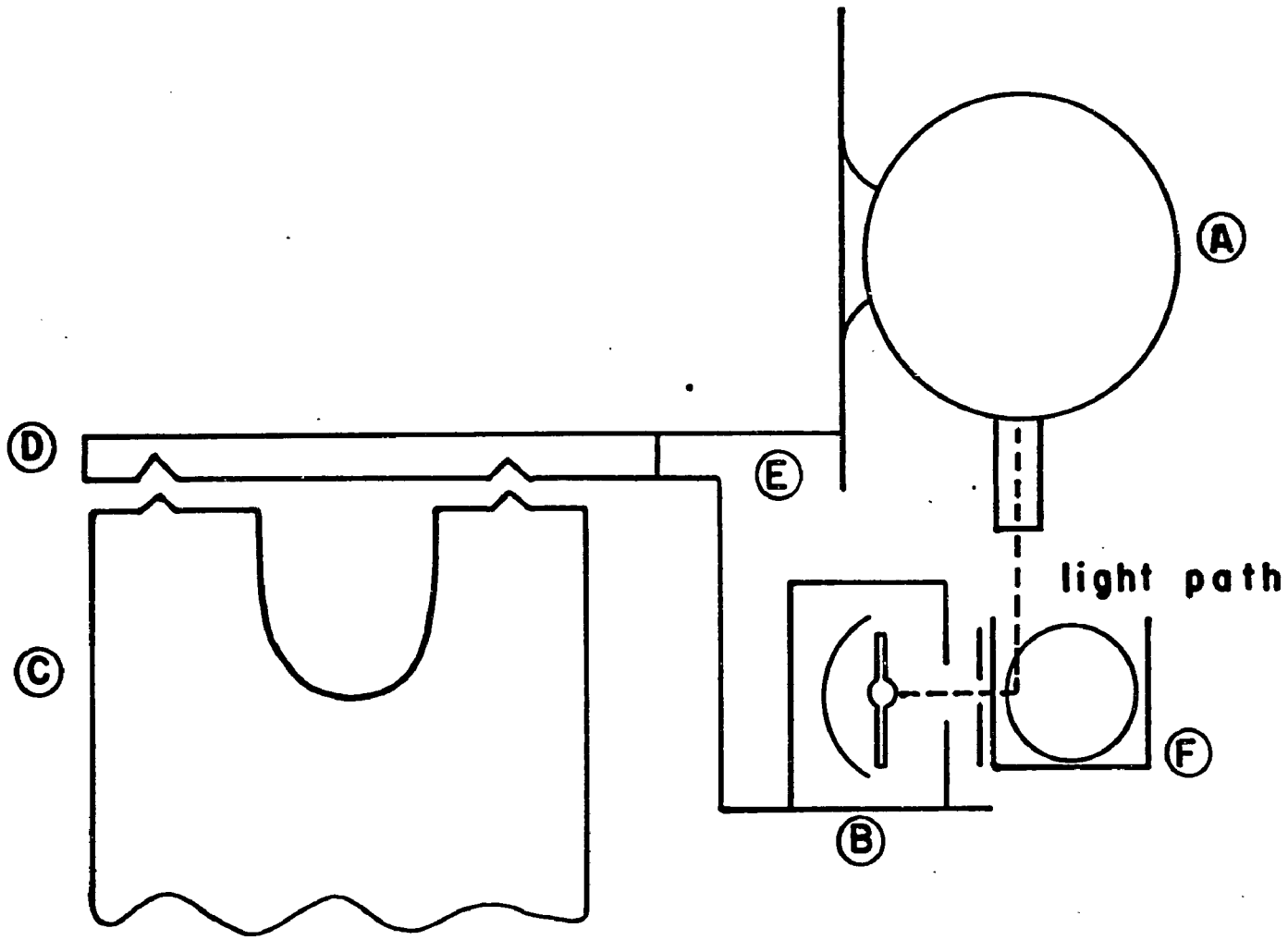

Figure 2. Photo-Optical System

and focused accordingly. The filming speed desired was set on the proper controls. The carriage speed was selected, and the controls for the hydraulic drive mechanism adjusted. If the carriage was to remain stationary during the run, the photography was begun at this point. If, however, the carriage were to move, it was first moved upstream beyond the point where photography was to be initiated, and then started downstream. When it reached the initiation point, the camera was turned on. In this fashion, any possible acceleration effects associated with the carriage motion were eliminated before photography was begun.

The films resulting from these runs were analyzed in detail to provide the desired information concerning the nature of the fluid motions in the wall region. This analytical procedure is described in another section.

Photographs of the equipment appear in Figures 3, 4, 5, and 6.

Flow system

Piping and metering. With the exception of the test section and the entry section preceding it, all piping was 2 inch, schedule 40, galvanized steel. The joints were all threaded except for the connections to the pump and the glass pipe test section. These were flanged. The holding tank was carbon steel and had a 150 gallon capacity. It was entirely closed except for the inlet and outlet ports and a

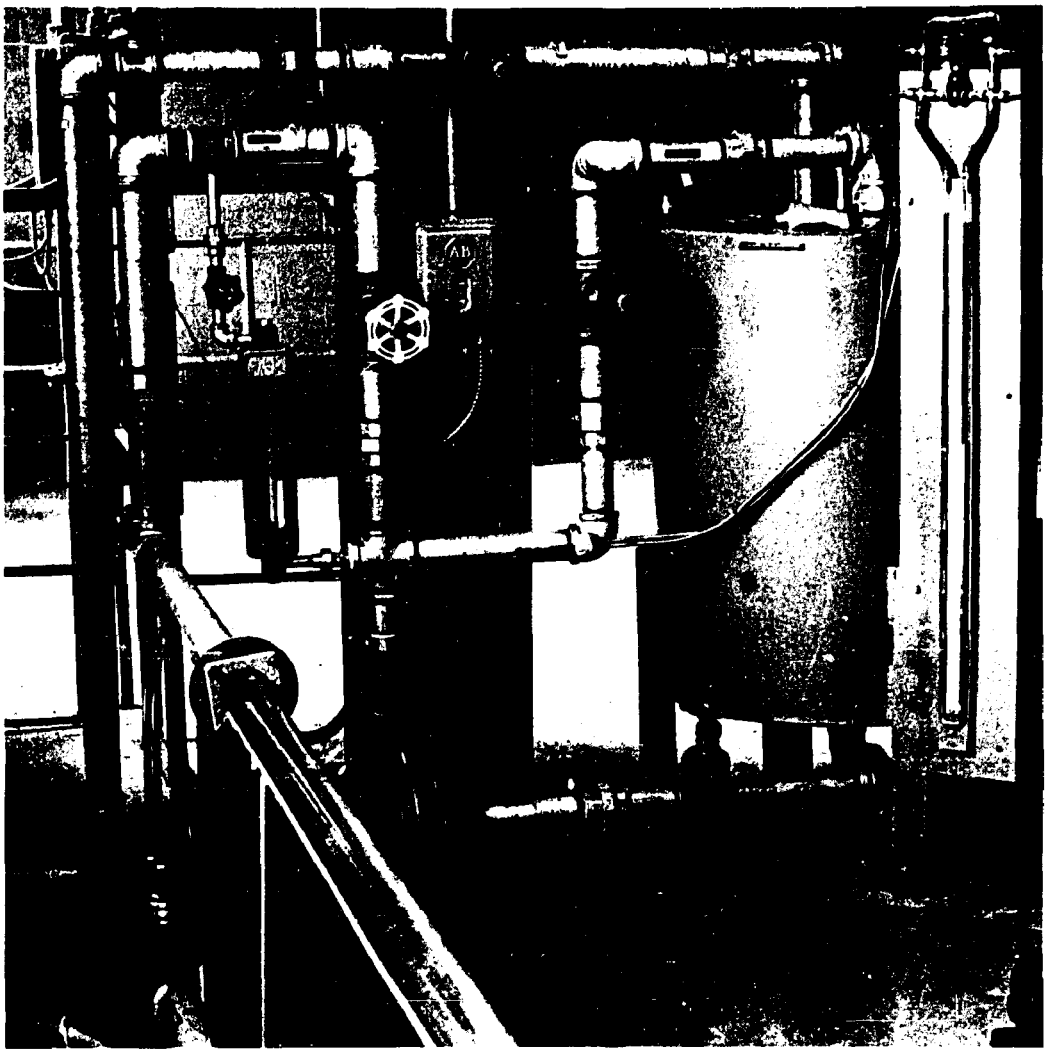

Figure 3. Flow Equipment

Figure 4. General View of Test Section

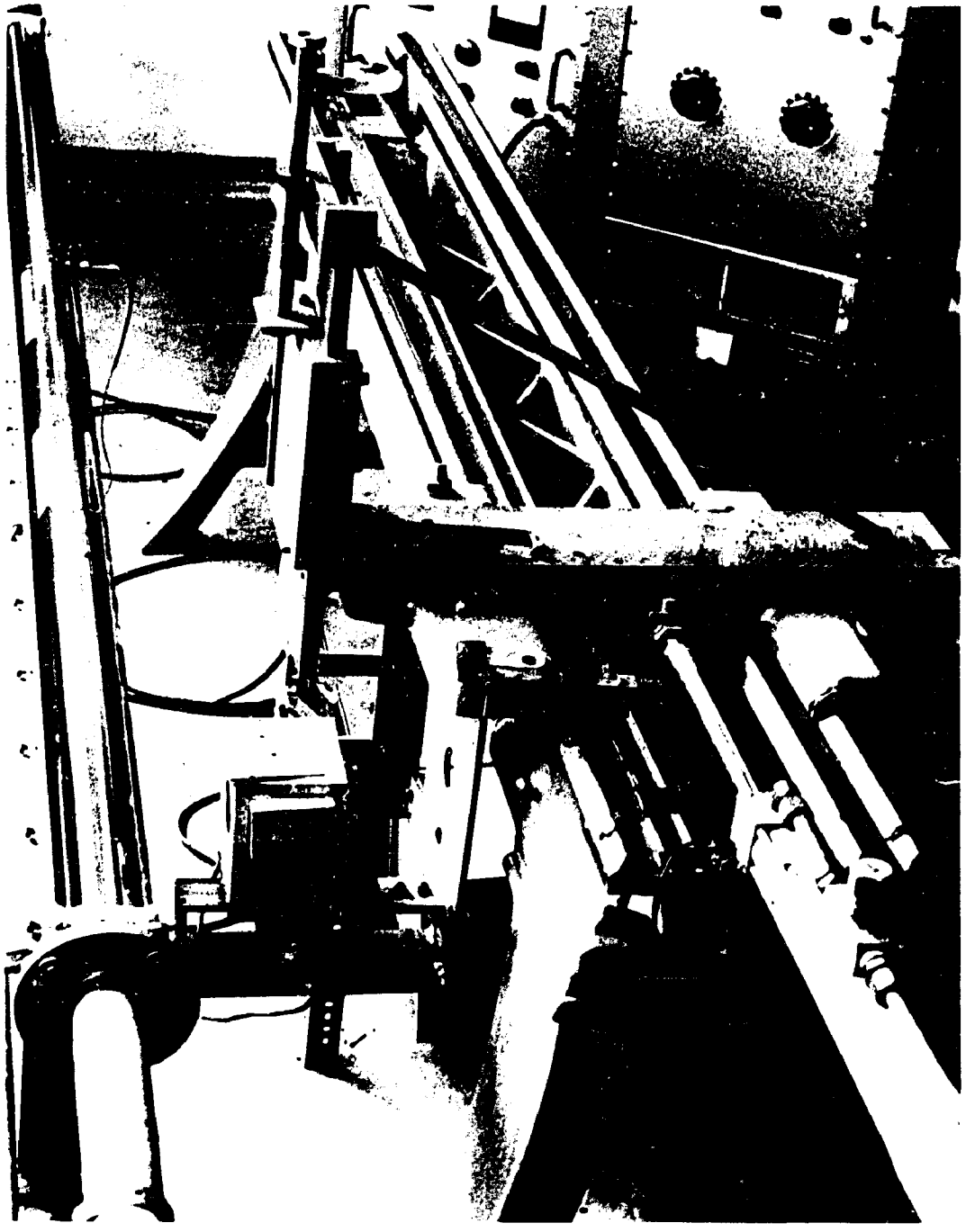

Figure 5. Detailed View of Test Section

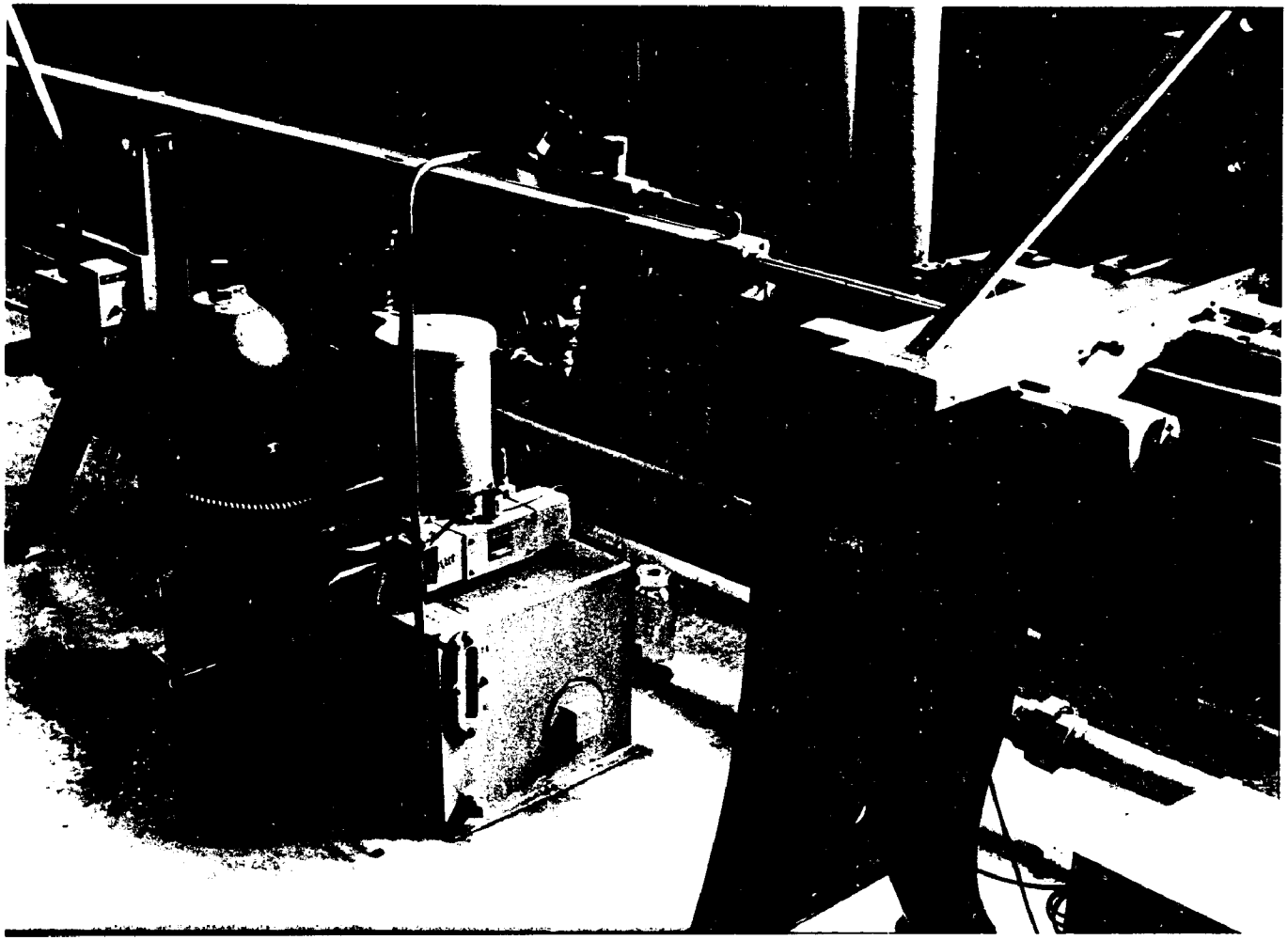

Figure 6. Hydraulic Drive for Carriage

vent line. Before the equipment was assembled, the interiors were thoroughly scrubbed with trichloroethylene to remove dirt and grease. After assembly the entire system was flushed with pure trichloroethylene which was then drained. The centrifugal pump was all iron with an eight-inch diameter, six-vaned impeller. It was rated at 50 gpm. at 70 feet of head for water at 1750 rpm. A larger motor was installed to provide similar capabilities for pumping the denser trichloroethylene. As Figures 1 and 3 show, the outlet line was fitted with a by-pass line and control valve, and two flow lines. One of the latter was of two-inch diameter pipe, and was used for flow rates in excess of 2.5 gpm. The other flow line was of 1/2 inch pipe and contained a rotameter. This line was used for low flow rates where more accurate control and flow rate readings than were possible with the larger diameter line and the orifice meter were obtained. By either route, the fluid proceeded to the four-foot steel section which just preceded the first of three ten-foot sections of Pyrex glass pipe. This pipe had an internal diameter of two inches. The sections were connected by Teflon gasketed flanges. The gaskets and joints were very carefully aligned and fitted to reduce their possible action as disturbance generators. The test section actually used was situated in the central portion of the last length of glass pipe, at least four feet downstream of the nearest joint. This was a precautionary measure to make certain that

the motions observed within the test section were not influenced by end effects. The most desirable condition, of course, would have been to use a continuous thirty-foot length of plastic pipe and eliminate the joints entirely. Unfortunately, the requirements that the pipe be transparent, and that the fluid flowing within it be clear and colorless, Newtonian, of low viscosity, and, most important, have an index of refraction equal to that of the pipe, eliminated all potential fluids except hydrocarbons. Of these, the ones of proper index of refraction also attacked the plastic. Thus, glass pipe was the only alternative, and ten-foot lengths the only practical lengths available. This question of the effect of the joints on the flow was examined theoretically and experimentally, and the results are discussed in a later section. It can be safely concluded that in the present study the joints had no effect on the motions observed within the fluid in the test section.

The twenty-four-foot length of glass pipe which preceded the test section was designed to assure that fully developed turbulent flow existed within the test section. Schlichting (53) calculated the entry length needed for pipe or channel flow to establish a fully developed profile in laminar flow. He obtained values of the order of 80-200 diameters. Turbulent profiles require much shorter entry

lengths. Latzko (30) presented the relation

$$\frac{X}{D} = 0.693 \ (N_{Re})^{1/4}$$

for the entry length required to establish a turbulent profile in a pipe. If the upper Reynolds number of this study is substituted into this relation, an entry length of 10.4 diameters is predicted. However, Hinze (20) says that this relation gives values which are always less than those measured experimentally. Kirsten (25) measured entry lengths experimentally and found that 50 to 100 diameters, depending on N_{Re}, usually were sufficient to establish the flow. Nikuradse (41) found that for disturbed entries 25 to 40 diameters were sufficient. Hinze in reviewing these values states that 40 diameters can be used as a minimum value. In the present case, the entry was disturbed, and the entry length of nearly 145 diameters satisfies even the most extreme requirement. Thus it may be safely assumed that fully developed turbulent flow existed within the test section. This assumption was later checked by hot film anemometer measurements and found to be valid.

The end of the test section was connected to a six-foot section of steel pipe which was in turn joined to the return line. Within this section a Selas Flotronic filter with Series F type Micro-Filter element was positioned. This element removed all particles of diameter greater than 5 microns. The fluid was continuously passed through this

filter. The filter porosity is, of course, much greater than the average particle diameters of the solids used, but it was designed to primarily remove any extraneous dirt or agglomerations from the system. An element of 0.5 micron porosity would have required impractically high pressure drops for high flow rates, and so was not used. Periodic examination of the filter element showed that agglomeration of the magnesium oxide was not occurring, and it seemed reasonable to assume that the majority of particles were still of the order of 0.6 microns.

At the very end of this section a packing gland was located which afforded the means of moving a positioning scale axially within the test section. A thermocouple well was also located here, and during runs the temperature of the fluid was continuously recorded.

The glass pipes and lead-in pipes were supported by steel cradles which were bolted to the concrete floor. The return line was bolted to the vertical supports of these cradles.

It was necessary to know the average flow velocity since the Reynolds number was a basic parameter in the study. This was measured by either the rotameter, for flow rates of 2.5 gpm. or less, or the orifice meter, for larger flow rates. The rotameter was calibrated by weighing the efflux collected at a particular scale setting for a timed interval. The calibration curve appears in Figure 7.

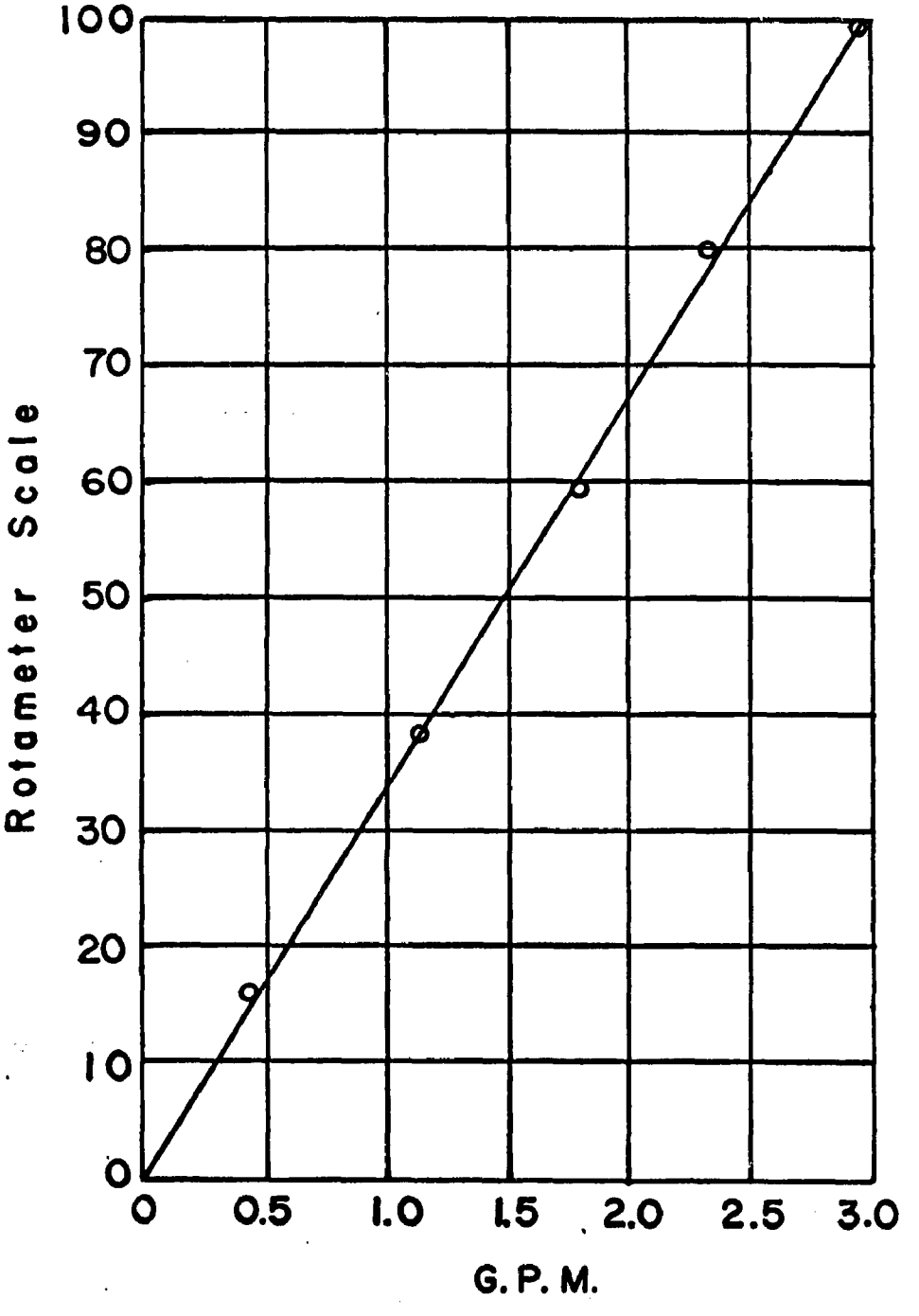

Figure 7. Rotameter Calibration

For higher flow rates, and consequently for most runs, the orifice meter was used. This consisted of a standard flange tapped orifice flange and a stainless steel, sharp edged orifice plate. A mercury manometer was used to measure the pressure differential across the orifice plate. This orifice plate was preceded by 36 feet of straight pipe which contained a single union 20 feet upstream of the orifice. This assured the proper flow configuration through the orifice. The meter was calibrated by the timed weighing technique described above, and the calibration curve appears in Figure 8. For the lower flow rates where the two calibration curves overlap, the independently measured calibrations agree very well.

Over a period of a number of experimental runs there was an unavoidable temperature rise in the fluid due to the pumping energy input. This necessitated an approximate setting for Reynolds number by use of the meters, and a calculation of the actual Reynolds in which the temperature rise was taken into account. The difference was always quite small. For any particular run, the period of time involved was so short that no temperature rise of any significance was possible during the run itself.

Fluid. Since glass pipe had to be used in the system, for the reasons described earlier, the problem then became one of selecting the liquid which would match the refractive index of the glass and have the other desirable properties as

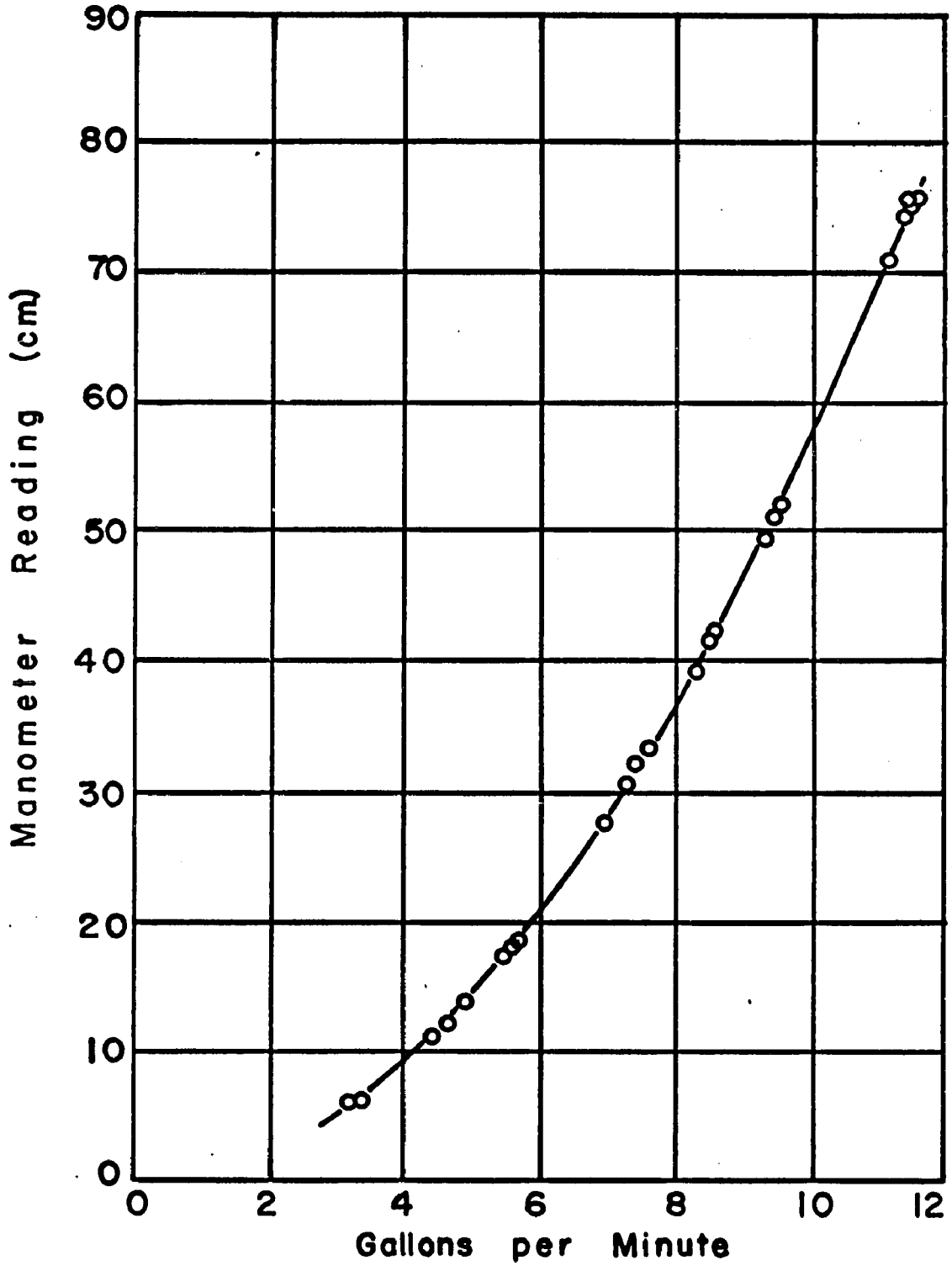

Figure 8. Orifice Meter Calibration

well. Trichloroethylene was the most satisfactory fluid. Its pertinent properties are listed in Table 1. Most important is the fact that its refractive index is 1.474 at 25°C. The Pyrex glass pipe has a refractive index of 1.4727 for sodium D light and 1.477 for pure blue light. Since the light source used was not monochromatic, no attempt was made to achieve agreement in the third decimal place of the refractive indices of the pipe and fluid.

TABLE 1

NEU-TRI^{R} TRICHLOROETHYLENE*

Properties:

A clear, colorless, nonflammable liquid, free of suspended matter

Boiling point at 760 mm. Hg	87.1°C.
Specific gravity at 25/25°C	1.459
Specific gravity at 60/60°F	1.473
Refractive index at 25°C	1.474
Viscosity at 20°C., centistokes	0.384
Viscosity at 60°C., centistokes	0.287

*NEU-TRI^{R} of the Dow Chemical Co., Midland, Michigan.

The experimental technique required that the fluid elements be marked for visualization by small particles inhomogeneous with the trichloroethylene. Ideally, the particles should be small in size and of the same density as the fluid. The possibility of a mixture of liquids which would be inhomogeneous with the main fluid and yet have the same density was considered, but the difficulty of dispersing

such particles in sufficiently fine form, and maintaining this dispersion at high concentration without coalesence upon repeated circulation was too great to warrant extensive study. Solid particles of very small size were available, but they all had densities greater than the fluid. Fortunately a compromise could be reached. If the particles of solid material were sufficiently small, the fact that their density was greater than that of the fluid would be compensated by the small size, and they would still faithfully follow the fluid motions. "Seemag" grade magnesium oxide was selected as the solid. Its particle size was excellent, and its shape and density were acceptable. It also did not react with the trichloroethylene, and, being inorganic and highly dispersed, showed no tendency to agglomerate. The particle shape was rather important since a particle nearly equal in the three dimensions was considered better than plates or flakes. One reason is that such a particle appears much the same under the lighting conditions used regardless of the orientation, but a plate or flake seen edgewise would be very different from one seen broadside. The general crystal structure of magnesium oxide and statements from the manufacturer indicated that it would be three dimensional in the manner described above. This was supported by examination with an electron microscope. The most important feature, however, was the particle size. Seemag as analyzed by the manufacturer with a Fisher Sub-Sieve Sizer was described as

having an average diameter of 0.5-0.6 microns, with approximately 0.6% retained on a 325 mesh screen. The approximate particle density was 3.59 as compared to trichloroethylene which has a density of approximately 1.46.

The particles were dispersed in pure trichloroethylene, and the mixture filtered through a 50 micron and finally a 5 micron filter. Since the initial dispersing procedure did not produce a great enough concentration of particles in the fluid, the entire process was repeated until the desired concentration was reached. At one point pure trichloroethylene was distilled off and a concentrated residue retained. This was later found to be unnecessary. The most desirable concentration was determined by trial and error. Various concentrations were prepared and photographed under conditions similar to those used in an actual run. These photographs were examined for particle content and degree of particle-particle interaction. The objective in this situation was to arrive at a concentration where a sufficiently large number of particles appeared in each frame of the film and yet were dispersed enough so that contact between particles was not a problem. The first is necessary if one hopes to define the fine scaled turbulent motions, since if a dilute concentration is present, the separation distance between particles will possibly be greater than the scale of the turbulent motion, and therefore no measurement of it would be possible. This emphasizes another reason why extremely small particle

diameters are necessary in a study of this type, for only if the particles are very small compared to the scale of the turbulence can one hope to achieve a large enough concentration to delineate this motion and yet not have particle-particle interaction. The concentration finally accepted fulfilled both objectives. The resulting fluid used in all runs exhibited a particle count in any given frame of the order of 50 to 100 or more, and particle-particle collisions were observed only very rarely. A frame usually had dimensions of 0.069 x 0.095 inches and might be thought of involving a volume of fluid of the order of 1.8×10^{-4} cubic inches. A rough calculation of concentration gives a value of 55.6 particles/cubic inch, but the volume occupied by all particles, assuming a cubic shape 0.6 microns on an edge, is less than $1 \times 10^{-6}\%$ of the total volume. These particles were uniformly distributed throughout the fluid. The fluid appeared clear and colorless in normal lighting, and even after standing undisturbed for months in a sealed large diameter vessel the particles did not settle out of suspension. Under proper lighting conditions Brownian motion was visible. This motion was, however, of such relatively small magnitude compared to the fluctuating motions of the fluid that it was never apparent when the fluid was flowing. Even motion pictures taken at high speed of laminar flows failed to reveal any evidence of Brownian motion, and it was

concluded that these motions would not be a factor when the analysis for turbulent motions was undertaken.

Although the particles did not settle out of the suspension upon standing, they are still subject to the force of gravity. This would cause a downward movement as the fluid flowed through the test section. An estimate of the extent of this movement may be made by considering the terminal velocity of a spherical solid particle suspended in a non-turbulent fluid. Since this treatment ignores the effects of turbulence and Brownian motion it represents an extreme case. The particle diameter selected for calculation is 5 microns which again is the worst possible case. The terminal velocity is

$$u_t = \frac{d^2}{18\mu} (\rho_f - \rho_p)g = 1.79 \times 10^{-3} \text{ ft./sec.}$$

The important time for consideration is the period during which the particle is viewed. A reasonable value for this time is 3×10^{-3} seconds so the particle can drop 6.4×10^{-5} inches while in view. Comparing this to the viscous sublayer thickness at $N_{Re} = 50,000$ of approximately 4×10^{-3} inches shows that the worst possible case gives a movement of approximately 1.6% of the sublayer thickness. For a smaller particle diameter and lower N_{Re} the effect is much less.

The addition of solids to a liquid could conceivable affect the viscosity, especially its Newtonian character.

While magnesium oxide does not show this characteristic, and therefore was very unlikely at the existing dilute concentrations to affect the fluid, there are colloidal materials which in very small quantities drastically change liquid viscosities. Therefore a check of the fluid viscosity both before and after particle addition was made. A long capillary tube viscosimeter was used, and the variation in shear rate necessary for determination of departures from Newtonian viscosity was obtained by varying the height of the constant head tank above the capillary inlet. The measurements for pure and particle containing trichloroethylene gave congruent straight lines when $\frac{d\bar{U}_x}{dr}$ was plotted against $\Delta Pr/2L$, which showed that the two fluids had identical, constant (with respect to shear rate) viscosities. The slope of this plot indicates the viscosity, and it was found to be $3.61 \times 10^{-4} \frac{lbm}{ft\text{-}sec}$ at 27.5°C. This compares with the published values of 3.64×10^{-4} lbm/ft-sec. The curves appear in Figure 9.

The question as to how well the suspended particles follow the turbulent motions warrants some discussion. The particular situation at hand is a special case of the broad field concerned with particle-fluid motions in turbulent flow. Of this field, a recent article by Soo (57)[1] states,

> Apart from the studies of a single solid particle in the turbulent field of a fluid, studies of dynamics of a gas-solid suspension as a whole have

[1]Soo (57), p. 33.

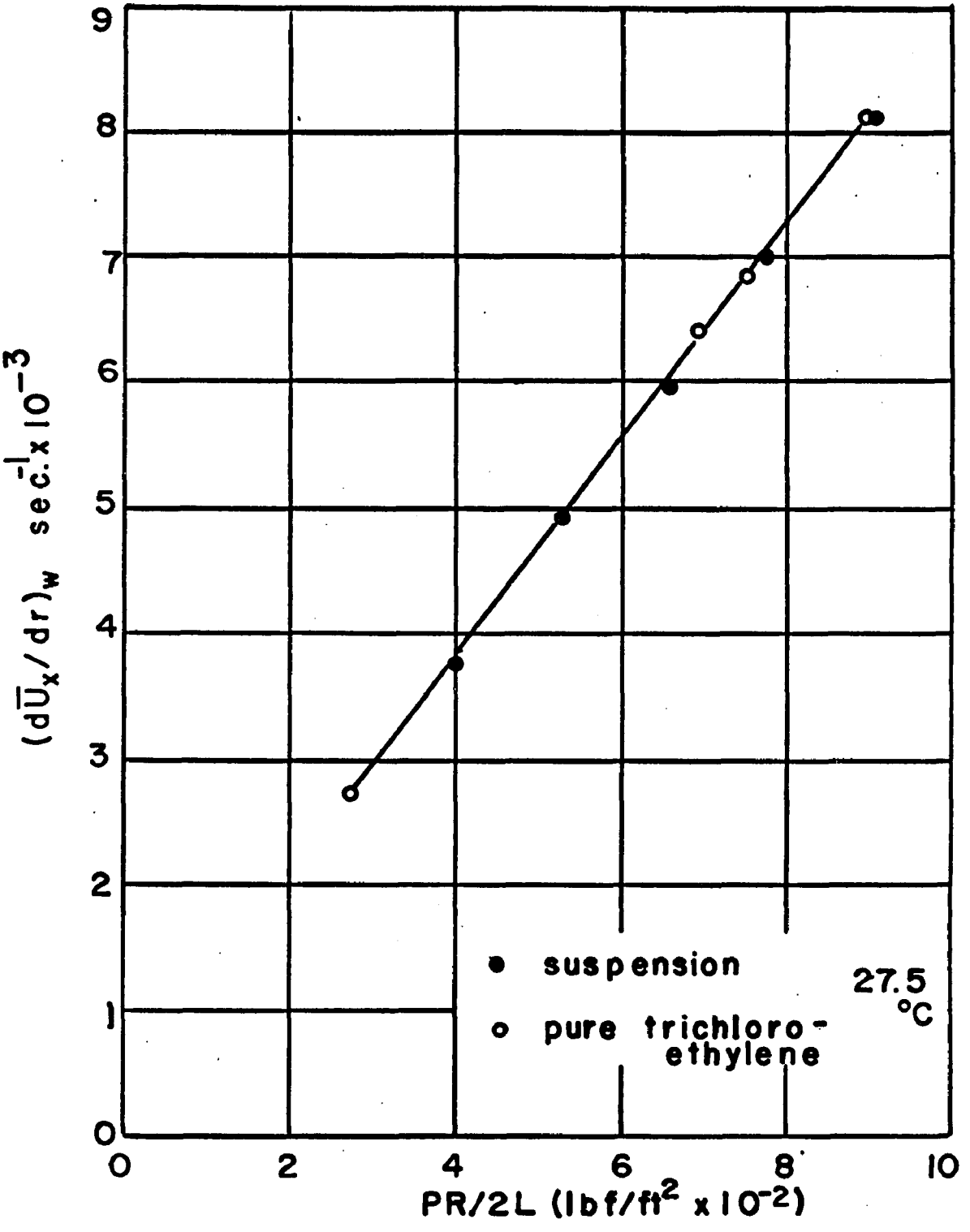

Figure 9. Viscosity Measurement

> either excluded turbulence or have been completely empirical. . . . A solution is not even available for the statistical formulation of simple turbulent pipe flow, where the turbulence is nonhomogeneous. Even when one assumes an isotropic turbulent field, the solution of the problem of motion of a single particle is at best academic.

In other words, the problem has not been solved except for a very few simple cases. Most theoretical treatments which exist require a large number of simplifying assumptions to even permit the relations to be written. Fortunately, the present case does fit some of these assumptions, and, moreover, the very small particle size permits additional simplification. Nevertheless, a rigorous theoretical or experimental proof that the particles follow the turbulent motions cannot be given.

Experimental studies of this problem have utilized particles of much greater dimensions than those used in the present study. The smallest particles used in reported experiments were of the order of 50 times the diameter of the present particles, and in most studies the size was much greater than this. For example, Soo (57) used glass spheres of 100-200 microns diameter. Kada and Hanratty (24) used glass and copper spheres of 0.0039 and .0079 inches diameter respectively.

Since both experimental and theoretical studies show the importance of the particle size on the fluid-particle interactions, extrapolation of experimental results for large spheres to the present case must be done with reservations.

For example, larger particles with densities greater than the fluid will settle due to gravity, and a stratification or particle concentration gradient will occur in the pipe. In the present study, no such effect occurs because the particles, while denser than the fluid, do not settle. Particles of dimensions of the same order of magnitude as the scale of turbulence would extend over a large enough distance so that they could be influenced by the different velocity fluctuations which could exist over this distance. Very small particles which are much smaller than the scale of turbulence would be influenced by only the velocity fluctuations over the distance equal to their dimensions, and thus would most likely be affected by a single fluctuation at any one time. In the wall region, the fluid has zero velocity at the wall, and there is a steep velocity gradient over a small distance. For particles of finite size, slip must occur at the wall because the particle extends out from the wall a distance equal to its own diameter and experiences the accelerating forces of the fluid over that distance. Obviously, the smaller the particle diameter, the more nearly it will represent the fluid motions in the wall region. Particles of 0.6 or even 5.0 microns diameter can obviously approach to distances very near the wall and still follow the fluid motions. In addition, the steep velocity gradient operating over the diameter of larger particles can cause particle spin and secondary motions, but this effect is much less

pronounced for extremely small particles. Finally, the fluid elements are deformable and in turbulent flow experience stretching and other deformations. Solid particles do not deform under the forces which deform the fluid, so large particles of order of the dimensions of the fluid element will not remain with the element during such motions. Particles which are very much smaller than the elements will. This lack of slip between particle and fluid element does not create disturbances in the fluid which can occur when slip is present. For all these reasons, the above caution regarding the extension of experimental results to the present case was given. Nevertheless, the trends shown by the experimental data can be utilized. Of special value are those concerned with particle size and concentration effects. In all the experiments, the particles more nearly followed the fluid motions and created fewer side effects as the particle size and concentration were decreased, and as their density approached that of the fluid. Kada and Hanratty (24) using the particles described earlier found that for volume concentrations of less than 1.5% in water, the presence of the particles had little or no measurable effect on the diffusion of mass in turbulent flow.

Hinze (20)[1] in introducing this subject stated,

> In the other extreme case, namely, when the concentration of particles is very low, we may

[1]Hinze (20), pp. 352-353.

> neglect the interference of the particles and regard each particle as being alone in the turbulent flow field. If the particles are big compared with the scale of turbulence, the main effect of the turbulence on the particle will be to increase its flow resistance, and the particles will, at most, more or less follow the slow large-scale turbulent motions of the fluid. If, on the other hand, the particles are very small compared with the smallest scale of the turbulence, they will tend to follow all turbulence components of the fluid.

The present case satisfies both restrictions. The particles exist in very low concentrations, and they are very small compared to the smallest scale of turbulence. For example, Mickelsen (37) measured a Eulerian microscale of 4500 microns for turbulent flow of air in an eight inch pipe. From Lee's (32) data, measurements in water at $N_{Re} = 41,000$ yield a microscale, λ_g, of 0.234 cm. Neither of these were measured in the wall region, but even though the scale of turbulence is known to decrease as the wall is approached, it does not decrease to the point where it has a scale of 0.6 or even 5.0 microns. The lower limit to the scale of turbulence is set by energy considerations since the rate of viscous dissipation of turbulent energy increases greatly as the scale of turbulence decreases. A great amount of extremely small scale turbulence would dissipate the turbulence energy at such a high rate that turbulence could not be maintained by the conversion of mean flow energy which is its source. Thus, turbulence of an extremely small scale cannot be present in any significant amount. Since the

particles used in the present study are much smaller than the lower limit of the scale of turbulence, they not only can follow the fluid motions, but also provide assurance that they are not masking fine-scale motions because of their size.

As a prelude to a more realistic and correct treatment, a simple calculation may be made to determine if it is reasonable to expect the particle to follow the fluctuations. As a model, assume that a particle is surrounded by a fluid element initially at rest which suddenly undergoes an acceleration a_f. Because of the impulsive start of the motion, this is an extreme case. The particle within this element will be accelerated according to the forces exerted upon it, and conceivably could have an acceleration a_p quite different from that of the fluid. For simplicity the only force assumed to act is that described by Stoke's law, $F_p = 3\mu d\ (u_f - u_p)$. As the analysis in Appendix I shows, other forces are acting, some in a negative direction to the above force, but they will be small for small velocity differences and are neglected for this simple case. From this model and the assumption that the fluid element accelerates from zero velocity to u_f in time t, the relation

$$u_f = u_p \left(\frac{d^2\rho_p}{18\mu t} + 1\right)$$

is obtained. Clearly, if $(d^2\rho_p/18\mu t) \ll 1$, then $u_f = u_p$. For an extreme case take $u_f = 0.5$ ft./sec., d = 5 microns

instead of 0.6 microns, and t equal to the time of a single motion picture frame, i.e., 1.25×10^{-3} sec., the relation becomes

$$u_f = u_p\ (.0076 + 1).$$

For this simple analysis of a very extreme case the difference in fluid and particle velocity is negligible.

In a far more realistic treatment of this question, Hinze (20) presents a modification of Tchen's (62) theoretical treatment of the motion of a small particle suspended in a turbulent fluid. This treatment involves a rather restrictive list of conditions and assumptions, and the development is rather involved although it is basically a force balance on the particle. These are presented in Appendix I along with an outline of the development. The relation which is pertinent to the question at hand is

$$\overline{u_{ip}^2} = \frac{a\ \Gamma_{fL} + b^2}{a\ \Gamma_{fL} + 1}\ \overline{u_{if}^2}$$

where

u_{ip} = Lagrangian turbulent velocity of particle

u_{if} = Lagrangian turbulent velocity of fluid

Γ_{fL} = Lagrangian integral time scale for fluid (this term is usually considered a measure of the longest time during which, on the average, a particle persists in motion in a given direction).

$$a = \frac{36\mu}{(2\rho_p + \rho_f)d^2} = 9.24 \times 10^4 \text{ (for the present case)}$$

$$b = \frac{3\rho_f}{2\rho_p + \rho_f} = 0.502 \text{ (for the present case)}$$

where

μ = fluid viscosity

ρ_p = particle density

ρ_f = fluid density

d = particle diameter

The effect of the extremely small particle diameter is apparent. For all intents and purposes, $\overline{u_{ip}^2} = \overline{u_{if}^2}$, i.e., the particle motions equal the fluid motions. However, it must be recalled that a number of assumptions are included in the developed relation, so the treatment is not rigorous. The degree to which the present case approaches the assumed situation is discussed in the Appendix.

There have been other theoretical developments, notably one by Friedlander (12). In this one too the effect of the small particle size is overwhelming so that the particle motions follow the fluid motions in spite of the density differences.

These theoretical relations have not included the effect of the presence of a solid boundary on the particle fluid motions. Soo and Tien (58) treated this problem theoretically for a simplified flow system. They considered

the effect of an infinite wall on a single, spherical particle suspended in a semi-infinite turbulent fluid. The particle diameter was assumed to be smaller than the microscale of the turbulence. Local isotropy and fully developed flow were also assumed to exist. The pertinent relation produced was

$$\frac{\overline{u_p^2}}{\overline{u_f^2}} = \frac{\sqrt{\pi}}{K}\left[1 - \frac{2\sigma}{y_o^3}\left(1/2 - \frac{1}{K^2}\right)\right] e^{1/K^2}\,\mathrm{erfc}\left(\frac{1}{K}\right)$$

where $\overline{u_p^2}^{1/2}$ = intensity of particle velocity fluctuation

$\overline{u_f^2}^{1/2}$ = intensity of fluid velocity fluctuation

σ = a reduced volume

y_o = distance particle is from wall

$$K = \frac{2}{\lambda_T b}\left(\overline{u_f^2}\right)^{1/2}$$

λ_T = Lagrangian time microscale of turbulence

$$b = \frac{9\mu}{2a^2(\rho_p + \rho/2)}$$

a = particle radius

They present a plot of $\dfrac{\overline{u_f^2} - \overline{u_p^2}}{\overline{u_f^2}}$ versus K with $\dfrac{2\sigma}{y_o^3}$ as a parameter of distance from the wall. This plot shows that

for values of $K < 0.2$, the value of $\frac{\overline{u_f^2} - \overline{u_p^2}}{\overline{u_f^2}}$ is zero,

i.e., at $K = 0.3$ the ratio is less than 0.03. For the present study, K may be evaluated as follows using Lee's measurements at $N_{Re} = 41{,}000$ in water for $\overline{u_f^2}$ and λ_T terms. For this calculation "a" is taken as 2.5 microns.

$$\overline{u_f^2}^{1/2} = 2.33 \text{ cm/sec}$$

$$g = 0.234 \text{ cm.}; \quad \lambda_T = 2.46 \text{ sec.}$$

$$b = \frac{9(.0055)}{2(6.25\times10^{-8})(3.6 - \frac{1.46}{2})} = 13.9\times10^3$$

$$K = \frac{2\ (2.33)}{(2.46)(13.9\times10^3)} = 1.36\times10^{-4}$$

K is clearly less than 0.2, which again emphasizes the strong effect of particle diameter.

Later in the same article the authors show the effect of the wall on particles of 100 microns diameter. Due to the steep velocity gradient and the resulting particle rotation, a magnus effect becomes important. Why this is probably not so for the small particles of the present study has already been discussed. In addition, it can be said that such an effect or the results from it were not observed in the motion picture.

All of the preceding arguments were made to show that the fine particles used in this study adequately follow the

fluid motion so that their motions in turbulent flow may be assumed to be the same as the turbulent fluid motions. While the arguments were not rigorous, the evidence strongly supports this contention. Moreover, no invalidation of the assumption was found either in the theoretical or the experimental evidence considered. The consensus of most authors on this subject agrees with Hinze's statement that if the particles are small enough they will adequately follow the turbulent fluid motions.

The question as to whether the trichloroethylene wets the solid and the possible effects of the particle behavior if it does not is now considered. Although no measurement of the contact angle of the air-magnesium oxide-trichloroethylene system was available, examination of the values for similar systems and for fluids of similar surface tension indicate that the solid is wet by the liquid. Actual experience with the materials indicated that this assumption was justified. In addition, the suspension was prepared far in advance of the time of use, and it experienced continual agitation over this period of time. Both factors would tend to overcome any resistance to wetting. Therefore, there is no reason to believe that the solid surface was not wet by the fluid. Despite this conclusion, it might be of value to consider the effects on the particle motions which might occur if it were not wet. First, very large air bubbles

surrounding the particle cannot exist because agitation within the flow would quickly shear them off. Thus, only a thin film of air can surround the particle. This air-solid particle would not be much larger than the solid particle, and would have a density more nearly equal to that of the fluid. The air film would necessarily be tightly bound to the solid surface, and slip between the film and the particle would be nil. The forces due to the fluctuations of the ambient fluid would act on the air-solid particle in the same fashion as for the solid particle, and it has already been demonstrated that the relative velocity between the solid particle and the fluid element is very small. Thus one cannot expect the resulting shear to remove the air film in a steady state case. It is quite reasonable, therefore, to expect that the presence of an air film on the particle will not affect its motion to any appreciable extent. Of course, such a film would have great effects for heat and mass transfer to the solid, but this is of no concern in the present situation.

Photo-optical system

This section describes all the equipment and procedures used to obtain the photographs of the flow. It also discusses the different camera viewpoints and the advantages of each.

Camera. As was discussed in the introduction, the very nature of turbulent flow, i.e., random, rapid motions, requires that some means other than visual examination be provided for any detailed observation of its characteristics. Not only is a permanent record of these motions required for comparison when flow conditions are changed, but some means must be provided to display the rapid motions at a reduced speed. The high speed motion picture camera is ideal for these purposes. It provides the means of slowing the motions to an intelligible level and, equally important, provides a permanent record for comparison. For the study of turbulent flow, it has a great advantage over high speed still photography because it provides an ordered progression of time and a continuity of motion. One can watch time dependent sequences develop. In still photography one is forced into a position of random sampling. The task of taking a large enough quantity of single photographs to depict a time dependent sequence of events, and then interpreting this sampling without having knowledge beforehand of the events or order of occurrence is an almost insurmountable one. The camera used in this study was a 16 mm Fastax WF3 high-speed motion picture camera with a film capacity of 100 feet (4000 frames). It has a rated framing speed of from 150 to 8000 frames/sec., but was operated in this study at between 650 and 1000 frames/sec. depending on conditions. This limitation was set for two reasons. First the amount of light

available to expose the film was limited even though an extremely powerful source was used. This is because much of the light input passes directly through the fluid and is not transmitted to the camera by the particles (recall that the direction of view is at right angles to the direction of light input). It was possible to obtain exposures as high as 2000 frames/second, but only at the cost of a considerable reduction in quality of the images and content. The second reason for the limitation is that at higher speeds the real time recorded on the 100 feet of film becomes drastically reduced so that there is a greater chance of a developing or sequential type occurrence being missed. For example, at 1000 frames/sec. the entire 100 feet of film will be exposed in approximately 4 seconds, and at 2000 frames/sec. the time is 2 seconds. For these reasons, it was decided that the best course of action would be to use the speeds of 650 to 1000 frames/second. At these speeds, the shutter speeds are 5.1×10^{-4} and 3.3×10^{-4} seconds respectively.

The high-speed motion pictures record a motion which occurs very rapidly in real time and permit the observer to view that motion in a greatly extended time interval. For example, at $N_{Re} = 50000$ the local mean axial velocity at $y^+ = 25$ is 0.82 ft./sec. Under the conditions of these experiments the magnified field of view covers a real axial length of 0.095 inches. A particle of fluid would traverse this field in 0.0097 seconds which is too fast for the

unaided eye to follow much less discern any fluctuating motion. At 800 frames/sec. this particle would appear in approximately 7 frames of film and travel 0.095 inches. If now the film is projected for viewing at 7 frames/second, this same motion has been extended over a period of one second, an advantage of 100/1. This advantage not only permits more detailed observations, but permits more accurate measurements as well. An additional improvement is obtained by moving the camera with the axial flow as will be explained later. Since this greatly enhances the capabilities of the system, further discussion will be deferred until then.

The camera has a timing light which automatically imprints in the film margin timing marks at the rate of 120 marks/second. These marks permit the calculation of framing rate, but more important they permit an accurate calculation of the real time which has elapsed for a particular occurrence, regardless of the relative time the viewer is using. This was used extensively to measure velocities and the duration of events, and the procedure will be discussed in the appropriate section.

Film. The combination of high speed photography and limited available light for exposure placed severe requirements on the type of film to be used. It was found that Kodak #2475 Recording film (formerly Royal-X Pan), which is the fastest film available, performed adequately under the conditions of this study, and was used exclusively for

particle films. This film, after development, produced a black and white negative print wherein the particles appeared as dark spots on a light background. This negative print was used in all subsequent analyses. The enlarged photographs shown in Figures 23, 24, and 26 were made from these negatives and appear as positive prints. It should be noted regarding these prints that considerable image quality was lost during enlargement and printing, and the positives are used here solely for illustrative purposes. All analyses were made on the negative motion pictures because their quality and content, even when enlarged 100 times in projection, were superior to the positive prints.

Lighting. Dark field illumination such as was used in this study requires that the direction of light imput be at approximately right angles to the direction of view. Thus the light eventually reaching the camera must first be reflected or refracted by the small particles suspended in the fluid. As the concentration of these particles was relatively dilute, only a very small fraction of the total light input eventually reached the camera. Most passed directly through the essentially clear fluid. The brightness of the particles is dependent upon the brightness of the light source, and not the total illumination. Also, a law of physics states that given a light source of a certain intrinsic brightness the brightness of any image formed from the source by whatever means cannot exceed the intrinsic

brightness of the source. The light energy per unit area may be increased by focusing, but not the intrinsic brightness (Sears, 54). Applied to the particular case at hand, this means that the brightness of the particles cannot be increased by lamps of higher wattage or by focusing into the field the beams of large light sources unless the intrinsic brightness of the source is increased. One may, of course, illuminate a larger area and therefore see more particles, but the intensity of the brightest particle is fixed by the source. The field of view in the present case was quite small so a source of large dimensions was not needed. The lamp selected was an Osram HBO-109 super pressure mercury arc lamp. It has a very small arc (0.3 x 0.3 mm) suitable for the present purposes, and the highest intrinsic brightness of any comparable light source, 140,000 candles/sq. cm. This lamp was operated by a D.C. power supply at 100 watts. The power supply was equipped with a "low ripple" attachment to assure more uniform operation of the arc regardless of fluctuations in the line voltage to the power supply. The lamp body was quartz.

The lamp was enclosed in a metal housing with an aperature centered at the arc. The light was focused by a front surface, spherical mirror located behind the arc at a fixed position to give an optimum image of the arc. Focusing of the image in the field of view was accomplished by movement of the entire housing along metal guides. Adjustment in

three directions was possible. Adjustable slits were fastened to the housing to provide a narrow line of illumination in the field of view, and increase the contrast between the illuminated and dark field. The beam was, however, wider than the depth of field of the optical system, so the latter determined the depth of view and not the light beam. A photograph of the lamp, housing and supports appears in Figure 10. The lamp also appears in the photographs of the mechanism used to move the photo-optical system with the flow as is described. Those are Figures 4 and 5.

Optical arrangements. The over-all optical system is depicted in Figure 2, and in the photographs of Figures 4 and 5. In addition to the lamp already described, there are two other important parts. First there is the viewing cell mentioned earlier. This is a cell open at the top which completely encloses the glass test section. It is shown in Figures 4 and 5. The base and one vertical side are the support cradle for the pipe. In the rear vertical support a number of adjustment screws are located. These are used in the alignment of the test section with the line of travel of the camera, and will be discussed when this matter is described in a later section. The ends of the cell are sealed to the pipe. The front, or face of the cell toward the light source, is 1/4" plate glass and runs the entire length of the pipe, as does the cell. This watertight cell can be filled

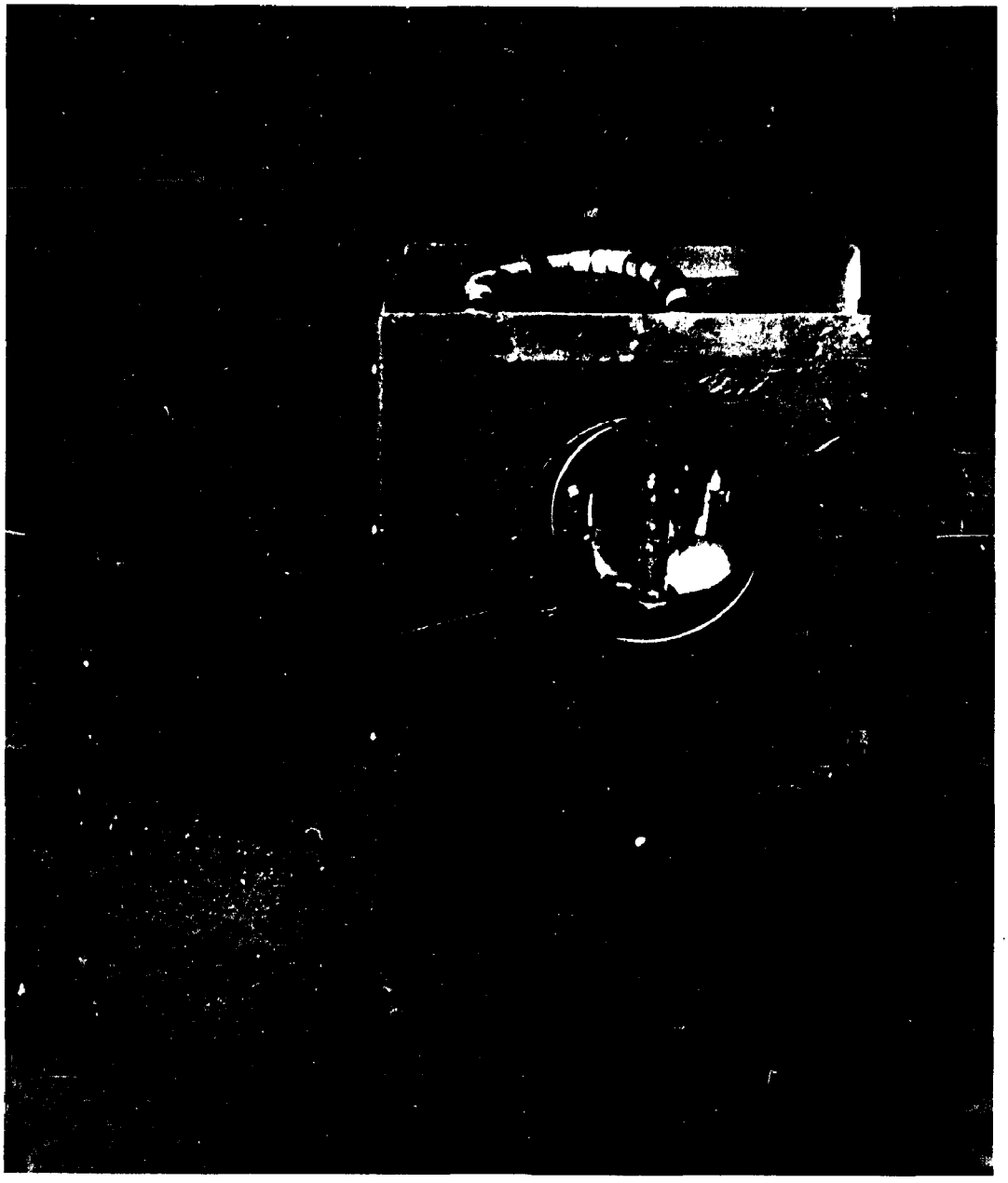

Figure 10. Lamp and Support

with pure trichloroethylene so that the entire test section is submerged in the fluid. Since this fluid has essentially the same index of refraction as the glass pipe, and since the fluid is inside the pipe as well, the refraction of light due to the curved pipe walls is minimized, and the wall area can be viewed from above as indicated in Figure 11. This result is very important as it allows the studies to be made in circular pipes. Without this view cell and the tricholorethylene within the pipe, the wall area, and particularly the sublayer, would not be visible for study.

The cell serves a second purpose as well. The intense light beam focused on the exposed pipe wall would rapidly heat the glass in the area of focus, and could cause convection currents which at low flow rates might introduce extraneous motions into the pictures. The plate glass and cell fluid effectively absorb this heat so that the problem is eliminated. In addition, the movement of the light source with the flow during the runs prevents the local regions of the cell or pipe wall from becoming heated, although this is not likely under most circumstances of operation anyway. This question of local heating was examined experimentally by photographing laminar flows with the light stationary at a particular axial position. Not only are these conditions most conducive to producing heat effects, but the laminar flow would most readily show these effects if they existed. No such effects were observed.

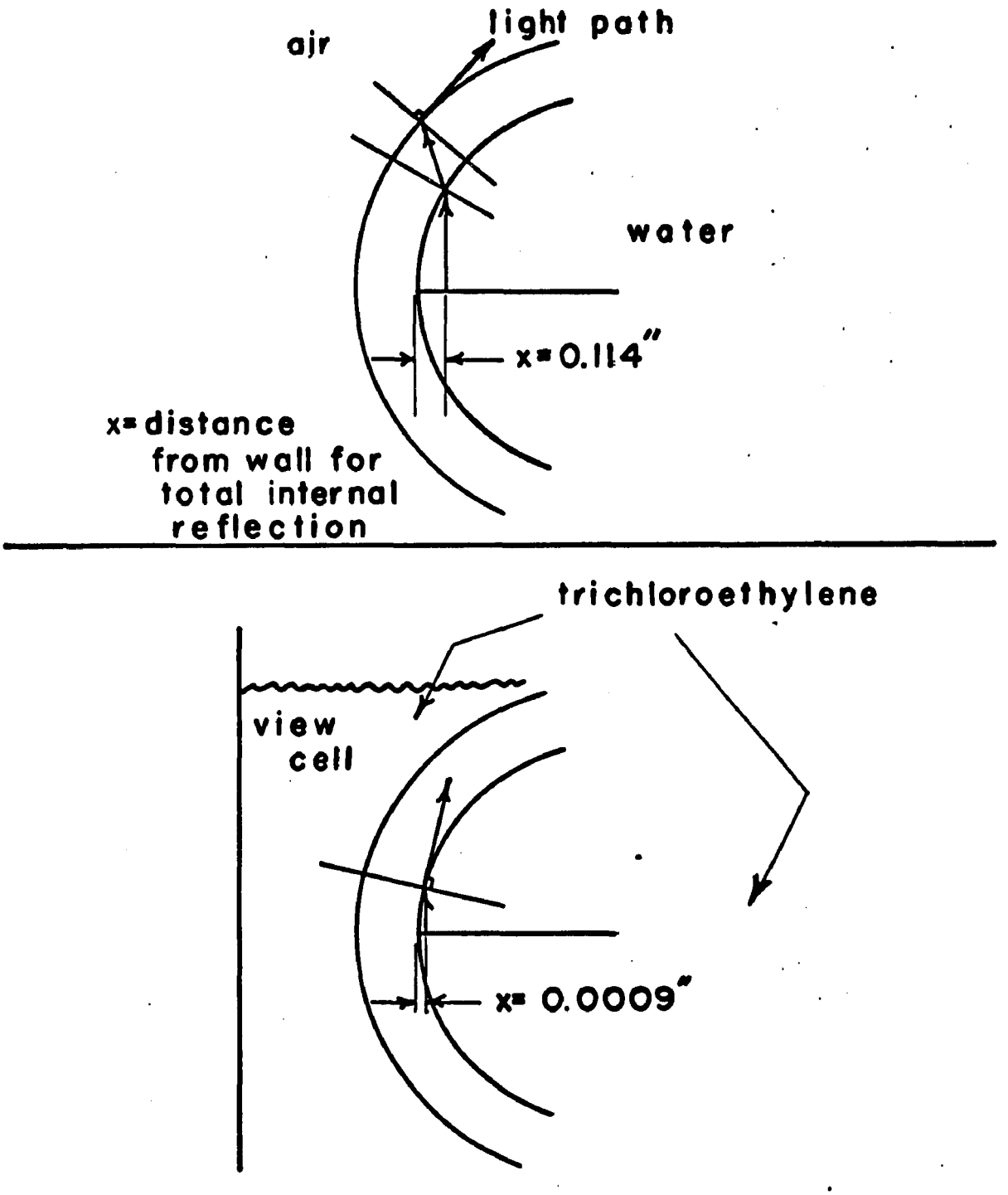

Figure 11. Refraction Effect

The lenses of the camera comprise the second part of the optical system. These lenses were adapted to produce magnifications of 4.3X and 2X. Some magnification of the field of view was necessary for detailed investigation of the fluid motions because the sublayer and wall region are of such small dimensions. For example, at N_{Re} = 20,000 the thickness of the region out to $y^+ = 15$ is of the order of 0.025 inches in a 2-inch diameter pipe. The amount of light from the particles which reaches a unit area of film for exposure is inversely proportional to the extension tube length between the lens and the film plane which produces the magnified image. Since the amount of available light from the particles was limited, any increase in magnification required a proportionate decrease in framing speed for photographs of comparable quality. Thus one must pay for increased information from magnification by reduced information from slower framing speeds or poorer quality images. The above magnifications represent a compromise. It was decided that higher magnifications would be sacrificed for higher framing speeds because the latter were felt to be more necessary. The lower magnifications were also chosen for a second reason. As the magnification increases, the field of view decreases. At higher magnifications the field of view would become very small, and certain aspects of the fluid motion which were larger in scale than the field would not be defined. The 4.3X magnification was found to be most

satisfactory as it provided sufficient enlargement of the wall region to permit detailed investigations, but still provided a large field of view.

The field of view available at 4.3X was 0.095 inches measured parallel to the pipe wall, and 0.069 inches measured along a radius perpendicular to the direction of view. For 2X the respective dimensions were 0.205 inches and 0.147 inches. The dimensions were measured by photographing a ruled scale with the appropriate lenses, and measuring the image obtained.

Each magnification also had a depth of field associated with it. The depth of field is defined as the thickness of a plane perpendicular to the direction of view in which all objects are in focus. For very high magnifications this depth is sharply defined, but for low magnifications, such as those used in this study, there is a degree of subjective judgment as to what is really in focus and what is not. The depth of field was determined by photographing with the appropriate lenses for each magnification a hairline mounted on the inclined face of a 45° right angle prism. The resulting photographs showed a line which was sharply in focus over a given distance, less well focused over another distance, and so on until it was complely out of focus. By measuring the length of the line to the degree of focus desired, and knowing the magnification, the depth of field can be

calculated from the following relation

$$\text{depth of field} = \frac{L}{M} (\sin 45^\circ)$$

where L is the length measured on the photograph, and M is the magnification. This was done for each magnification at the f stops used in the experimental runs. The gradual deterioration of the line focus in the photographs introduced some arbitrariness into the selection of a working depth for the actual experimental films, but after careful examination of image quality of the particle films and the depth of focus photographs, the depth of 0.027 inches was selected for 4.3X and 0.041 inches for 2X. The degree of choice was not great. For example, the 4.3X magnification must have a working depth between 0.022 and 0.027 inches.

The field of view is thus seen to be a volume of fluid which for 4.3X is .095 x .069 x .027 inches in axial, radial and line of sight respectively. This is depicted in the drawings in Figure 13. Since the field of view is a dimension at a particular magnification, the dimensionless or y^+ distance of the wall region encompassed by a single frame will vary with the Reynolds number. Thus at N_{Re} = 20,000 the full frame width will include a y^+ of approximately 45 while at N_{Re} = 50,000 this same width will include a y^+ of approximately 90.

Mechanism to provide camera motion. During the preliminary investigations leading to the experimental techniques eventually used, it was found to be very desirable to move the camera with the mean axial flow. There were two important reasons for this. The difficulties with lighting, magnification, and framing speed have already been discussed. If the camera is held stationary at a particular axial position, the framing speed must be increased to slow down sufficiently the mean axial velocities so that the fluid will remain in view for long enough period of time to permit analysis of its motions. This increase in framing speeds results in a decrease in image quality if the magnification is held constant, or necessitates a decrease in magnification to maintain image quality. In either case a decrease in information results. Also, the problem of real time examined in a single 100 foot roll of film is present. This too has been discussed previously. If the time is reduced to too small a value, the number of reels exposed must increase greatly if a reasonable sampling of the random events of turbulent motion is to be obtained. The second reason for the movement was the discovery that with the camera following the selected fluid elements, the development of certain motions could be readily observed, and the various measurements could be more easily made. This will be discussed at length later in this section.

Since the major problem was in slowing down the axial flow, the process of moving the camera and light source downstream with the flow would greatly reduce the relative motion between the camera and the axial flow. Returning to the example used earlier, consider the case where the camera is moved downstream at 0.56 ft./sec. The local mean velocity at $y^+ = 25$ is still 0.82 ft./sec., but now the relative velocity is only 0.26 ft./sec. Performing the same calculation as before, it is found that the particle of fluid appears in approximately 24 frames instead of 7 as before. In order to accomplish the same result without camera movement, the framing speed would have had to be nearly 2500 frames/sec. as compared to 800 frames/sec. Additionally, there is the added feature of following a particular element for a given time and distance. The departures from axial flow caused by the turbulent motions are also more readily apparent because they exhibit larger <u>apparent</u> angles of deviation from the axis. Thus, as later calculations will show, angles of the order of 10° and 20° can appear as 90° deviations from the axis when the proper axial motion of the camera is used. This permits these angles to be more accurately measured, and also makes minor deviations more visible. Since this relative motion only operates in the axial direction, it does not reduce the apparent radial or angular fluctuations. These, however, are small compared to the local mean axial velocities. Laufer's (31) measurements in air show that at

$y^+ = 25$ at 50,000 N_{Re} the u_r' fluctuation is only 5% of the local mean axial velocity, and the u_θ' intensity is approximately 12%. These velocities are readily slowed down for analysis at 800 to 1000 frames/second, and though they represent average values, even the larger fluctuations contained in this average will be visible in the motion pictures. In all these examples the highest Reynolds number studied in the experiments has been used since it provides the most severe conditions. Since the technique can adequately handle these conditions, it can easily handle the less severe conditions imposed by lower Reynolds number. In addition, at positions very near the wall the absolute magnitude of the fluctuating velocities decreases so again the above examples are extreme cases.

While the camera is moving downstream, it is essential that the focus be maintained and that no disturbing vibrations occur. To assure both of these conditions, an 8-foot lathe bed was aligned parallel to the test section, and bolted to the floor. The lathe carriage, designed to slide down the ground steel ways of the bed, was fitted with the necessary supports to carry the camera and lighting system. The carriage and supports were very heavy and not susceptible to vibrations. The supports for the camera and light source were adjustable to permit proper focusing, and the camera support had an adjustment screw for fine focusing. They appear in the photographs of Figures 4 and 5 where the posi-

of the lathe bed is shown. The final alignment of the test section to the line of travel of the camera was made by the adjustment screws in the rear face of the test section cradle. A microscope with a grid eyepiece was mounted in place of the camera, and the carriage was slowly moved down the bed while the pipe wall was sighted through the microscope. Adjustments were made until the wall over the entire length of the test section deviated no more than .03 inches from parallel. Over short sections used for most of the studies the alignment was much better. No further improvement of the alignment was possible because of the flexibility of the glass pipe and the necessity of not having any solid support on the top or front face of the pipe. Fortunately, this alignment was not a problem. The position of the wall was clearly visible in the field of view, and prior to each run it was aligned so that it would appear in all frames. This necessitated sacrificing part of a frame by having the wall position within the frame at some axial positions so that at other axial positions the wall would just be aligned with the edge of the frame.

Over the short sections used for most studies the alignment was quite good and the wall could be maintained at the very edge of the frame. It was only over long segments of the test section where the full effect of the misalignment was visible. These long sections were used for high Reynolds numbers and at these Reynolds number the y^+ region enclosed

by a full frame is much greater than that for low Reynolds numbers, so the result was that the loss of part of the frame did not really cause any loss of the y^+ region studied when compared to the lower Reynolds numbers. Vertical alignment was established by mounting a feeler gauge on the carriage and keeping it in contact with the pipe surface while adjustments were made.

The drive mechanism for the carriage consisted of an hydraulic piston with specially compensated valving and pumping apparatus to assure steady, vibration free movement. The piston was connected directly to the carriage. The rate of travel of the piston controlled the carriage movement, and was continuously adjustable from motionless to 1 ft./second. Once the control was set, of course, the velocity was constant. A photograph of the piston and support equipment appears as Figure 6.

The speed adjustment on the piston was necessary because the camera or carriage motion was to be matched to a particular local mean axial velocity which varied both with y^+ position and Reynolds number. For the wall views (to be described later) it was found that the best photographs were obtained if the carriage velocity was matched to the local mean axial velocity at $y^+ = 11$. For other views, other positions of matching were selected. When the carriage velocity matched a particular flow velocity, the resulting photographs showed zero relative velocity for that position, and gradu-

ally increasing relative velocities as the distance from this position was increased both wallward and outward toward the centerline. Naturally, the apparent direction of flow on one side of this plane was the opposite of the flow on the other.

Since this relative motion was measured in the later analyses, it was essential that the carriage speed be known quite accurately for each run so that absolute velocities could be determined. To record the carriage velocity, a nichrome ribbon with a constant and accurately known resistance per foot was cemented to an insulating strip on a non-bearing flat-ground surface of the lathe bed which paralleled the tracks down which the carriage moved. A sliding contact was established between this ribbon and an arm securely fastened to the carriage. A mercury cell was connected through a variable resistance circuit to the ends of the nichrome ribbon so that a constant voltage drop per unit length was maintained. Also permanently connected to one end of the ribbon was a lead wire which was one input to a Baush and Lomb VOM-5 recorder. The other input was from the sliding contact. As the carriage moved, the voltage drop measured between these two leads was recorded on the recorder strip chart which was driven at a known constant speed. The carriage velocity was determined from the slope of the line traced on the strip chart and the calibrated voltage drop

per foot of the wire. For constant carriage speed, the line was straight, and this provided an additional check on the constancy of carriage motion during a run. The variable resistances through which the batter was connected to the resistance ribbon were used to provide a selection of voltage drops within the wire appropriate for the various carriage speeds to be measured. A schematic drawing of this device appears in Figure 12. After each days experiments, the voltage drop per unit length of the resistance wire was calibrated using a precision potentiometer.

To check the recording device and the constancy of the carriage movement, a steel tape was mounted on the pipe surface, and high speed motion pictures taken of it while the carriage was moved downstream. The carriage velocity was recorded and calculated. Two different but representative velocities were checked in this fashion. The timing marks on the film and the scale image in the frames permitted an accurate calculation of the absolute carriage velocity for each inch or fraction of an inch of carriage movement. In actuality, 3 inch segments were examined. It was found that there was no variation in carriage velocity from segment to segment, i.e., it was constant. The velocity determined in this fashion agreed with the values given by the recorder. The photographically determined velocities were 0.680 and 0.208 ft./sec., and the recorder values were 0.679 and 0.209 ft./sec. respectively. The films also showed that

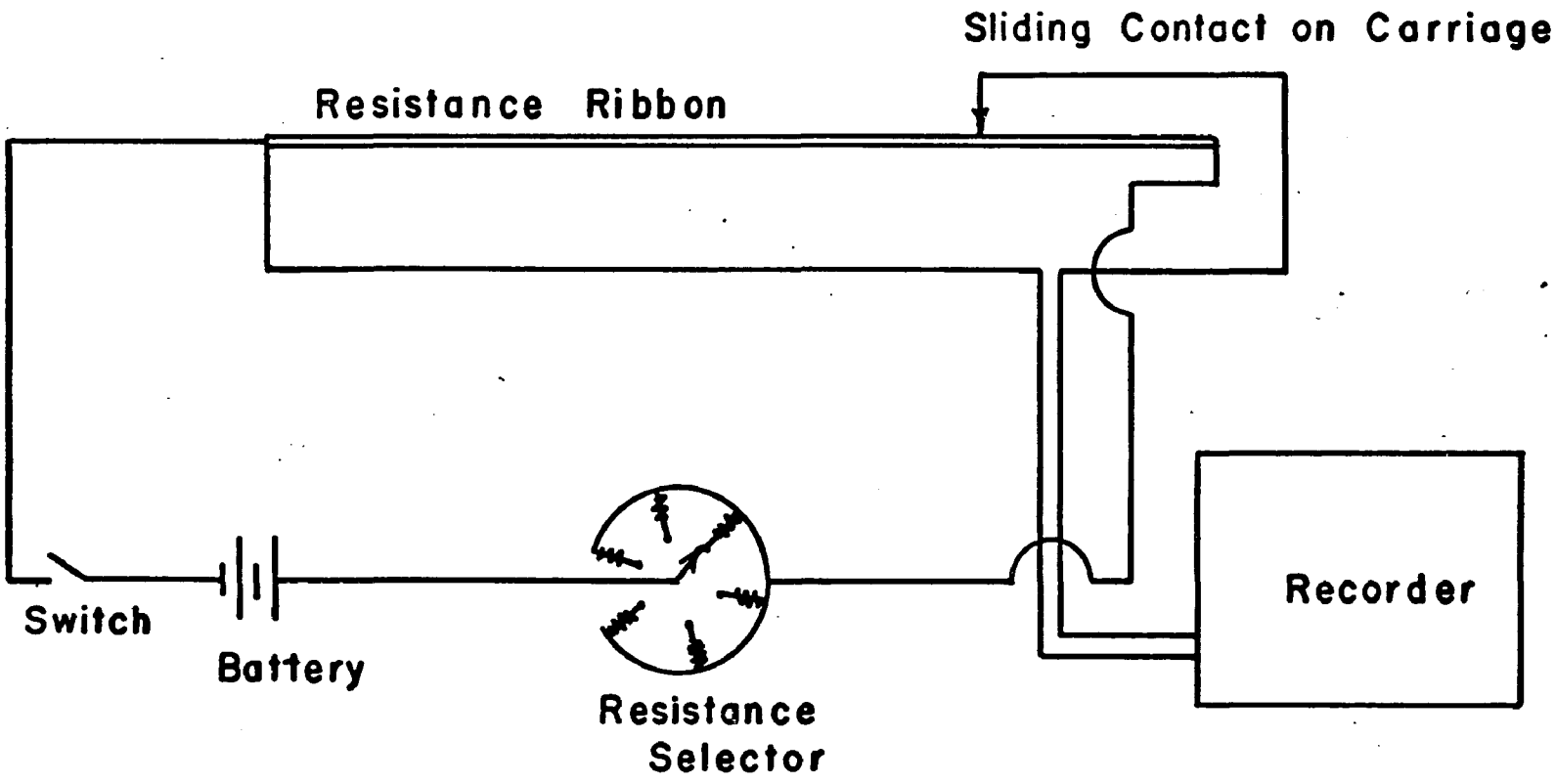

Figure 12. Carriage Velocity Measurement

there was no vibration of the system which affected the photographs.

Camera viewpoints

Although the camera line of sight of necessity must be at right angles to the light beam, there is some choice as to the position of focus. In this section the different positions used will be described.

Wall view. The following discussion will be much clearer if Figure 13 is used in conjunction with it. As part (a) of this figure shows, the light beam enters the field at right angles to the line of sight of the camera. The camera is focused on a horizontal plane AB (part c) at the vertical centerline of the pipe with the interior pipe wall aligned with the edge of the frame. Part (b) of this figure is included to show the orientation of the various planes in polar coordinates. In future references to this view, these planes will be used to describe the location of various events. If the camera were focused only at the geometric plane AB, the plane would coincide with the rx plane of the polar coordinates. However, as part (c) shows, the camera actually "sees" a certain distance on either side of this plane along the line of sight due to the depth of field of the lens system. Since the lenses present flat surfaces parallel to AB for the camera to view, these planes separated from AB by the one-half the depth of field will

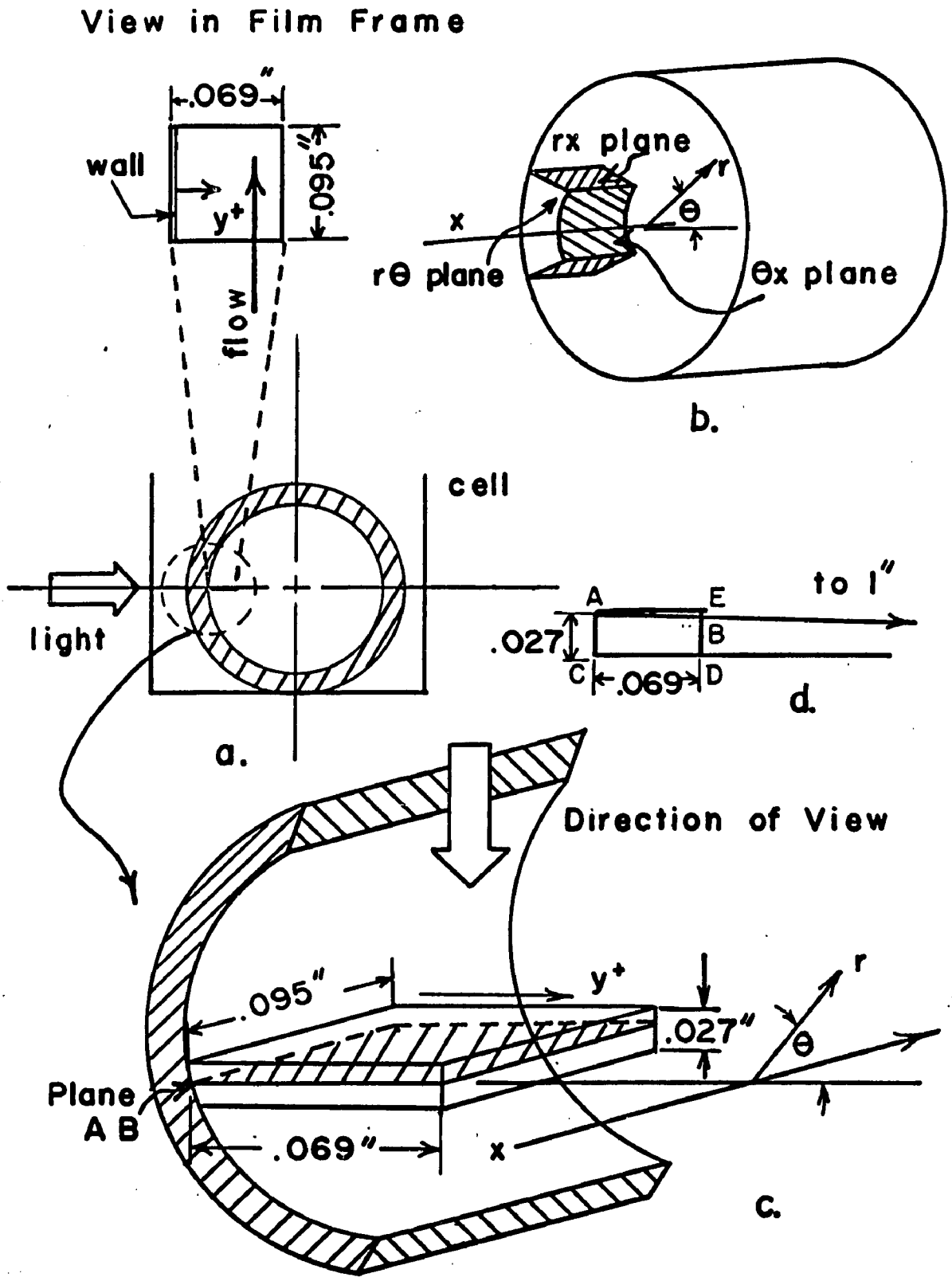

Figure 13. Wall View

not coincide with the rx planes at that position. However, because of the extremely small dimensions of the field of view, the actual difference is insignificant and no differentiation will be made in future discussions. Part (d) illustrates this point. AEDC is the optical field and ABDC is the polar coordinate field. This could, of course, be avoided through the use of rectangular coordinates, but they would cause confusion when other views are considered. Because of the depth of field, the camera actually "sees" a volume of fluid and not a plane, although the thickness of this plane is quite thin. Since the optical system cannot show three dimensional effects in the motion pictures, the particles within this volume all appear to be on a single rx plane, and in this view there is no accurate means of determining at which rx plane within the volume they are located. In most future descriptions, the positions of particles in this view will be described without regard to the possible separation in the θ direction. For most cases this separation is so small that it has no great effect on the observations so ignoring it does not create any problems. For those situations where it may be of importance, specific mention is made of it. Also, particle motions will be described in terms of movements, along the polar coordinates, i.e., x, r, and θ. To be absolutely rigorous, one cannot say this because of the incongruence of the optical and

coordinate planes, and the inability to determine motions in the θ direction. The differences occur only for the r and θ coordinates, and are very slight because of the small dimensions. Whenever necessary, and in the final analysis where the observations from different views are compiled, an attempt is made to provide a three dimensional picture. This three dimensional motion will have its most important effect on velocity measurements. The question of errors introduced in these cases is discussed in a later section and in Appendix II.

During the experimental runs, the light beam was focused through the slits into the desired field of view by adjustment of its position on the metal support guides. For the wall view, it was focused at the vertical centerline at the inside surface of the pipe wall. The camera was then aligned with the pipe wall so that the interior wall was just within the frame. The wall could be seen as a thin bright line due to the imperfect match of index of refraction between the pipe and the fluid. The outside surface of the pipe could also be seen if the position of the camera were moved towards it, thus it was assumed that this line was the inside wall. The assumption was checked by inserting a ruled scale into the pipe such that its initial graduation was in contact with the inside wall, and then examining it visually and photographically. The results showed conclusively that the bright line was the inside wall, and that it did not

extend any significant distance into the wall region. This is due to the thin layer of focus and illumination, and the very small curvature of the pipe wall over this thickness.

The refraction of the light beam from within the pipe at the pipe wall was calculated for the sublayer region. At a distance of 0.002" from the wall (equivalent to $y^+ \doteq 2$ at $N_{Re} = 50,000$ and less for other N_{Re} values) the incident beam had an angle of 86° 23', and the refracted beam an angle of 87° 19'. This shows that very little distortion occurs. A similar calculation was made to determine the distance from the wall at which the light beam would have to originate in order to be totally reflected internally at the pipe wall. This distance was 0.0009 inches. This is only an approximation because monochromatic light was not used, but it is a good estimate. This distance can be considered the distance which the wall refraction effect intrudes into the sublayer. Actually, due to the fact that at angles near the angle of total reflection a large amount of light is reflected, although some is transmitted, one can expect that a dark region slightly larger than 0.0009 inches will exist in the sublayer. Some light is transmitted over this region, however, so the motions within the region should still be visible.

Once the camera was aligned, it was locked in place on the support member so no further lateral movement was possible. It was then focused by a sliding and screw

adjustment in the vertical plane, and then locked in place here as well.

Top view. Figure 14 details the different aspects of this view. As part (a) shows, the light enters at right angles to the camera line of sight, but in this case the light is directed to the interior wall region at the top, horizontal centerline position of the pipe. The pipe orientation is the same as in Figure 13 so a comparison can be made. Since there is axial symmetry in pipe flow, this view is essentially rotated 90° from the wall view. The line of sight is now along the r coordinate, and the planes perpendicular to the direction of view are θX planes. The comments made before concerning the congruence of the optical planes and the geometric planes apply in this case as well, as do the comments about the three dimensional movement of the particles. These motions are considered to occur in the θX planes, and therefore would be motions parallel to the line of sight in the wall view, just as the motions of the wall view in the rx plane are parallel to the line of sight in this view. Although these viewpoints were used separately, careful analysis of each series of films permitted a three dimensional picture of the fluid motions to be constructed.

Since the wall of the pipe did not appear in this view, the camera alignment procedure became more elaborate. A positioning scale, which is shown in Figure 15, was inserted into the pipe from the downstream end by a long steel rod.

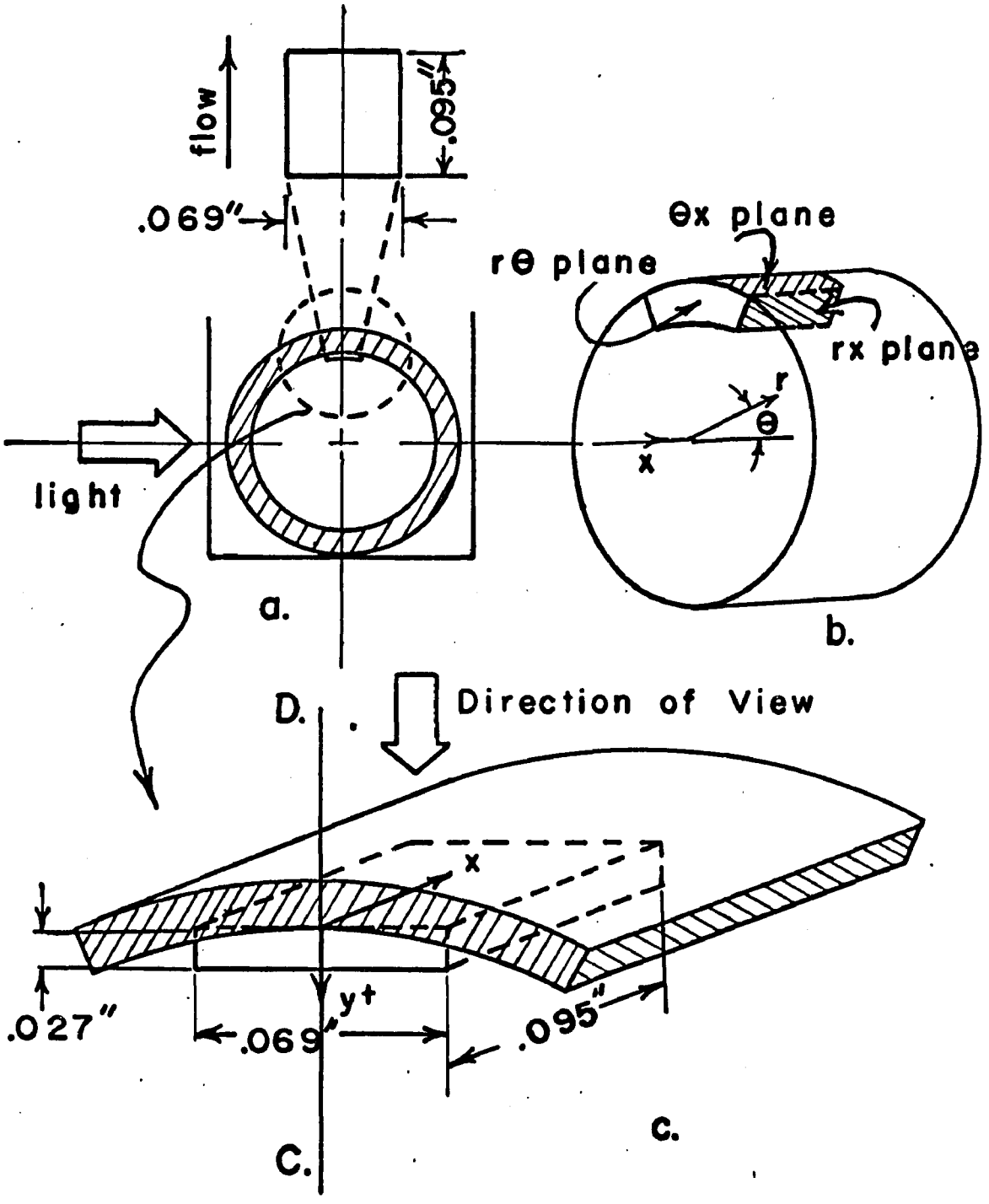

Figure 14. Top View

The brass collar supporting the scale was designed to push the edge of the scale against the inside pipe wall surface at the vertical centerline (that is at plane AB of Figure 13). This placement is shown in Figure 15. In this position, the scale coincided with the AB plane. The camera must be positioned not only with respect to rx plane of Figure 14 but with respect to the θX plane as well. For this view, the center of the frame was aligned with the rx plane which coincided with the CD plane of Figure 14, part (c). This was the pipe centerline as measured horizontally from the wall. To make this alignment, the viewfinder of the camera was sighted in on the appropriate scale reading which corresponded to the pipe radius, and the lateral movement mechanism locked in place. The other adjustment concerned the focusing of the camera on the θX plane at the inside pipe wall. This was accomplished by rotating the brass collar so that its surface was facing the camer. The camera was then focused on the surface such that the upper limit of the depth of field coincided with the surface. Since the collar was in contact with the pipe wall, this adjustment meant that the entire depth of field was available for viewing from the inside pipe wall radially inward. After this adjustment, the scale was retracted downstream out of the test section into the section of steel pipe which followed the test section. It therefore could not affect the flow.

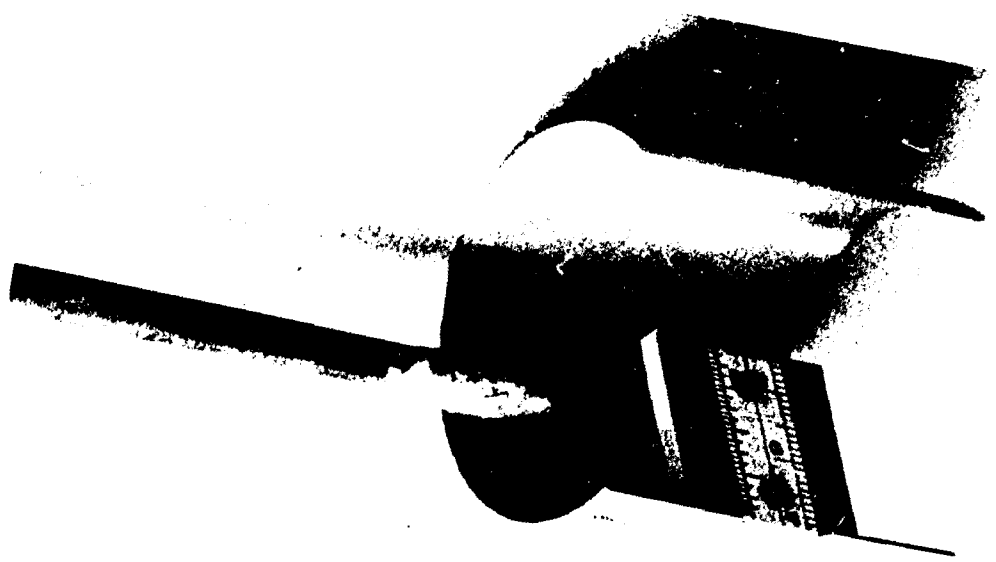

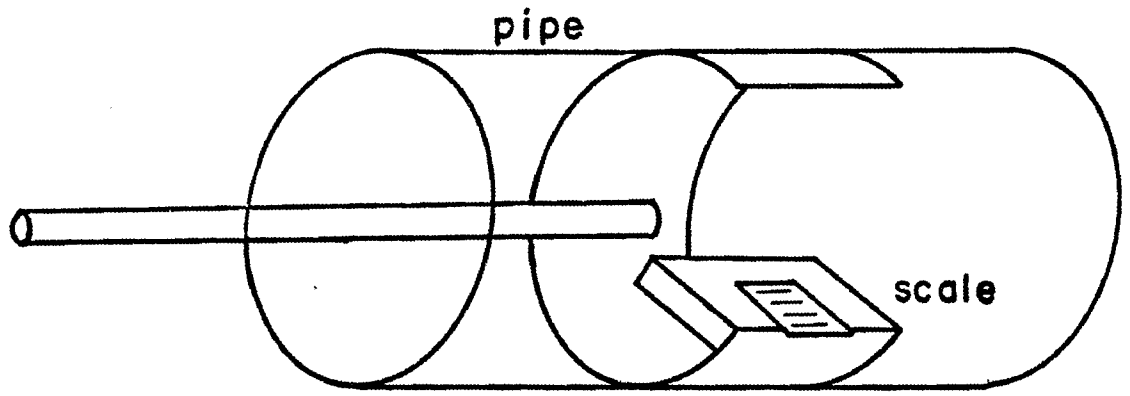

Figure 15. Positioning Scale

Trip wire. In a few cases the presence of a trip wire was required. The trip used in these cases was a circle of spring steel which when inserted into the pipe had an outside diameter just equal to the inside pipe diameter. The wire had a circular crossection and a diameter of 0.0032 inches. It was positioned axi-symmetrically, and was held place by its own tension. Both top and wall views were used in the series of runs with this trip wire.

Other views. The limited dimensions of the field of view permitted observations to only small y^+ positions when the camera was focused at the wall. In order to examine the fluid motions at greater y^+ values, it was necessary to focus the camera at greater distances from the wall as measured along the AB plane of Figure 13. The resulting views were essentially the same as the wall view, but displaced varying distances from the wall. In order to position the camera, the scale device described in the top view section was used. In this case, of course, the focus was at the plane AB.

Hot film Anemometer

A lintronic Model 40W Linear Constant Temperature Hot-Film Anemometer with a thermocouple-type root mean square meter was used for measuring local mean velocities and turbulent fluctuation intensities. This unit will not be described in detail here as a rather complete discussion has

been presented elsewhere by Hubbard (22). Basically the unit measures the velocity of the fluid by indicating the voltage requirement needed to maintain the constant temperature of the hot film of the probe. The internal circuitry provides a linear relation between the effects of the fluid velocity on the probe and the output signal. Two probe configurations were used. One was a right angle wedge probe where the sensing element or hot film was positioned on a thin glass wedge set at right angles to the probe axis. By inserting this probe through the wall of the pipe, the $\bar{U}_x$ and u'_x velocities could be measured. The other configuration had a flat surface at the end of the probe where the sensing element was positioned. This probe was inserted through the pipe wall with the sensing surface flush with the wall. It is particularly sensitive to u'_r fluctuations. Both probes were purchased from Lintronic, and as such were standard units. The sensing element of platinum was 1 mm. in length, 0.2 mm. wide, and had a thickness of 1.5×10^{-5} mm.

A spectrum analyzer was also used to analyze the output signals from the hot film probe for the presence of periodic disturbances. The model used was by Panoramic, and had a sonic analyzer which could measure the input signal in the frequency range of 20 to 22,500 cps, and a subsonic unit which analyzes the input signal in the range of 0.5 to 2,250 cps. Both had adjustments for setting the center

frequency, and for adjusting the frequency span examined. A more extensive discussion of this unit appears in Lee (32).

The probes were inserted into the pipe through a hole drilled into the pipe wall. Since the presence of this hole could conceivably have caused some disturbances during the photographic studies, it was not drilled until these were completed. As this hole was drilled in the pipe while it was installed in the system, it was not exactly centered. This necessitated an accurate determination of the probe position when it was installed, so that the velocity and rms measurements with respect to radial position could be made. The probe was mounted in a holding device and could be moved horizontally. The scale on the device was graduated in hundreths of an inch and had a vernier which could be read to the nearest thousanth of an inch. The vertical position of the probe was determined by optical means using a microscope.

Since this was apparently the first time a hot film probe had been used in a hydrocarbon system, the proper overheat ratio for the hot film had to be determined. Approximate calculations for the heat transfer from a cylinder in turbulent flowing air, water, and trichloroethyline were made, and knowing the proper overheat ratio for air and water, an approximate setting for trichloroethylene was obtained. Thereafter it was a matter of trial and error to obtain the setting which would give a straight line calibra-

tion curve of output voltage versus velocity. Because no extensive measurements with the hot film probe were planned, and satisfactory results could be obtained for the measurements desired without an absolutely straight line calibration curve, no extensive study of the most desirable overheat ratio was made. Indications from the study revealed that a straight line curve could be obtained at higher overheat ratios than those eventually used. These higher ratios were not employed because the system was not equipped with a heat exchanger to control the fluid temperature, and the equilibrium fluid temperature after hours of operation was too great to permit stable operation at the high overheat ratios. The overheat ratio used was 1.16.

The hot film probe is calibrated by causing some known or measured velocity to flow past it and recording the voltage output from the measuring circuit as this velocity is systematically changed. Usually a measuring device such as a pitot tube is used to determine the flow past the probe. In the present study, however, physical circumstances required that an alternate method be found since such a measuring device could not be placed in the test section without major changes in its design. For calibration, the probe was positioned within the test section very near to the pipe center. The velocity of flow past it was changed by changing the average axial flow rate as measured by the orifice meter and rotameter. The local mean axial velocity past the probe was

calculated from the average value by first assuming that a turbulent profile existed in the section. Then by using Brodkey's (1) extension of Pai's (42) equations, the over-all average velocity could be related to the maximum velocity. From these values, and Pai's relation for the turbulent velocity profile, the local mean axial velocity at the probe position for each average velocity could be calculated. These equations have been shown to be quite accurate, Brodkey (1), so the only difficulty is with the assumption of a turbulent profile. If it does not exist, then the calibration curve is in error. Since the calibration measurements are made with the probe at a fixed position, and the velocity profile measurements are made at a fixed Reynolds number by moving the probe, an error in the calibration measurements will be reflected in the velocity profile measurements, and a normal turbulent profile would not be obtained. This then provides an indirect check on the assumption for the calibration method. If the measured profile agrees well with the theoretical profile for turbulent flow, then one can conclude that the calibration was satisfactory since this agreement could not have been attained unless the necessary assumption made during the calibration step was true. If a poor measured profile is obtained, the results are inconclusive, but would indicate that a turbulent profile does not exist in the test section. The procedure is not all that one would desire, but for the limited purposes of the hot

wire measurements in this study, i.e., to determine if the flow in the test section is fully turbulent, it is adequate. The calibration curve appears in Figure 16.

A remarkable result of the use of the hot film probe in trichloroethylene was the excellent stability of operation. The literature contains many references to the difficulties encountered and inaccuracies introduced by the drift of the probe output when it is used in water. In the present study, once the fluid had reached constant temperature, the probe operation was completely stable for periods of hours, and never showed a systematic drift.

Dye injection

For a brief sequence of runs dye was injected into the wall area through the hole in the pipe wall where the hot film probe had been inserted. A glass tube of approximately 2 millimeters I.D. and O.D. approximately that of the hole was inserted into the pipe wall, but did not extend to the inside wall surface. Dye was injected through this tube, into the hole in the pipe wall and then into the wall region. A small centrifugal pump and needle valve were used to control the dye flow rate. With the light source and film sensitivity, Sudan III red dye was found to be most satisfactory.

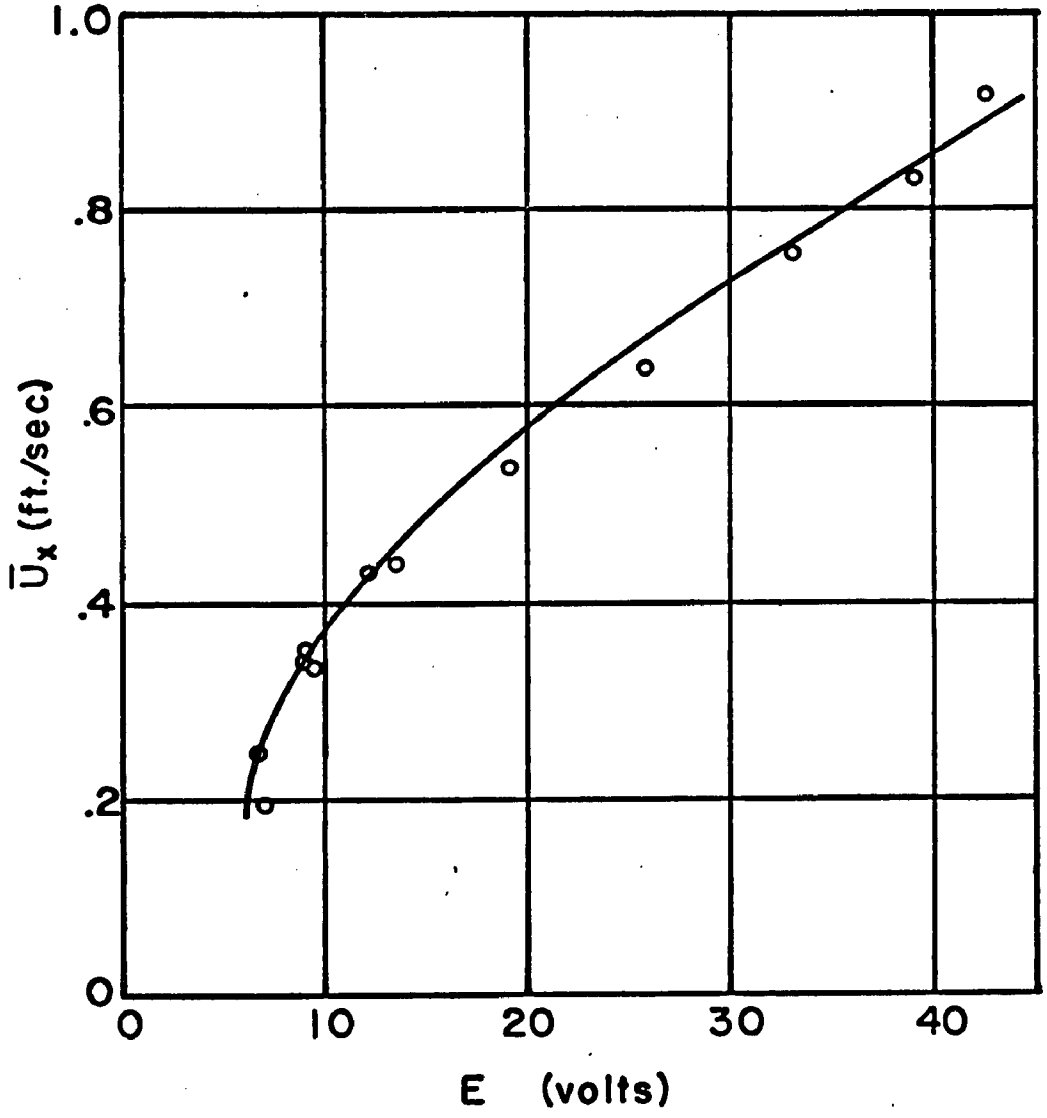

Figure 16. Hot Film Calibration

Discussion of method

The experimental method used in this study has some distinct advantages over other type visualization methods which inject or displace a dye or use birefringent fluid. Even if the latter could show sufficient detail to reveal the fine structure of fluid motions (this ability has yet to be demonstrated), the fact that the fluids are highly non-Newtonian in character introduces a number of uncertainties and unknowns into an already complex problem. For one thing, the mean velocity profile cannot be accurately predicted for such fluids. Dye or particle injection techniques require a mechanism to inject the material into the flow, and in the wall regions the affect of such a mechanism can be a source of concern. The present method, of course, requires no injection since the particles marking the flow are uniformly distributed throughout the fluid. This distribution provides another distinct advantage over dye injection methods. In these latter the tracer fluid is injected at a point or line, and the fluid motions cause the tracer to spread and assume various configurations. From these configurations, information concerning the fluid motion is deduced. The diffusion and spread of the dye is an unsteady state process. While it might satisfactorily delineate the fluid motions in a steady-state flow, for turbulent flow it is less satisfactory. This is especially true in the wall region where the fluid motions exhibit locally a distinct

unsteady state nature beyond that of the quasi-steady state turbulent flow. In this region, the combination of a developing dye field with a developing velocity field compounds the difficulty of interpretation. Another factor is the uneven distribution of dye after development has proceeded for a time. This leaves high dye concentrations in areas of low velocity and depletes the dye in the area of high velocity. Thus the motions of the fluid in the high velocity regions are not marked. With the uniformly distributed particles of the present study both of these disadvantages are removed. In addition the particles permit a more detailed study of the fine structure because they mark very small elements of fluid and not large regions as dye does. Finally, because the particles are not segregated or dissipated with time, they permit the study of a developing motion over a longer period of time than do injection methods.

For unsteady state flow, tracers injected at a point produce streak lines which define neither streamlines nor the paths of individual fluid elements. The particles, being distributed and marking local fluid elements, define these paths and thus are pathlines. This is a fundamental difference, and although for simple unsteady flows streaklines, streamlines, and pathlines may be calculated from one another and a knowledge of the velocity field, for unsteady turbulent motion this is impossible.

Methods of film analysis

All analyses of the fluid motions were made from the motion picture films because image quality was lost during printing. The motion pictures to be analyzed were selected solely on the basis of image quality without regard to content. This preliminary screening was necessary because it was felt that if films of widely different quality were used, there would be a strong possibility of attributing certain observations to flow behavior when in actuality they were due only to the failure or ability to see something because of a poor or good image. Only films of good, comparable quality were used in the detailed analyses. For analysis, the films were projected by a motion analysis projector onto a screen ruled into a rectangular grid. The speed and direction of projection could be controlled. The projected image magnified the film image by 93X so that the films taken at 4.3X showed the wall region magnified 400X on the screen. The increase in magnification by the projector made the observations and measurements easier by revealing all that was on the film on an expanded scale. It could not, of course, do more than this, so in a real sense the important magnification was the one at which the films were taken. This one sets the limits on content. The rulings on the screen were drawn to the scale of the magnified image so that each line of the grid corresponded to a given dimension of the wall region. To be certain that the proper

magnification and alignment were used for all analyses, the grid was marked with reference lines which corresponded to marks on a calibration film. This film contained an image of a grid where the spacing between lines was accurately measured with a microscope equipped with a micrometer eyepiece. By aligning the screen calibration marks with the corresponding marks on the projected image of the calibration film, proper magnification of the projected image was attained.

The projector was adapted to count electrically the number of frames of film projected. This was done by installing a miniature microswitch under the film advance sprocket wheel and connecting it through a switch to an electric impulse counter. As the sprocket wheel turned, it opened and closed the microswitch one time for each frame. The switch in the counter circuit was normally open, so the counter did not begin counting until it was closed, and stopped when it was released. This ability to count frames was necessary for the determination of real time as opposed to projection time which was much slower. The counter was periodically calibrated by using a strobotac to measure the sprocket wheel revolutions.

As was mentioned in the camera description, timing marks, which appeared as distinct dark streaks, were automatically imprinted on the film margin at 120 marks/second. By measuring the number of frames of film covered by the tim-

ing mark one could calculate the filming speed in frames/second. To facilitate this calculation, the length of the mark was measured, and knowing that a frame measured 7.6 mm from centerline to centerline of adjacent sprocket holes, the framing speed was calculated as follows

$$\text{frames/second} = (\frac{S}{7.6})/.00833$$

Then by counting the number of frames during which a particular event occurred, one could calculate the real time of occurrence. This proved to be an excellent means of timing events of very short duration because the high-speed photography caused even these events to appear over a large number of frames, very seldom less than 20 and usually more, and the low-speed projection permitted the event to be seen and the frames accurately counted. All of the timed events described in later sections were measured by this method.

Among the most important measurements made are those of particle velocities and trajectories. In each of the camera views, but in particular the wall view, the motions of particles or fluid elements across the projection grid was quite readily determined. In many cases the particles exhibited a straight or only slightly curved trajectory, so that by recording the grid coordinates at the beginning and end of a particular movement, and counting the frames elapsed, the velocity of the particle as well as the trajectory could be calculated. This procedure neglects the three dimensional movement of the particle, i.e., movement along the line of

sight, and so underestimates the velocity in most cases. Since some estimate of the extent of this three dimensional movement is available from the two views, the potential error can be estimated. This is done in Appendix II where the method of calculation is also presented.

The observation and measurement of trajectory and u_r or u_θ fluctuations is greatly enhanced by the fact that the carriage moves with the flow. This movement reduces the relative motion between the camera and the local mean axial velocity, and the apparent axial velocity is often of the same magnitude as the u_r or u_θ velocity. On the films these motions appear as deviations from axial flow. Since the camera moves with the flow, these deviating particles remain in view for a longer period of time, and therefore travel a greater observable distance. Also, since the trajectory or angle of deviation is calculated from the relation $\tan \alpha = B/A$, where α = apparent deviation angle, $B = u_r$ or u_θ, and $A = U_x$, any apparent decrease in U_x increases the angle α and makes the deviations more visible and more accurately measured.

The motion of the camera is matched to the local mean axial velocities at selected y^+ positions. At these positions the particle motions have approximately zero relative velocities, and a reversal of apparent direction of U_x velocity occurs as one moves from the wall toward this y^+ position and then beyond it. During any run, the carriage velocity

is constant, so if the position of zero relative velocity changes, it must mean that the U_x velocity has changed. This permits some observation of large fluctuations in the x component, but generally these fluctuations are not as readily observed or measured as u_r or u_θ. Other particular methods of analysis are discussed during the presentation of experimental results since they are more meaningful in that context.

In addition to the various measurements, the different films were carefully and systematically analyzed for qualitative information concerning the fluid motions. The position of occurrence and dimensions of various occurrences could be readily noted because of the scaled grid on which they were projected. From the observations of the movement of particles separated by various distances, some estimate as to the size of the disturbances could be obtained. If a group of particles covering a given region of the grid moved together as a deviating element, it could safely be assumed that they were all part of a single disturbed eddy. Since the scale of these disturbances in the wall region was less than the field of view, this method was quite effective. Often more than one group of particles could be observed within the field, each group moving differently from the other, but at the same time.

In order to determine the position of occurrence of any event from the projected image, it was necessary to

align the wall of the pipe as it appeared in the image with the line corresponding to the wall on the grid. Once this was done all positions relative to the wall were fixed. Due to the imperfect matching of the index of refraction, a thin dark line appears in the motion pictures at the wall position. This was described earlier and the verification that it was the interior wall was discussed. Earlier, some calculations pertaining to the extent of the effect of the refraction of the light were presented and discussed. At that time the estimated area affected had a width of approximately 0.0009 inches, although the possibility of a somewhat less affected area of greater width was also discussed. A check was made of these estimates by inserting the scale into the test section and taking still photographs of it. These photographs showed that the darkened area existed, but the presence of the metal scale and supports increased the width and particularly the density of the dark line. The still photographs showed a very dense, sharply defined line while the motion pictures without the scale showed a somewhat diffuse dark area within which particles were still visible. The line became darker as the wall was approached. This is in agreement with the theoretical calculations. Other still photographs were taken under lighting conditions where the reflections from the metal scale were almost eliminated, and these showed no encroachment of the dark region into the sublayer. The still photographs mentioned earlier,

therefore, represent an extreme case and are useful in setting the extreme limits of the effect of the refraction. It must be emphasized that in the motion pictures of the wall area the refraction effect does not approach these limits in size or density.

Careful examination of the motion pictures showed that particle motions were visible within the darkened region. This region was always very small compared to the frame width, and was very dark only within an extremely narrow line at the wall-side of the region. During the analysis, this dark line was aligned with the line on the grid corresponding to the wall. The lack of absolute precision in locating the wall causes some uncertainty in the location, with respect to the wall, of particular events, but this uncertainty was definitely less than 0.002 inches which gives a maximum uncertainty less than 2 y^+ units at 50,000 N_{Re}, and considerably less than that at lower Reynolds numbers.

The effect of refraction was not present in the top view, and it afforded an excellent opportunity to examine the sublayer region. The observations from this view generally confirmed those made in the wall view.

EXPERIMENTAL

Hot film measurements

Chronologically, the measurements with the hot film probe were made after the photographic study was completed. This was necessary since the use of the probe required that a hole be drilled into the pipe wall at the test section, and it was essential to avoid the possible introduction of disturbances due to the presence of the hole during the photographic study.

In the description of the equipment it was noted that an entry length was designed to permit the establishment of fully developed turbulent or laminar flow within the test section. Since the entry length actually used exceeded the calculated value, the assumption that the flow was fully developed seemed valid. Nevertheless when the unsteady nature of the wall region was discovered, it was deemed of value to measure the profile to confirm the assumption.

No extreme degrees of accuracy were attempted because extensive modification of the equipment would have been required to attain them. These refinements are primarily of importance when extensive measurements of turbulent characteristics are to be made, and the intent in this case was to measure a mean velocity profile.

The successful application of the hot film equipment in a liquid hydrocarbon system, and its excellent stability has been discussed in the equipment section. The importance of such stable operation for turbulence measurements may be estimated by reading any of the articles where such measurements in liquid systems have been attempted.

Although the calibration curve obtained for the overheat ratio of 1.16 was not a straight line, it was statisfactory for the desired measurements. The calibration curve appears in Figure 16. For accurate velocity fluctuation or Reynolds stress measurements, a straight line calibration curve is essential. No extensive examination of the conditions required to attain a straight line calibration curve was attempted in this system, but in one trial using an overheat ratio of 1.24 a much straighter line was obtained. Unfortunately as the fluid temperature increased the probe began to show very erratic operation. This was not the usual drift in a particular direction common to unstable operation in liquid systems, but a sudden jump of the output to a particular value at which it remained for a time, and then a jump in the opposite direction to a new value. Tapping the probe usually returned the output to the original high value. While acting in this fashion, the probe was examined under a microscope and tiny bubbles could be seen shedding from its surface. The fluid temperature at this

time was 41°C and since it has a boiling point of 87°C it was concluded that the erratic behavior was due to incipient boiling at the probe. The lower overheat ratio never showed this behavior. Since the system proved to be so stable, future experiments are planned using it to measure various properties of turbulent flow, i.e., spectra, Reynolds stresses . . . for liquid systems. For these studies, a heat exchanger to control the fluid temperature is planned.

The velocity profile across the pipe was measured for N_{Re} = 21,000. This profile is presented in Figure 17. Also presented in this figure is the profile predicted by Pai's (42) equation as given by Brodkey (1).

$$\overline{U}_x = \overline{U}_{x_{max.}} \left[1+a_1\left(\frac{r}{R}\right)^2 + a_2\left(\frac{r}{R}\right)^{2M}\right]$$

$$\overline{U}_{x_{max.}} = \overline{U}_{avg.}/\left(1+ \frac{a_1}{2} + \frac{a_2}{M+1}\right)$$

$$a_1 = \frac{S-M}{M-1} \qquad a_2 = \frac{1-S}{M-1}$$

with S = 13.5 and M = 20. The measured profile is unmistakably that of fully turbulent flow and agrees reasonably well with the predicted profile. The differences, especially in the wall area, most likely arise from the failure to correct for the presence of the wall and possible positioning errors. The film length of the probe is 0.039 inches, and this is equal to nearly one-half the sublayer thickness under the flow conditions, so this too contributes to the difference.

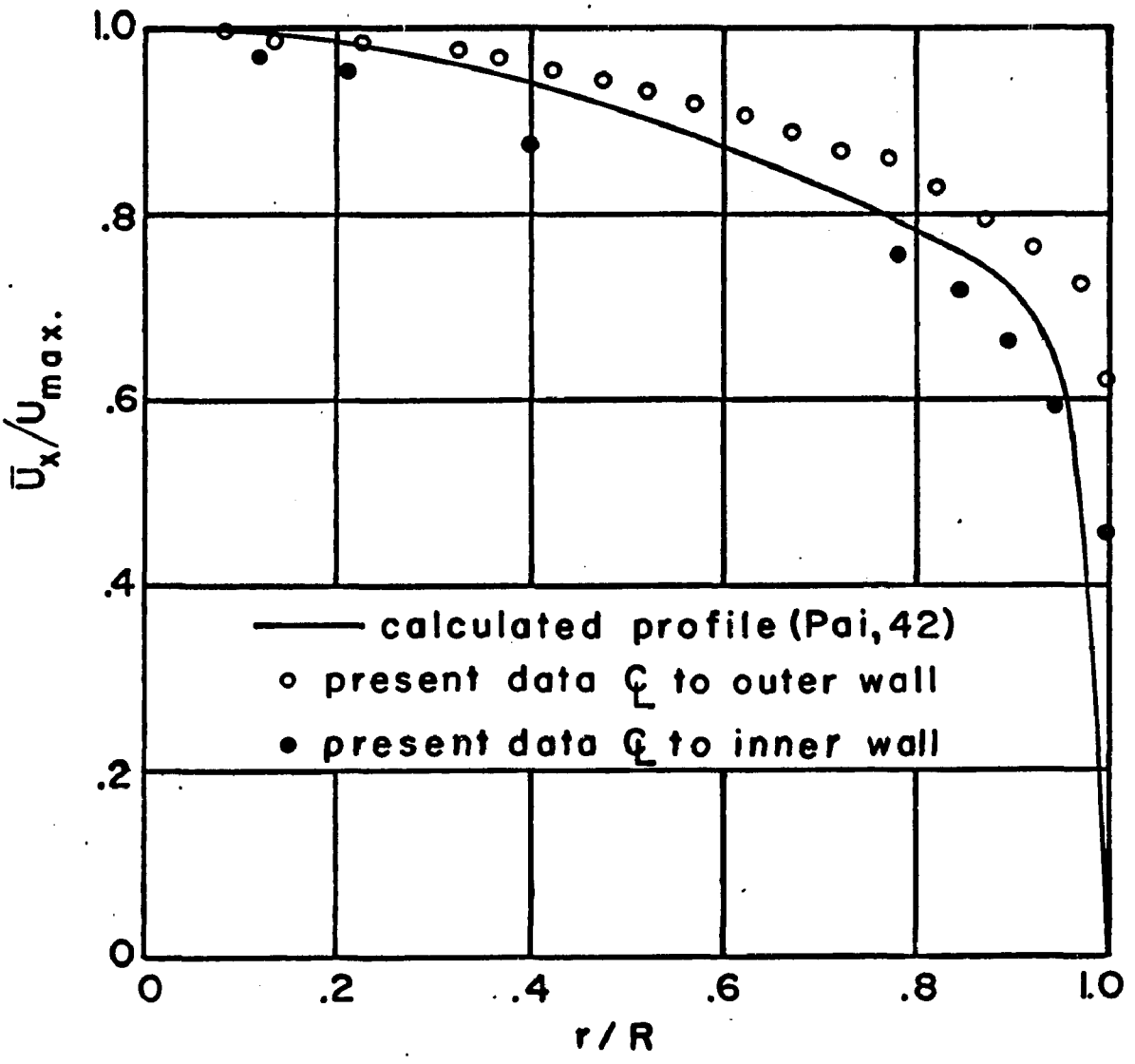

Figure 17. Mean Velocity Profile

Positioning errors can easily arise because, as was explained in the equipment section, a combination of optical and direct measurements were required to determine the location of the probe.

The data points for positions on either side of the proposed pipe centerline show a uniformity in that each set falls almost exclusively on opposite sides of the predicted curve. If one supposes that the original measurement of probe placement was slightly in error, a correction for this error would shift each set of points towards one another and into congruence with the predicted curve. Even without any attempt at correction, the measured profile satisfies the original intent. It establishes the fact that the flow is fully turbulent in the test section.

Simultaneously with the profile measurements data were taken for determining the root mean square (rms) value of the u_x fluctuation. In this calculation, however, the lack of a straight line calibration curve of the output voltage E versus velocity presented a problem. The relation for determining u_x' from the reading I of the rms meter is

$$u_x' = A \beta_1 I$$

where A is the slope of the calibration curve and β_1 is a calibration constant for the rms meter. With a curved line, of course, the slope is continually changing. However, if one is willing to accept certain inaccuracies the distribution

of u_x' with position can still be obtained. The rms metering circuit measures fluctuations about the mean value E which is known in this case for all corresponding I values. From this knowledge, the position on the calibration curve is fixed and the slope A at that point may be determined graphically. This procedure can be repeated for all I values. Of course, the graphical determination of a slope is subject to large possible errors, but fortunately in this case the slope is changing only gradually in the area of interest. If one does not place too great an emphasis on the absolute magnitudes obtained, the calculation is certainly worth doing. The resulting curve appears in Figure 18 along with the similar measurements by Laufer (31), Lee (32), and Cohen (3). Each of these latter was for pipe flow at 41,000 N_{Re}. No data are available for NRe = 20,000, but Laufer also measured the distribution at 410,000 N_{Re} and the results indicate only a small effect on the curves due to Reynolds number. Laufer's data are for air while Lee's and Cohen's are for water, and Lee's is a single run. For the measurements in water, severe problems with probe stability were experienced and neither Lee nor Cohen placed a great deal of confidence in the measurements as a result of this. The agreement between the measured curve and Laufer's data is reasonable. The curves certainly show the same general shape and increase in u_x'/u^* value as the wall is approached. The absolute values depart from Laufer's as the wall is approached, but the order

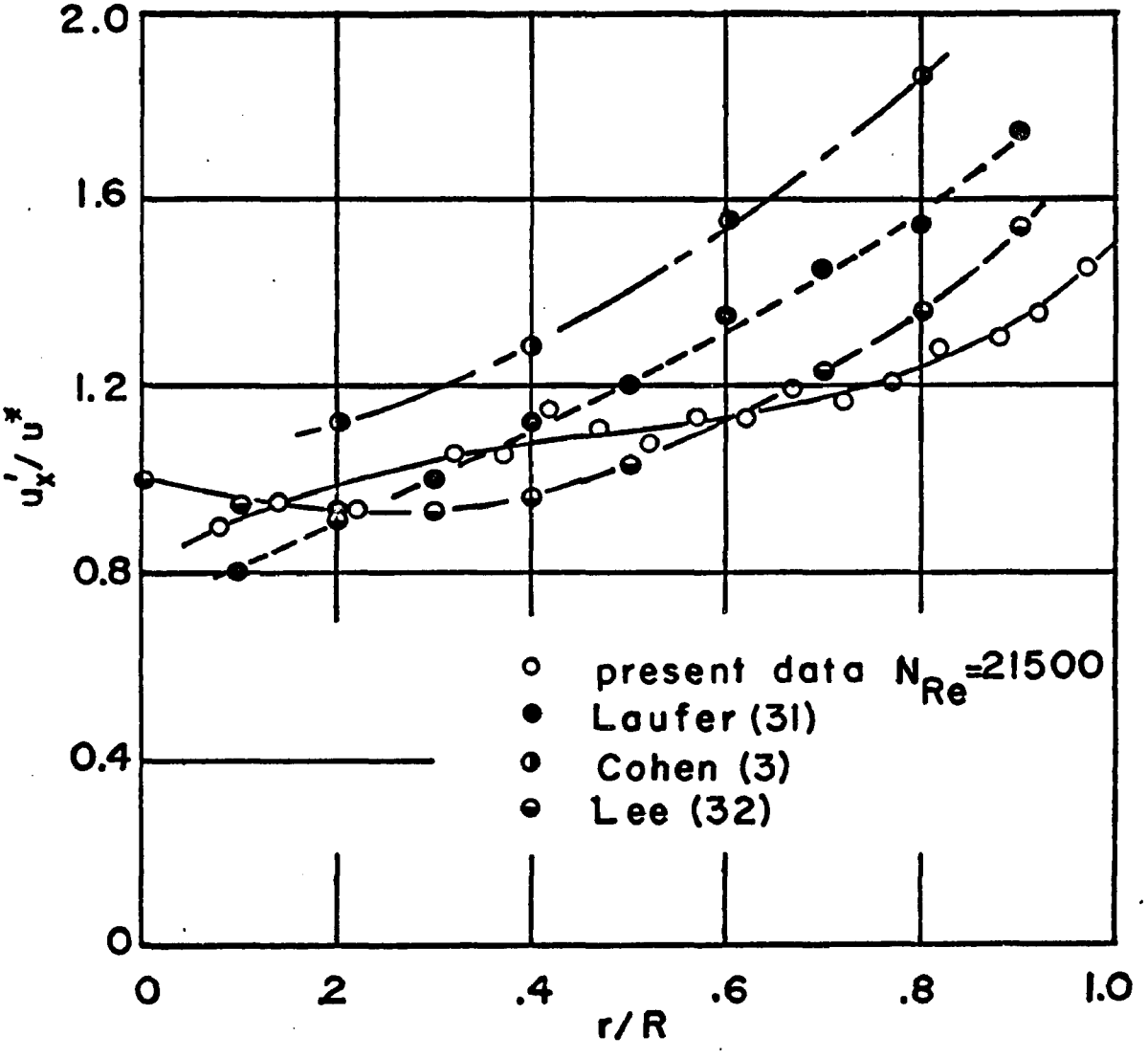

Figure 18. u_x' Distribution

of magnitude is the same. Because of the relative size of the probe and sublayer thickness, no attempt could be made to measure the fluctuations very near the wall as Laufer did in air. The comparison of the measurements by Laufer in air with the present measurements in a liquid is acceptable provided the Reynolds number similarity is true. There is no reason for not believing that it is so, and with stable probe operation in liquids the validity can be rigorously tested.

With the same wedge probe as was used above, in position at approximately the pipe centerline, the output signal was examined on a spectrum analyzer for evidence of periodicity. Intially a wide frequency span was examined, and when it showed no regularity, narrow frequency spans were examined. In particular the lower bands of the order of the frequency of occurrence of wall region ejection were examined. Also, multiples of the pulsations which might originate within the centrifugal pump were scanned. In all cases no regular periodicity was observed. The output appeared to be completely random.

A second probe, described earlier as a surface probe, was positioned with the film flush with the inner wall of the pipe. This probe is particularly sensitive to fluctuations normal to the wall, and it was used to detect any regular periodicity originating from mechanical sources which might intrude upon the wall area. None were detected. The probe

was also used in an attempt to observe the effects of the ejection process but this was unsuccessful. This is not surprising since the ejection process is random in nature and any attempt to discern such events against a basically random background is not likely to be successful. In addition, later analysis of the motion pictures showed that the ejection process at N_{Re} = 20,000 did not penetrate to the wall very often so even the expected high intensity pulse could not be observed very often. In addition to visual observations of the cathode ray tube screen of the spectrum analyzer, time exposure photographs were taken of the screen with a sixteen second sweep period and a full scale width of 0-20 cps. This is approximately the frequency of ejections. Nothing which could be related to the ejection events was observed.

In summary, the hot film examination produced three valuable results. It established the presence of a fully developed turbulent flow in the test section, it produced an u_x' distribution which agreed with other published data, and it demonstrated that the fluid did not possess any regular periodicity such as might arise from mechanical vibrations.

General description of wall area characteristics

In the next section a detailed description of the fluid motions in the wall region will be presented. These descriptions are the result of extensive examinations of

numerous motion pictures taken of different flow conditions and from different views. Since the description of the motions is quite complex, each step of the process is described in detail separately and in the order in which it occurred. Additionally, the observations from each different camera view are described separately, although they are, of course, descriptions of the same events seen from a different position. This enables the reader to be oriented to the particular advantages and disadvantages of the different views, and thereby permits a more meaningful and critical interpretation of the descriptions. While this format results in a clearer, more detailed description of the individual occurrences, it necessarily presents a somewhat disjointed picture of the entire process. This section therefore is designed to give to the reader a very brief, unencumbered, over-all view into which the more detailed descriptions may be placed in their proper perspective.

All that will be described here and elsewhere is much clearer when seen in the motion pictures, and therefore a motion picture made up of selections from the original films is available for loan.

The single most important feature of the wall region ($0 \leq y^+ \leq 35$) in fully developed turbulent flow is the fact that it is periodically disturbed by the ejection of discrete fluid elements from the wall area outward toward the center of the pipe. These ejections are very local events,

and occur randomly in both space and time. The ejection of these low $\overline{U}_x$ velocity elements into regions of much greater $\overline{U}_x$ velocity causes turbulence to be generated, and this in turn disturbs the entire wall region, even to the wall itself. The existence of these events means that the fully developed turbulent flow in the wall region is not in a quasi steady-state condition but in fact exhibits a locally unsteady nature which taken as an average produces the steady-state nature of turbulent flow.

The actual ejection of fluid is only a part of a sequence of events which to one degree or another appear with the ejection in a definite order. Of course there are variations of the sequence and all of the steps do not appear all of the time nor in the exact fashion described, but on the average it proceeds as follows.

First the fluid in a relatively small region near the wall experiences a deceleration of the local mean axial velocity. This generally occurs in the y^+ span of $0 \leq y^+ \leq 35$ and as such could be interpreted as a thickening of the sublayer. This is followed by the entry into the region from upstream of a large mass of fluid which possesses the steady-state local mean axial velocity. This fluid tends to accelerate the retarded fluid in the region, but because it does not extend all the way to the wall it only succeeds in creating a region of high shear at the boundary between it and the retarded fluid. This is quickly followed by the

ejecting of a low $\overline{U}_x$ velocity fluid element outward from the wall into the high velocity region. The resulting interaction of these fluid streams causes a great amount of chaotic motion which spreads both outward and wallward. This is then followed by a mass of fluid entering from upstream with a greater $\overline{U}_x$ velocity than the interacting fluid. This mass sweeps the field of the fluid and re-establishes the local mean axial velocity profile.

The basic character of the process is not a function of Reynolds number, but the frequency of occurrence and intensity is.

The character of the disturbed motions changes as the distance from the wall is increased. By a $y^+ \doteq 70$ position, the characteristics of the wall region are essentially lost and the character of the outer region has asserted itself. The wall region motions are of small scale, local in nature, and exhibit abrupt, intense movements. The outer region has a larger scale with less abrupt movements and less intensity of fluctuating motions. No ejections originate anywhere but within the wall region.

The ejection process as a function of Reynolds number

The motion pictures of the wall area for Reynolds numbers of 2300 to 50,000 were examined for evidence of the ejection process and to determine the effect of Reynolds number on the character and frequency of its occurrence. In

all the photographs the wall view was used at a magnification of 2X or 4.3X.

For N_{Re} = 2300 the velocity profile exhibited in the motion pictures showed only a very gradual change in local mean axial velocity from the wall out to the edge of the field of view, a distance of $y^+ \doteq 22$. Since the turbulent profile would exhibit a much steeper gradient than this, the flow was assumed to be laminar. Also, there is a complete absence of any departures from the smooth flow parallel to the wall.

At N_{Re} = 5360 the turbulent velocity profile is quite evident. Local velocities were checked by the timing method described in an earlier section, and were found to agree well with velocities predicted by Pai's relations for the velocity profile. This flow displays the first evidence of the unsteady nature of the wall region. It appears as an occasional deceleration-acceleration sequence of the local mean axial velocity. No significant departures from the axial flow were observed, but generally the flow appeared more agitated than previously.

Upon increasing the Reynolds number to 11,280 the deceleration-acceleration sequence of the local mean axial velocity was observed to occur with increased frequency, about once per second on the average, and was more clearly defined than in earlier cases. The deceleration process is the gradual replacement, within a local area near the wall, of

fluid, which possesses the local mean axial velocity of fully turbulent flow, by fluid of a reduced axial velocity. This latter enters with the mean flow from upstream, and usually does not affect the fluid below $y^+ \doteq 3$. This retarded state persists for a brief period and then is partially removed by the reappearance from upstream of fluid having the normal local mean axial velocity. The majority of the particles are moving axially, but some few have significant departures from the axial in both directions. These constitute the first notable departures from purely axial flow. At this Reynolds number the first evidence of an effect called "two layer velocity" occurred. This is the observation of two masses of fluid at identical radial positions having distinctly different axial velocities. With the optical system used, these masses could be separated by a maximum distance of 0.027 inches along the line of sight. This phenomenon will be discussed in greater detail in a later section.

When the films taken at N_{Re} = 21,000 were studied, the full nature of the wall region was revealed. The entire sequence of events surrounding the ejection process were repeated a number of times in excellent detail. Here for the first time was unmistakable evidence of the ejection of fluid from the wall region outward, and the subsequent interaction with the mean flow. The majority of ejected elements

originated in the region $5 \leq y^+ \leq 15$, but some originated as near the wall as $y^+ \doteq 2.5$. The events occurred at random intervals, and between events the fluid in the region was still in an agitated state due primarily to the effects of the preceding event. During the early stages of the event process and the ejection itself, the "two layer velocity" effect was observed.

Upon increasing the Reynolds number in steps to 50,000, the analysis showed that the changes which occurred were not in the basic character of the ejection process, but in the intensity and frequency of occurrence of these events. With each increase in Reynolds number there was an increase in the number and intensity of ejection events, so that by $N_{Re} = 52,000$ the events occurred so often and at such close intervals that even in the periods between events the fluid was highly agitated, and it was extremely difficult to determine where one event ended and the next began. Also, there was an increase in the intensity of the created turbulence, and therefore the effect was more clearly felt in the regions very near the wall.

Initially, in order to assign a quantitative value to the relationship between frequency of occurrence and Reynolds number, an attempt was made to count the individual events which occurred during a given time period. This method was satisfactory for Reynolds numbers of 20,000 or lower, but above $N_{Re} = 30,000$ the difficulty of separating individual

events from each other and the intervening fluctuations became so great that confidence in the counts was greatly reduced. It was possible to obtain widely different counts for the same motion pictures depending upon the criteria employed for separating events. Since the difficulty increased with increasing Reynolds number, there was no way to compensate for the possible error. In all cases it was possible to duplicate a count within reasonable limits if the same film sequence was viewed a number of times in succession. If one returned to the film after an interval of a week, the original count could not immediately be duplicated, but after a number of viewings one could duplicate it within the same limits as the first trials. For example, one case at N_{Re} = 40,000 the first count gave 18 events and the second 21. In order to prevent an error due to a change in criteria over a period of time, all the films used in the event count analysis were viewed in sequence during a single time period with two counts made in succession for each film. This final counting was done, however, only after the films had been carefully examined a larger number of times to establish a proper criteria. The results appear in Figure 19. Each point on the graph represents the results of a single film. The increase in the number of occurrences with Reynolds number is unmistakable and consistent. The ratio of the number occurring at N_{Re} = 50,000 to those at N_{Re} = 20,000 is

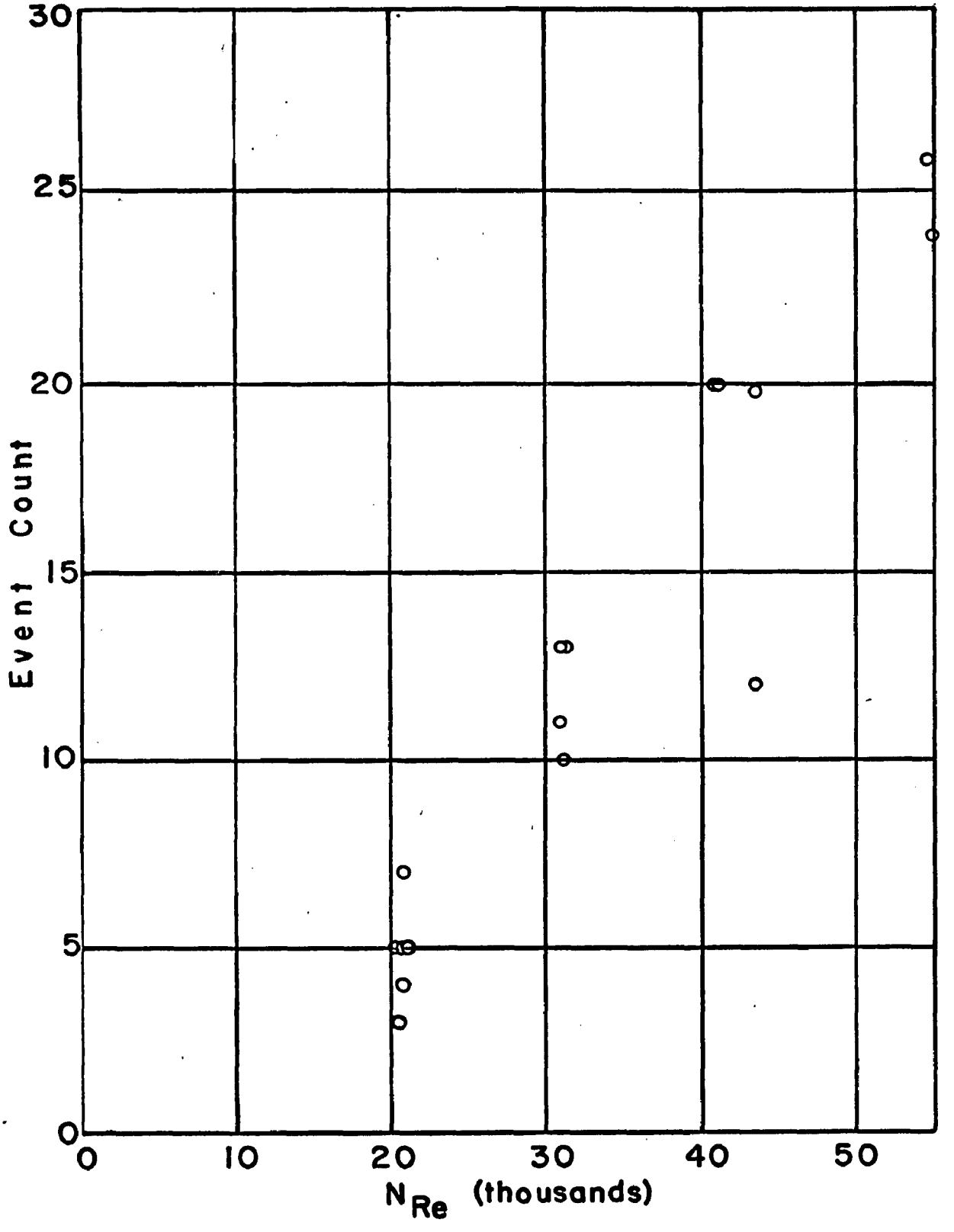

Figure 19. Event Frequency

approximately 5/1. All counts are for approximately a six second interval of real time.

Because of the difficulties encountered in the preceding method of analysis, an alternate method of obtaining essentially the same information was devised. An electric counter was used to count the number of motion picture frames in which the fluid in the wall region was significantly disturbed. From this count and the knowledge of the actual number of frames per second at which the film was exposed, one could determine the percentage of the total photographed interval during which the wall region was significantly disturbed. In this method it is not necessary to separate individual events if they overlap or if the intervening disturbances are very intense. If they exceed a minimum intensity they are included. It is necessary, however, to establish a minimum for what constitutes a significant disturbance of the wall region. There were nearly always some departures from purely axial flow visible in the wall region. To include each small fluctuation would defeat the purpose of the analysis since the intent is to relate the measurement to the ejection event and not its after effects. Extensive examination of the films permitted a lower limit to be established quite readily since the intensities of the motion directly connected to the ejection event are quite pronounced. To improve on the consistency of the measurements, the films were examined in succession over a

single continuous period with two timings given to each film. The duplication of results by the method was much greater than the preceding. For example, in one case at N_{Re} = 40,000 the two timings gave values of 55.2% and 51.7%. Good agreement between measurements made after an interval of weeks could be obtained. Figure 20 shows the results of this analysis. Each point is the average of two measurements for a particular film. The films used were the same ones examined in the number count. As before, the increase with Reynolds number is unmistakable and consistent. The wall region is significantly disturbed approximately 16% of the time at N_{Re} = 20,000 and nearly 68% of the time at N_{Re} = 50,000. This is a ratio of 4.3/1. Both the ratio and the general shape of the curves show that the two methods are in agreement. The unusually low values at N_{Re} = 43,000 can probably be attributed to the inferior quality of the photographic image on the film used for those analyses. This poorer quality could easily have obscured some of the significant motion.

In summary, the analysis shows that the nature of the events in the wall region is independent of Reynolds number, but shows a strong dependency on it with regard to frequency of occurrence and intensity.

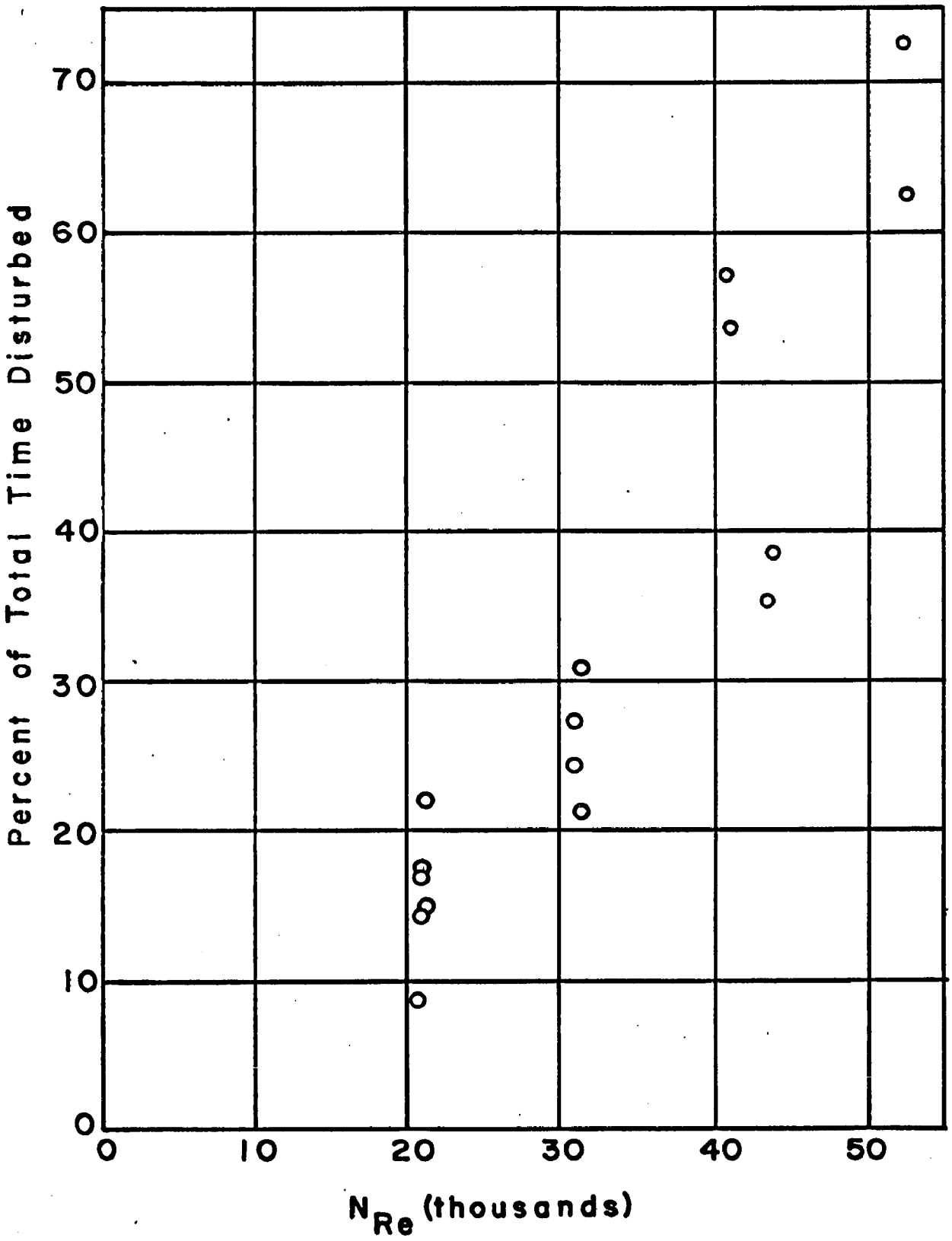

Figure 20. Disturbed Percentage

Detailed description of events--
wall view

In the descriptions of this section, the camera position was that described as the wall view in the experimental procedures section. It would be of value to the reader to refer to this description to properly orient himself before proceeding.

In the preceding sections various aspects of fluid motion in the wall region were briefly discussed, and a condensed description of the ejection process was presented. In this section the details of this process will be examined, and each step of the event will be discussed in the order of its occurrence. It must be recalled that the ejection process is basically random in its nature, and therefore the following events do not always occur exactly as described. At higher Reynolds numbers the frequency of occurrence and the high state of agitation often act to obscure or eliminate certain of the steps. The ejection of fluid elements is, however, the primary feature of the wall region, and it is always recognizable. What follows then is a composite picture derived from a detailed event analysis of numerous motion pictures taken of different flow conditions. The notes of the detailed analysis of each motion picture are too voluminous to present here, but they are preserved and could be examined to reveal the individual variances as well as the general consistency of the process.

Deceleration. The first step of the process usually involved a deceleration of the local mean axial velocity of the fluid. The area of fluid affected was greater than 0.095 inches in length (this is maximum length of field), but the distance from the wall affected was of the order of the frame width of 0.069 inches. Evidence from other sources indicates that the dimension affected along the line of sight was of the order of 0.027 inches. Thus in the r and θ dimensions the event was quite small and local in nature. The deceleration effect was really the gradual replacement of fluid possessing the normal local mean velocity with fluid from upstream that had a local mean axial velocity of smaller magnitude. The actual extent of the deceleration varied greatly from a barely perceptible difference to cases where the entire field above a particular y^+ value was moving in essentially plug flow (i.e., little or no velocity gradient above $y^+ \doteq 10$ to edge of frame) at a reduced velocity. The disappearance of a velocity gradient from the region is a striking effect since in normal turbulent flow the region possesses a very steep gradient. The velocities of individual particles which were representative of the particular region of flow were measured for the deceleration period and the period preceding it. These velocities, measured during a number of different occurrences, are presented in Table 2 along with the local mean axial velocities calculated using

TABLE 2

DECLERATION VELOCITY

Run No.	Before y^+	Decel-eration U_x	Calcu-lated U_x	During y^+	Decel-eration U_x	Calcu-lated U_x
164	4	.11	.095	5	.11	.122
	5.8	.11	.135	8.7	.11	.192
				10	.11	.213
165	6.4	.113	.146	8.7	.113	.192
				6.4-30*	.113	.146-.38
168	4.6	.182	.11	11.5	.82	.235
	6.4	.182	.146	8.7	.182	.192
225	10.6	.332	.338	16.4	.332	.29
	9.0	.332	.318	12.3*	.332	.379
				12.3	.332	.379
224	7.4	.332	.278	18.5	.432	.46
				7.4	.117	.278
				9.0	.262	.318
				30	.45	.55
				12.3*	.332	.379
221				20.5*	.575	.62
				27.5	.658	.697
				18*	.605	.586
223	9.5	.46	.42	16-21	.46	.56-.628
155	14.5	.353	.27	16	.167	.285
	7	.193	.16	8	.125	.18
	11.5	.365	.235	8.7	.09	.192
	20	.331	.32			
	2.9	.09	.07			

*Denotes absence of usual velocity gradient.

TABLE 2--continued

Before Deceleration		During Deceleration	
Δ	% $100(\frac{\Delta}{Calc})$	Δ	% $100(\frac{\Delta}{Calc})$
.005	+58	-.012	-9.8
-.025	-18.5	-.082	-43
-.033	-22.6	-.103	-48.4
.072	+65	-.059	-31
.036	+24.7	-.033	-22.6
-.006	- 1.8	-.267	-70
.024	+ 7.5	-.053	-22.5
.084	+30	-.010	-5
.039	+9.2	+.04	+13.8
.08	+3	-.047	-12
.033	+20.6	-.03	-6.5
.130	+55.3	-.101	-36.3
.011	+3.4	-.056	-17.6
.02	+28.5	-.11	-19.6
		-.047	-12.4
		-.04	-6.5
		-.03	-4
		+.02	+3.4
		-.10	-17.9
		-.17	-27
		-.118	-41.4
		-.055	-29.4
		-.102	-53

$\Delta = U_x$ measured - U_x calculated.

Pai's equation. These latter are, of course, mean velocities while the measured velocities are instantaneous and include the turbulent axial component. One might be reluctant, therefore, to compare any of the measured velocities with each other or the calculated to obtain evidence of deceleration, because one does not know just what the effect of the turbulent component is for any single particle. The situation, however, is not that hopeless because it must be recalled that while these measurements are for individual particles, they are representative of an entire mass of particles all of which exhibit the same general velocity. Therefore, while no single absolute velocity should be considered too strongly, the properties of the group as a whole can be significant when compared to the calculated values or to the other measured values taken as a whole. Also, of course, the presence of the plug-like flow cannot be explained as a result of a turbulent fluctuation or an error in measurement, but definitely shows that the normal turbulent profile is distorted by reduced velocities. The motion pictures make this abundantly clear since they provide the continuity of motion which permits comparisons of the adjacent periods of flow. Referring to Table 2, if the measured velocities of the fluid which preceded the deceleration are compared with the calculated local mean velocities it is found that 71% of the measured velocities were <u>greater</u> to some degree than the calculated. Conversely, nearly 91%

of the measured velocities of the deceleration period were slower than the calculated local velocities. Since the same measuring procedure was used in both cases, the same errors in the measurement are likely to occur. Yet for one period the large majority of velocities are greater than the calculated and for the next period the overwhelming majority of the measured velocities are smaller than the calculated. A change of such magnitude cannot be attributed to experimental error. The departures in each group from the calculated are not surprising since they are instantaneous velocities and would be expected to differ from the average. The errors in the measurement of the velocities usually act to produce values which are too low (see Appendix 2). The measurable part of the error is only of the order of 3% or less of the total velocity, and while this is a factor in considering the absolute values of the velocity it cannot be used to explain the consistent manner in which the velocity measurements of the observed decelerated fluid fall below those of the fluid velocities succeeding it. The totality of evidence supports the observation that the deceleration period is a decrease in the mean axial velocity within a rather small area of the pipe wall. The local mean axial velocities, for the y^+ positions at which the retarded flow velocities were measured, were calculated for a laminar profile distribution. It was found that the magnitude of the retarded flow velocity was much greater than that which would

have existed for a laminar profile. The particular effect is usually of rather short duration relative to the ejection step.

Acceleration. This step in the sequence of events closely followed the deceleration step. It demonstrated the greatest variation in character, but since these variants occurred at this particular stage of the development, they are considered under this section. These variations did not correlate with any flow parameters, but seemed to occur quite randomly even to the extent that two successive events occurring in the same experimental run could differ markedly at this step. This naturally causes some difficulty in describing its nature, but since it generally appeared in two forms these will be described.

Most frequently a large mass of fluid entered the retarded field from an upstream position with an axial velocity greater than that of the fluid within the field. The direction of flow was generally parallel to the wall or at a small angle directed inwards towards it. Usually it entered the field above a $y^+ = 15$ position and then proceeded across the field. This step was always followed very quickly by the ejection step. Sometimes the ejection would occur just as the fluid entered the field, while at other times it occurred after the acceleration process was begun, but always before the entire field was completely accelerated.

When the fluid had a slight wallward trajectory it displaced the field fluid wallward as well as axially. The instantaneous velocities of representative particles of the entering stream were measured for various runs, and the results appear in Table 3. The general agreement of these velocities with those calculated for the local mean velocity indicate that this stream of fluid may well be the normal steady-state turbulent velocity re-establishing itself. The area involved in these movements was at least the size of the field of view (.095" x .065") and indications were that it was considerably larger, especially in the axial direction.

The entry of this stream into the retarded field often resulted in an immediate interaction between it and the particles in the field. It tended to sweep all before it and accelerate it downstream out of the field. On other occasions it entered the field but seemed to be on a slightly different rx plane than the field particles because it did not immediately affect them. In these cases a "two layer velocity" was evident where the higher axial velocity stream would move past lower velocity field particles which were apparently at the same r position. Gradually as it proceeded across the field it would begin to affect the field particles and accelerate them. As it began to interact, the "two layer velocity" effect began to disappear. When this stream has a slight wallward trajectory, the

TABLE 3

ACCELERATION VELOCITY

Measured Velocity U_x	y^+ positions traveled	Angle to Wall	Calculated Velocity, U_x
.464	12-16	0	.374-.431
.459	24.6-14.5	3°	.517-.411
.491	28.7	0	.546
.458	11.5	0	.366
.494	16-20	0	.438-.481
.540	25-32	3°	.52 -.57
.570	20-30	4 1/2°	.48 -.56
.572	24.6	0	.518
.491	16.4	0	.438
.584	34	0	.57
.203	5.7-12.3	0	.226-.379
.50	3.3-16	6 1/2°	.569-.438
.449	20.5-12.3	5	.481-.379
.714	31.8	0	.72
.714	42	0	.765
.611	15.9	0	.68-.729
.714	32-26	0	.729-.68
.582	15.9	0	.552
.331	11.6-9.5	0	.47-.421
.303	5.3-3.2	0	.273-.142
.748	53	0	.8
.517	29-12	6°	.547-.374
.498	24.6-9	5.5°	.517-.318
.404	14.5-5.7	3°	.410-.226
.535	33-21	4°	.575-.485
.515	18.5-9	3°	.461-.318
.282	20-14	6°40'	.32-.265
.223	8.7-5	4°	.19-.120
.238	11.5-8.7	7°	.235-.19
.37	32-23	6°	.386-.34
.361	21-16	3°49'	.325-.285
.496	29-20	4.5°	.373-.380
.33	11.5-6.4	5.5°	.235-.145
.26	14-5	6°	.265-.120

particles which penetrate deeply into the sublayer are retarded and often lose their identity and flow out of the field within the sublayer. Others re-emerge with the ejected fluid.

The entering stream usually did an effective job of accelerating and displacing the fluid above a particular y^+ position. Below this position it only very gradually began to affect the retarded fluid. Therefore at the time of ejection there was often a very sharp interface between the accelerated and the retarded fluid. This creates a very high shear and high vorticity layer.

The other manifestation which was observed at this stage occurred much less often than the preceding. The fluid entered the field from upstream with a large wallward velocity and at a small angle to the wall. As in the previous case, the mass of fluid involved was larger than the field of view. The particles penetrated into the wall region and many entered the sublayer. Most of these latter lost their identity and were captured by the sublayer fluid and passed out of the field with it. Often as this mass of fluid was proceeding wallward there was a simultaneous ejection of wall region fluid outward. These elements were on a smaller scale than the wallward flow. The two opposing flows coexisted but did not interact although they were clearly passing one another. This implied that they were on separate rx planes separated by some distance along the line of

sight. The axial and radial components of the wallward flow were always greater than the corresponding velocities for the outward ejection. The angle of approach to the wall was approximately 5^{o}-15^{o}, while the angle of ejection on the same coordinate systems was approximately 170^{o}. From the analysis of the films and the velocity measurements it was concluded that these were two separate flows and not two parts of a larger circulation. There were cases where the wallward flow interacted with the outward ejection and temporarily retarded it. Gradually, the wallward flow diminished and the outward ejections dominated the field. The above description is also another example of "two layer velocity." Table 4 contains some measurements of the radial and axial velocities of the wallward flow and the angle of approach to the wall. For some flows the radial velocity was nearly 20% of the local mean axial velocity. The small angle of approach to the wall, and the rather close agreement between the measured axial velocity and the local mean axial velocity calculated for the y^{+} span over which the other velocity was measured indicates that wherever the wallward flow originated it has by the time of observation acquired the local mean axial velocity.

Ejection event. The ejection of fluid elements from within the wall region outward toward the pipe centerline is both the most striking and most important part of the ejection process which characterizes the fluid motion in the wall region. An ejection

TABLE 4

WALLWARD FLOW

Velocity	Angle to Wall	Axial Velo.	Radial Velo.	y^+ Span	Approx. Calc. Axial Velo.
.268	15°13'	.259	.075	26-11.5	.357-.235
.268	15°10'	.259	.073	23-8.7	.340-.192
.345	8°13'	.341	.050	29-19	.373-.310
.676	5°24'	.673	.064	21.2-11.6	.628-.47
.669	7°15'	.664	.084	31.8-15.9	.728-.552
.631	5°37'	.628	.062	37.1-18	.746-.586
.559	7°8'	.555	.069	26.4-13.8	.685-.465
.756	9°3'	.746	.121	42-16	.765-.555
.665	11°8'	.652	.128	64-21	.817-.627
.615	11°19'	.603	.121	64-37	.817-.795
.597	14°5'	.579	.146	58-26	.80-.68

is described as the swift and sudden movement outward from the region of the pipe wall of small element of fluid which was formerly flowing axially within the wall region. The frequency of ejection is a function of Reynolds number, increasing as it increases. Its basic character, however, is independent of such mean flow parameters. The process is random with respect to time and position along the pipe wall, and shows no regularity in time of duration or in the intervals between occurrences within any given set of conditions. Since they are fundamentally random events, they demonstrated a certain degree of variation, but the basic character of the ejection event is unchanging and always recognizable.

The ejection of fluid from the wall region occurred after the deceleration step and while the acceleration step

was in progress. Since the two often occurred in conjunction, the motion pictures were carefully examined for evidence that the accelerating stream was a direct causitive factor of the ejection step, but no such relation was discovered. At times there was some interaction between the fluid composing the entering stream and the fluid from which the ejection arose, but most often the interaction occurred only after the ejection had begun. The mass of fluid from which the ejections arose was part of the retarded region near the wall. It possessed all of the properties of this region, including a relatively undisturbed or only mildly disturbed axial velocity. The particles which appeared in the ejected element were clearly in view within the field, moving axially, parallel to the wall, before they were ejected outwards. It was concluded therefore that the accelerating stream and the ejection were two separate parts of an over-all process, but apparently neither caused the other. The ejections originated within the fluid in the field. There was no method of determining how their creation was connected, if at all, to the larger circulations and disturbances of the main stream.

Once the steps preceding an ejection had occurred, the ejection itself proceeded very rapidly from the early stages to the fully developed stage. At this stage there was a continuing ejection of fluid outward for varying periods of time, and then the ejection step gradually ceased.

Some indication of the duration of this step is given in a later section. The element of fluid constituting an ejection was very local in character. On numerous occasions the ejection first appeared at a particular position within the field, and while it was in progress other ejections occurred at adjacent downstream positions. At times these ejections appeared to be moving in a connected fashion, i.e., were correlated, but at other times there appeared two or more simultaneous ejections within the same field which were quite unconnected. Recalling that the field of view was approximately 0.095 inches long, one can obtain some idea of the size and local nature of the elements. Movement in a connected fashion is described as the movement of two or more particles in such a way that, although they are separated by a distance, they clearly describe similar paths, with regard to speed and trajectory, during the same interval of time. The maximum distance over which this occurs is called the distance of connected movement. This was used as a guide to identify the different local ejections when more than one was occurring at a particular time. In all cases observed, the distance of connected movement was less than the length of the field of view, 0.095 inches, and most often of the order of 0.06 - 0.03 inches. This dimension was measured axially along the pipe wall and may be considered the base of the ejected element.

Most of the elements originated within the section of the wall region bounded by $5 \leq y^+ \leq 15$. Table 5 shows the region of origin of the majority of the ejections as well as the position nearest the wall from which an ejection was observed to occur. In it one can see that even below $y^+ = 5$, and in fact at $y^+ \doteq 2.5$, a few ejections originated. Below these positions, significant departures from the purely axial flow were observed, but they never escaped the region as an ejected element. It will be shown later that much of the activity in the sublayer region resulted from the ejection process.

It will be recalled that the deceleration-acceleration sequence preceding an ejection distorted the velocity profile in the wall region and often created a high shear layer. The degree to which this occurred and the position of the high shear interface varied greatly since each step was independent of the other, and each showed wide variation. A later section will show this quantitatively. There are, therefore, a number of separate factors which affect the ejection element. On the average, it will have an axial velocity component representative of the y^+ region from which it came. However, the local mean axial velocity at a particular y^+ position is not that given by the normal turbulent velocity profile for local mean velocity, but is influenced by the degree of distortion of this profile by the deceleration-acceleration sequence. Since in many cases the axial velocity

TABLE 5

EJECTION VELOCITY AND ANGLE

Run No.	Re	Eject. Angle	Actual Velo.	Radial Velo.	y^+ Span[a] Meas.	y^+ Span of Origin of Most Particles	Ratio Radial Velo. / u*	Position of Deepest Origin
165	20,650	11°	.159	.032	6-20	5	1.135	
		7°	.134	.016	7-17		.567	
		7°	.134	.016	5-14		.567	3
		17°	.124	.036	8-29		1.277	
		18°	.128	.04	17-32		1.418	
		9°	.141	.022	7-14		.780	
166	20,650	6°	.209	.023	9-23	4-12	.816	
		1.5	.175	.005	7.5-9		.177	
		5	.175	.016	6-10		.567	
		6.5	.223	.025	11.5-17		.887	
		14	.231	.057	11.5-29	7.5-15	2.021	5
		15.5	.252	.068	17-35		2.411	
		8	.248	.036	11.5-20		1.277	
		15	.233	.06	20-35		2.128	
		12.5	.220	.047	15-32		1.667	
		10	.236	.04	7.5-17		1.418	
167	21,166	12	.176	.037	14-29	6.4-16	1.312	4
		15	.223	.058	17.3-35	6.4-8.7	2.057	
		13	.139	.031	11.5-20		1.099	
		6	.222	.024	7.5-11.5		.851	
		9.5	.175	.029	16-27		1.028	
168	21,080	7	.21	.026	13-32	4-7.5	.922	3

TABLE 5.--continued

Run No.	Re	Eject. Angle	Actual Velo.	Radial Veol.	y^+ Span[a] Meas.	y^+ Span of Origin of Most Particles	Ratio Radial Velo. / u*	Position of Deepest Origin
225	31,240	7	.231	.027	3.3-12	4-9	.675	2.5
		4	.229	.016	3.3-5.7		.40	
		6	.242	.026	5.7-12		.65	
		6.5	.294	.033	7.4-20		.825	
		4	.408	.026	4 -16		.65	
		15	.362	.092	12-29		2.3	
		14	.380	.093	12-33		2.33	
224	30,640	5	3.15	.026	9-21	7.4-12.3	.650	4
		5	.341	.029	11-25		.725	
		5.5	.248	.024	11-18		.600	
		5	.336	.028	9-25		.700	
		5	.352	.030	6.5-21		.750	
		4	.302	.022	6-16		.55	
		3.5	.380	.024	14-29		.600	
		12	.366	.078	20-50	10.7-25	1.95	6
		9.5	.338	.055	20-45		1.375	
		3.5	3.54	.022	7-25		.550	
		10	.362	.063	12-45		1.575	
		8.5	.308	.046	16-37		1.15	
		6.5	.298	.033	11-21	5.7-14	.825	
		12	.276	.059	12-33	5.7-12	1.475	3
		7.5	.431	.057	16-29	9.5-21	1.425	
		15	.212	.054	9-25		1.35	
		18	.244	.075	12.3-33		1.875	
		20.5	.306	.108	16-41		2.70	
221	40,670	18	.135	.041	4-16	5.3-11.6	.796	4

TABLE 5.--continued

Run No.	Re	Eject. Angle	Actual Velo.	Radial Velo.	y^+ Span[a] Meas.	y^+ Span of Origin of Most Particles	Ratio Radial Velo. / u*	Position of Deepest Origin
		9	.515	.079	16-42		1.534	
		13	.441	.097	9.5-47		1.883	
		7	.498	.063	9.5-32		1.223	
		5	.594	.051	11.6-32	1.	.990	
		11	.465	.118	5.3-53	5.3-16	1.728	
		14.5	.473	.118	5.3-53		2.291	
		10	.620	.108	9.5-42		2.097	
		13	.461	.103	7-37		1.999	
		13	.536	.120	9.5-48		2.330	
		9.5	.686	.112	11.6-42		2.174	
223	41,090	11	.469	.089	16-37	11.6-18.5	1.728	3
		10	.486	.087	18-42		1.689	
		9	.510	.077	14-42		1.495	
		8.5	.392	.058	11.6-31.8		1.126	
		12	.471	.099	11.6-37		1.922	
		11	.683	.132	21-47		2.563	
		5	.561	.049	16-32	9.5-16	.951	7
		7.5	.52	.068	11.6-37		1.320	
		6.5	.52	.068	11.6-37		1.107	
		9	.43	.066	9.5-26		1.281	
		7.0	.441	.052	14-26		1.009	
		8	.436	.059	9.5-21		1.146	
		8	.415	.057	7.4-26		1.107	
		7	.383	.048	7.4-26		.952	
		12		.019		4-11.5	0.074	
155	20,230	21		.032			1.134	

[a]This is only region selected for measurement and does not mean particles originated here.

in the region of origin of the ejections is still retarded at the time of ejection, the axial velocity of the ejected fluid will be retarded. The randomness and possible variations within each of these steps emphasize the strong dependency of the ejection event on local conditions. This element was ejected outward toward the unretarded region of much greater axial velocity. As the elements entered this region, they interacted with the fluid there, and the resulting motions were very violent and chaotic. Not only was there interaction between the ejected fluid and the mean stream, but when more than one ejection element appeared within the same region or time span, the interaction occurred among all three or more fluid masses. The motions might be characterized as very disorganized with the particles having short, abrupt movements and sudden changes of direction and speed. The general movement of the entire region was, of course, downstream, but the chaotic motions spread out in all directions, and the more violent ones reached even to the sublayer and wall. In this manner the inner parts of the sublayer region were disturbed by the ejection. The end result, in addition to the creation of this turbulent motion, was that the ejected element was disrupted and accelerated axially at the expense of the mean stream, and was convected downstream. The chaotic motion continued as it proceeded downstream. Since the elements originally possessed an

outward directed radial velocity component, the fluid continued to spread outward.

The ejected element originally possessed an angle to the wall of the order of 5^{o}-20^{o}, directed downstream, but as it entered the region of higher axial velocity it was accelerated downstream at a much reduced angle. The typical trajectory of an ejected element was a slightly curved path directed downstream at a relatively small angle to the wall. No tight rotation of the fluid elements was observed except on a very few occasions. The distance which an element moved outward before being accelerated and disrupted depended upon the position of the high shear interface, i.e., the nature of the profile in the wall region. In some cases the interface occurred very near the position of origin, and the elements were almost immediately affected. In some few cases, however, no interface appeared within the field (this often occurred during the wallward flow or when the deceleration took the plug-like flow form), a distance which ranged from a $y^{+} \doteq 40$ to 75. In these instances the ejected element left the field essentially unaffected and with a substantial radial velocity component. There was no way of ascertaining if in these cases a shear region formed beyond $y^{+} = 75$.

The velocities and trajectories of the ejected particles were measured and the results appear in Table 5. The method of measurement is discussed in the section on experimental procedures and Appendix II. These measurements are,

of course, only approximate, but they are sufficiently accurate to contribute valuable information about the ejection process. The angle of ejection showed a considerable variation from event to event, but this is not surprising in view of the earlier considerations. The largest angle observed was 21°, and the distribution ranged from 1.5° to 21°. The minimum angle measured has no real significance. The particles chosen for these measurements were representative of the particular ejection, and a number of particles within each element were selected. Within any given element there occurred a distribution of angles, but this was much smaller than the distribution among the different ejections. The angle of ejection was plotted against Reynolds number, and the distribution appears in Figure 21. It can be seen that the distributions are all similar for the Reynolds numbers considered, and, therefore, that there is no dependency of the ejection angle on Reynolds number. Figure 22 is a frequency distribution curve for the ejection angle and includes values for all Reynolds numbers. The most frequent angle of ejection is 8.5°.

The independence of the ejection angle with regard to Reynolds number has some interesting consequences. If one refers to Tables 2 and 3, it is seen that while a deceleration and acceleration do occur, the resulting velocities are still a function of Reynolds number and reflect the normal distribution of local mean axial velocity. The axial velocity

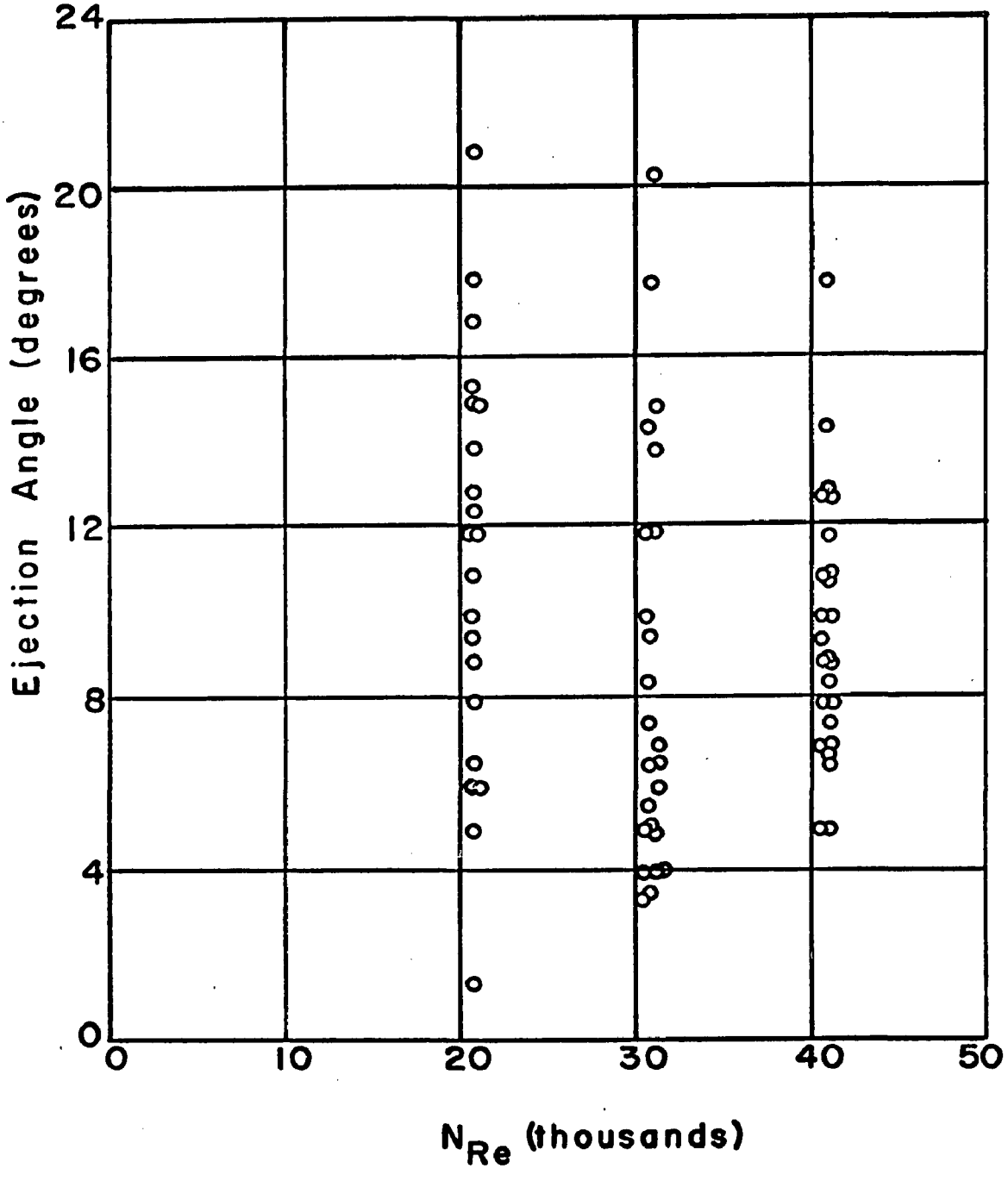

Figure 21. Ejection Angle Distribution

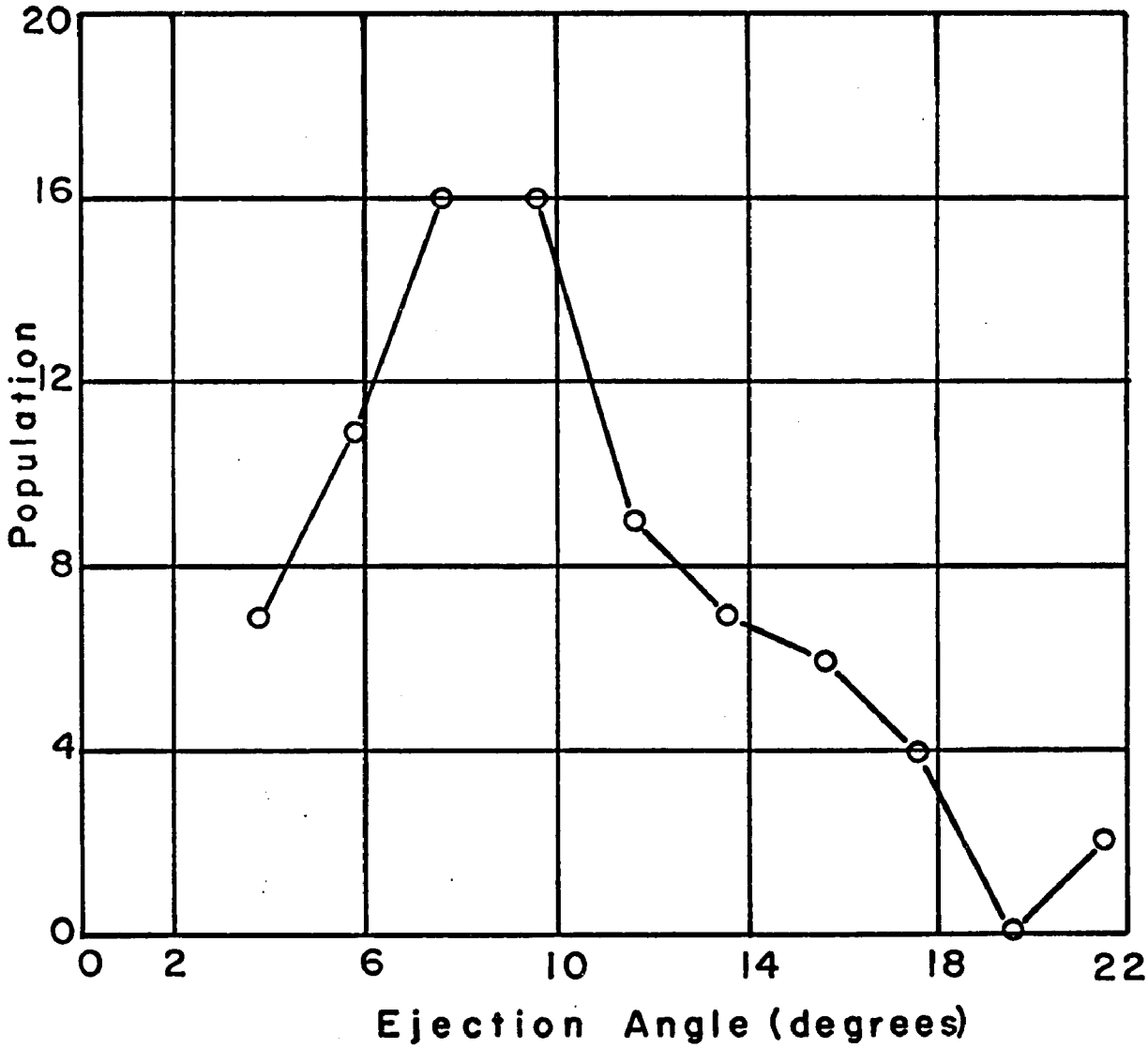

Figure 22. Frequency Distribution of Ejection Angles

component of the ejected element, since it originates in this region, must also have this dependency on Reynolds number, i.e., it is larger for larger N_{Re}. However, if the ejection angle is independent of Reynolds number, then the radial velocity component must increase with increasing Reynolds number, for this is the only way the angle can remain unaffected. This, of course, is clearly evident in Table 5. It is clear that whatever the mechanism is that causes the ejection, it must in some manner be related to the mean flow parameters as reflected by the Reynolds number. Unfortunately, the very randomness of the ejection process, which gives such a wide distribution of angles within any set of flow conditions, and its very strong dependency on local conditions precludes the possibility of correlating the present measurements with mean flow parameters.

The measured radial velocity component ranged from a very small percentage of the axial velocity component to a high of 30% or more. The most common value was 10% - 20% of the axial component. It must be remembered, of course, that these are instantaneous measurements and not average measurements of fluctuating intensities such as a hot wire would give.

Figures 23 and 24 show two ejections in a sequence of still photographs. It will be noted that in each case the sequence begins with the particle at approximately $y^+ = 23$ and that the motion proceeds out to a $y^+ \doteq 60$. This should

not be interpreted as evidence that the ejection began at $y^+ \doteq 23$. This segment of the ejection trajectory was selected because in the still photographs it most clearly showed the radial movement due to the large displacement. Ideally, the segment occurring within $y^+ = 30$ should have been selected, but this did not reproduce well from the motion picture, and the sequence would have been meaningless. This is a result of two factors. First it is very difficult to show by a series of still photographs the relative velocities and continuity of motion that a motion picture image provides. Secondly, the image quality of the print made from the motion pictures was much poorer than the original and much detail and even particles were lost due to this decrease in quality. To show the ejection in $y^+ \leq 30$ region would have required a considerable enlargement of the motion picture film (recall that for analysis the projected image was nearly 100 times that of the film image). At such magnifications the print is useless as nearly all details are lost. The Figures 23 and 24 therefore represent a compromise between a desire to show an ejection event and practicality. In Figure 23 the ejection is apparent because it involves the later stages of the event when the outward movement after interaction prevails. The axial velocity of the particle is nearly that of the local mean velocity indicating that acceleration has occurred. The particles of interest are marked with arrows. The wall view is used, and all motions in the photographs

are relative to the carriage velocity which is indicated. Adjacent to the photographs is a series of sketches drawn to scale which show the apparent trajectory. The actual trajectory is also plotted to scale. The particle motions are in the rx plane, and the ejection angle to the wall is approximately 10.5° directed downstream.

Figure 24 shows a slightly different case. As before, the outer segment of the ejection was selected primarily because it is most visible in the still photographs. However, unlike Figure 23 the particles in this case still have a decelerated axial velocity as evidenced by the fact that they are moving at approximately the carriage speed which is below the local mean axial velocity at all y^{+} positions traversed by the particles. This is clear from the sketch of the apparent profile where the carriage motion is taken into account. Since the particles are not accelerated by the axial velocity as they travel outward, one must conclude that locally the mean axial velocity is decelerated, and that the normal velocity profile does not exist there. This implies that the high shear interface exists further out, or as the motion pictures show, a sharp interface will appear within the region when higher velocity fluid enters from upstream. As before, the apparent trajectory is plotted, but now it is very different than the actual trajectory because the particle motions so closely approximate the carriage velocity. The actual trajectory is also plotted.

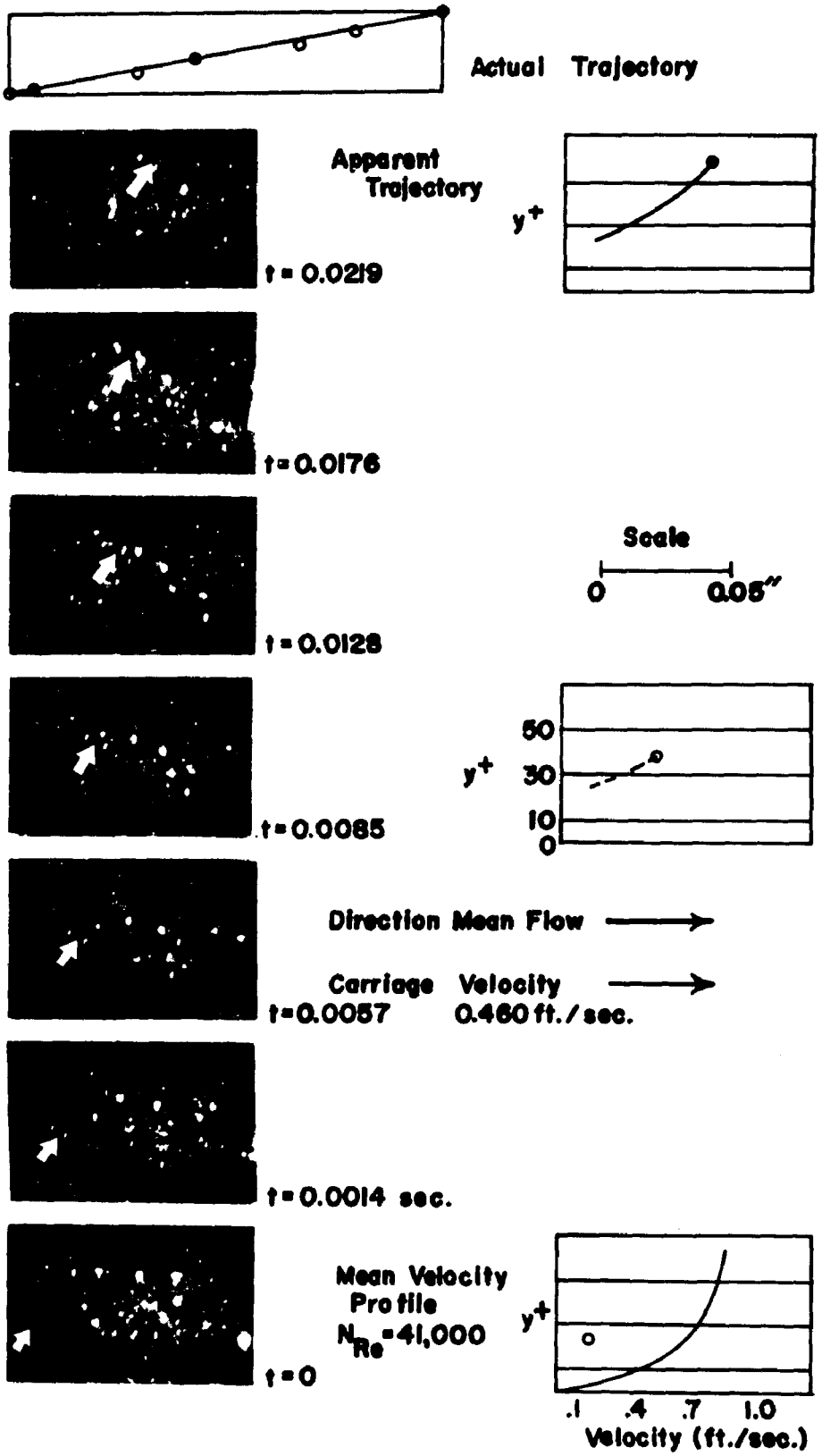

Figure 23. Fluid Ejection- Wall View

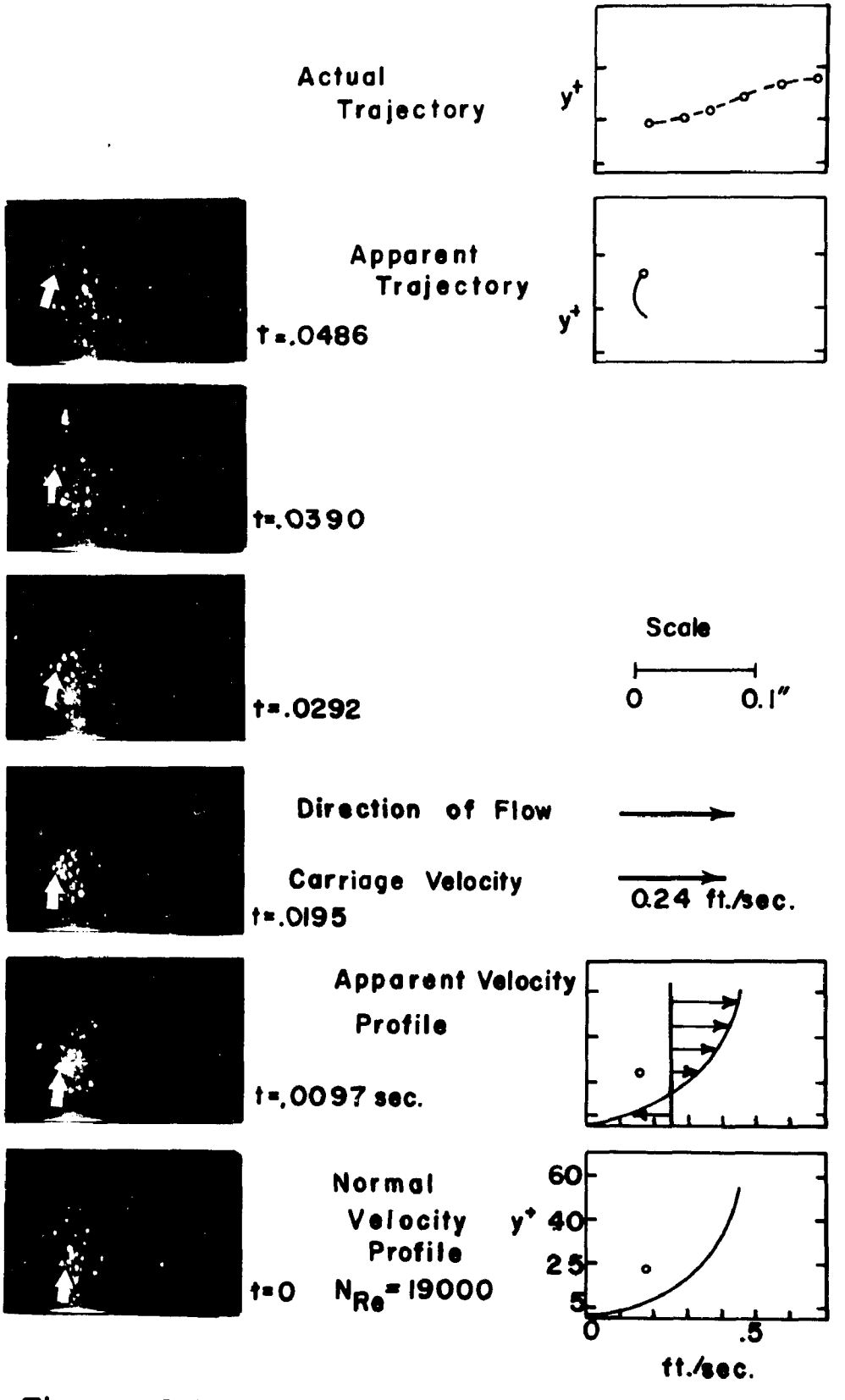

Figure 24. Ejection- Wall View

These sequences give only a faint indiction of what can be discerned on the motion pictures but they do indicate the ejection event and even the retardation of the local wall region during the ejection process. For a full understanding, the motion pictures must be carefully scrutinized under highly magnified projection.

Sweep. The ejection part of the process is usually terminated by a stream of fluid which enters the field from upstream and which possessed a greater axial velocity than much of the fluid within the field. This stream usually had no radial component and did not contain any high intensity, small scale turbulence. At times the stream immediately interacted with the fluid in the field and accelerated it downstream. In effect it swept it clear of the remaining retarded fluid and re-established an approximation to a normal turbulent velocity profile in the area. On some occasions the entering stream did not interact with the particles, but appeared to pass them much in the fashion of the "two layer velocity." After a time, however, the entering stream seemed to encroach upon the field fluid and eventually interacted with it. In both cases the interaction usually produced some chaotic motion. While this action terminated the cycle of events, it did not mean that all disturbances in the wall region disappeared. There remain minor disturbances.

Two layer velocity. The effect called "two layer velocity" appeared in the motion pictures as two large masses of particles, each possessing a distinctive velocity, which occupied the same radial or y^+ span but did not interact with one another. It should be emphasized that the comparison was made between entire layers and not individual particles. A few examples of this appearance have been described in conjunction with other aspects of the ejection phenomenon. Since the paths of these layers often crossed or were otherwise opposed, the implication from the visual analysis of the films was that they occupied two different rx planes and were separated by some distance along the line of sight. The depth of field of the optical system was such that it afforded a distance of approximately 0.027 inches along the line of sight to be in focus. This preliminary conclusion was supported by quantitative measurements.

Some distinction should be made between the shear layer, and the "two layer velocity." Both, of course, are shear layers of a sort, but they occur in different planes. The shear layer occurs as a result of a large $\overline{U}_x$ velocity difference over a small r distance, and appears as a rather sharp interface between two θx planes. The "two layer velocity" occurs as a result of different $\overline{U}_x$ velocities in two rx planes. This will perhaps be made clearer by referring to the sketch below.

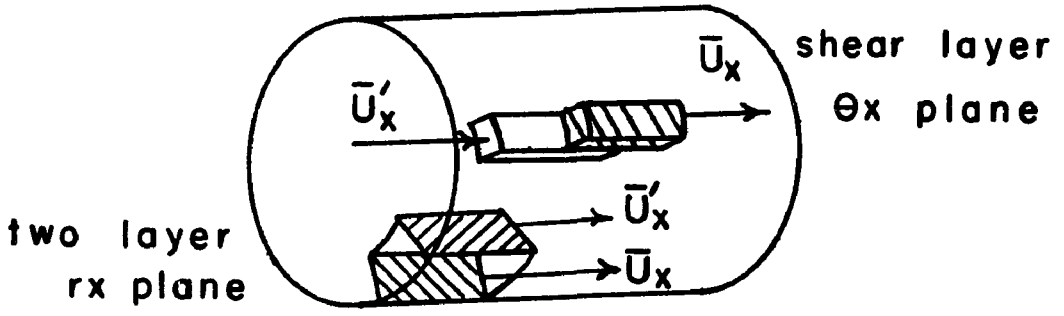

Fig. 25.--Shear Layers.

This phenomenon was usually observed in association with the events of the ejection process, but did not appear each time an ejection occurred. Its appearance usually was noted when the normal course of the ejection process required two streams of different character to interact, i.e., during the acceleration step, during the ejection, or during the sweep after the ejection. In all of these, if the streams were on different planes perpendicular to the line of sight, a "two layer" effect would be possible. On the few occasions when it was not associated with an ejection, the deceleration of the local mean stream had occurred so the same factors applied.

Although other evidence indicates it cannot be so, it seems of value to briefly consider the effect of the wall curvature on this observation. For the wall view, the line of sight is at the pipe wall through horizontal planes parallel to the horizontal diameter of the pipe. See Figure 13. The optical system has a depth of field of 0.027 inches along this line. If one places the upper extremity of this

field at the pipe wall where the horizontal pipe diameter intersects it, one would have the lower extremity at a plane removed 0.027 inches from it along the line of sight. Since the pipe wall is curved, a point on this lower plane directly below one on the upper plane will be slightly nearer the wall. The velocity gradient is quite steep near the wall, so the question is whether this displacement is sufficient to cause a large enough velocity difference between the points in the two planes to explain the "two layer" effect. This calculation appears in Appendix III, and clearly shows that the effect of the curvature is too small by several orders of magnitude to be a factor. Also, it was noted that the effect was not seen at all times but only at certain times. The presence of two layers moving in distinctly different directions also could not be explained by the curvature.

The axial velocities of selected particles representative of each layer were measured, and relative velocities calculated. The ability to make these measurements, and the accuracy of the measurements was enhanced by the fact that the camera was moved at a particular axial velocity in the flow direction. Thus in most cases the slower moving particles had practically a zero or even a negative axial velocity relative to the camera while the faster ones moved axially past it. This eliminated the necessity of discriminating between two similar appearing velocities, and permitted the measurement of even small relative motions. This

same general procedure also enhanced the measurement of ejection angles mentioned earlier. By keeping a radially moving particle in view for a longer time with the moving camera, an angle of 10°, for example, can appear as an angle of 60°-70° in the motion pictures.

The results of these measurements appear in Table 6. It should be stated that the results in general reflect the tendency to select for measurement those examples for which the relative motion between layers was most evident and therefore of large magnitude. The upper limit of the relative velocities, therefore, has more significance than the lower. The ratio of faster to slower velocities has a maximum of 2.9/1. The most common ratio, however, is 1.5/1.

The table also includes a comparison of the absolute axial velocity of the higher speed layer with the calculated local mean axial velocity for the same y^+ position. In general the agreement between the two is quite good, and one can conclude that the higher speed layer is most likely something approaching normal turbulant flow while the slower speed layer is retarded flow. One sequence of measurements in Table 6 is for the previously mentioned case where a wallward and outward flow coexisted. They also support the general view of the effect.

There are other observed properties of this "two layer velocity" effect which shed additional light on its origin. In discussing its appearance in association with other steps

TABLE 6

TWO LAYER VELOCITY

Relative velo. absol.(ft/sec)	Ratio higher velo. / lower	Actual velo. of higher absol. (ft./sec)	y^+ range where occur	Calc. profile velo. ft./sec.
.216	2.9+	.326	.20	.319
.189	2.7	.299	23	.340
.112	2.0	.222	5	.122
.119	2.0	.229	11.5-20	.223-.319
.129	1.7	.316	18	.31
.136	1.7	.323	16	.304
.136	1.7	.318	---	---
.120	1.7	.302	---	---
.117	1.6	.299	---	---
.078	1.4	.260	---	---
.105	1.6	.287	20.2	.32
.123	1.7	.305	17.3	.312
.066	1.4	.247	14.9	.289
.066	1.4	.247	14.4	.289
.161	1.5	.481	25-45	.521-.60
.132	1.5	.464	22.5-16.5	.502-.442
.254	1.8	.580	29-37	.55-.578
.225	1.7	.557	16.4	.438
.202	1.6	.534	15.4	.423
.147	1.5	.471	33-20	.569-.476
.139	1.4	.465	7.4-12	.278-.374
.174	1.5	.489	12-9	.374-.318
.163	1.5	.495	20.5-16.5	.481-.442
.161	1.5	.493	33-29	.569-.55
.138	1.4	.470	20.5	.481
.179	1.5	.503	41-33	.59-.569
.221	1.7	.553	20.5-16.4	.481-.438
.225	1.7	.550	33-20.5	.569-.481
.210	1.6	.542	24.6-16.4	.518-.438
.169	1.5	.501	20.5-28.7	.481-.55
.104	1.3	.436	20.5	.481
.155	1.5	.487	29	.55
.127	1.4	.457	14.5	.411
.171	1.3	.687	31.8-9.5	.728-.421
.180	1.4	.70	37.1-21.2	.746-.628
.085	1.2	.605	26.4-15.9	.685-.552

TABLE 6.--continued

Actual velocity	Angle to wall	Radial velocity
.268	15°10'	-.075
.268	15°13'	-.073
.345	8°13'	-.050
.124	17°	+.036
.128	18°	+.040
.141	9°	+.022

of the ejection event, it was observed that often the effect would disappear as the degree of interaction of the two layers increased. This implies that the two layers were separated but gradually approached one another or became sufficiently energetic to interact.

Figure 26 shows the "two layer velocity" in a series of still photographs. All that was said previously regarding image quality of the prints applies here as well. As a result, the bright particles mark the fluid involved in the event, but the less bright particles, which in the motion pictures show the extent of the masses involved, are missing. As before, all motions in the photographs are relative to the carriage velocity which is indicated. The wall view was used as shown by the sketch. Adjacent to each photograph is a sketch drawn to scale depicting the radial and relative axial position of the two masses. The normal local mean velocity profile and the apparent velocity profile clearly show that the relative motion of the fluid masses cannot be

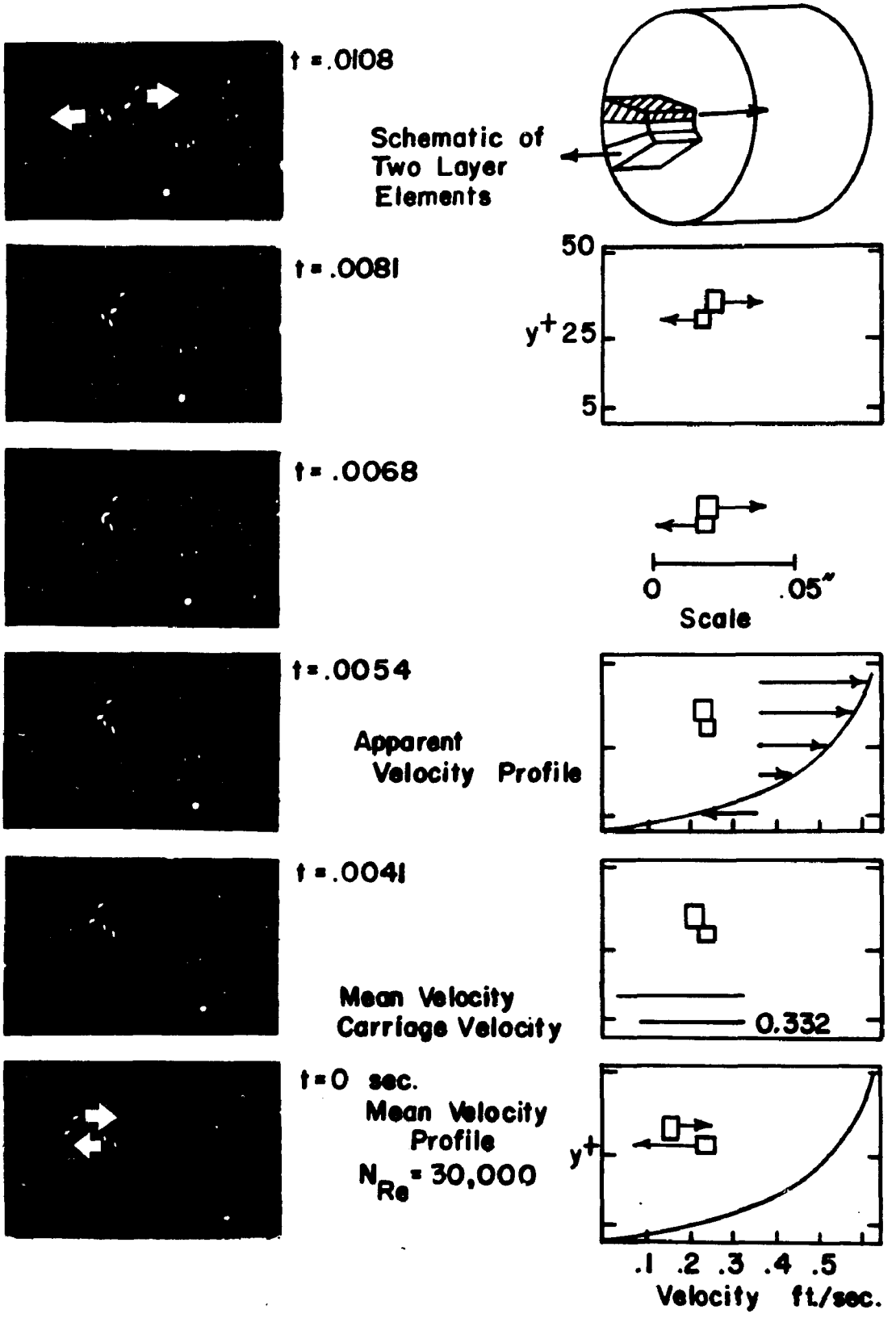

Figure 26. Two Layer Velocity

attributed to this cause. The two masses appear to approach each other along the same radial-axial coordinates. Actually the masses are both moving downstream along the same line but at different velocities. One mass is moving just slightly slower than the carriage velocity as evidenced by its apparent lack of motion. It is obviously retarded with regard to the normal axial velocity. The approximate relative velocity of the two masses if 0.163 ft./sec., and the ratio of the velocities is 1.49/1. In the photograph the masses appear to just overlap, but in the motion pictures the masses are larger so considerable overlap is involved. If the masses were truly on a collision course they would necessarily interact. They obviously do not, so they must be separated by some distance in the θ direction as shown by the sketch. This distance cannot exceed 0.027 inches.

The nature of the two layer velocity is clear. In itself it is not a new phenomenon but is, in fact, only a result of the local, small scale nature of the ejection process. The retardations and ejections occupy and initially influence only a small area both axially and along the direction of sight or the θ direction. The movement of the relatively unaffected mean stream flow past this area results in a "two layer velocity" until the two flows interact.

The existence of "two layer velocity" implies that the segment of the wall along the line of sight involved in the ejection process is of the order of the depth of field or

0.027 inches. This dimension cannot be fixed accurately because the observance of the event really only fixes one of the boundaries of the ejection area, and therefore one cannot know how far it extends in the other direction. However, since the effect was observed so frequently, and the ejection process itself is quite random, it seems unlikely that one could observe the effect with any frequency if the dimensions of the ejection process were different by an order of magnitude from the above value.

Further details of the ejection step

Since earlier analyses indicated that the basic nature of the ejection event was unchanging with respect to mean flow parameters, a more detailed analysis of motion pictures taken for N_{Re} = 20,000 was made. These films were selected because they contained a sufficiently large number of events, and yet each event was clearly defined and separated from the effects of the other. At higher Reynolds numbers the separation is less clear. The description that follows, therefore, strictly applies only to this particular Reynolds number, but the general characteristics will apply to all conditions, and the particulars may be modified approximately according to the observed dependency of certain factors on Reynolds number.

The duration of each ejection step from the beginning of the ejection to the sweep step and the interval between

ejections were timed. The results appear in Table 7. They show that there was no regularity or trend associated with the intervals between ejection events. Neither was there any regularity in the duration of an ejection. The maximum duration was 0.552 seconds and the minimum 0.063 seconds. Using a class width of 0.1 seconds, the most common duration of an ejection was in the class 0.1 to 0.2 seconds. The average of the population within this class was 0.148 seconds. For these flow conditions, the intervals between ejections was greater than the ejection duration, but since it is known that the frequency of occurrence increases with Reynolds number, this ratio must change. This measurement proves what had been qualitatively observed. The ejection process occurs randomly with respect to time.

It has been mentioned in previous analyses that between ejection events the wall region including the sublayer region continued to show evidence of disturbance, albeit with reduced intensity. A study of these motions in the present analysis supported that view. During ejections, disturbances extended well into the sublayer, at least to $y^+ \doteq 2$, and even to the wall itself.

The data of Figure 20 showed the percentage of the total time that the flow was significantly disturbed. The duration measurements of Table 7 provide an indication for the same flows of the contribution to this time made by the

TABLE 7

TABULATION OF INTERVAL AND DURATION OF EVENTS, RE=20,000

Run No.	Interval Start-A	Duration (A)	Interval (A-B)	Duration (B)	Interval (B-C)	Duration (C)	Interval (C-D)	Duration (D)	Interval (D-E)	Duration (E)
127		.324 sec		.284 sec		.443				
155		.141		121		.066		.092		.075
164	1.022	.063	1.237	.089	2.12	.199	.849	.552		
165	1.700	.078	1.29	.141	1.47	.145	.267	.113	.081	.199
166	1.42	.148	.364	.178	.809	.263	1.61	.118		
167	.671	.134	1.85	.355	.607	.228				
168	1.84	.372	.606	.218	.093	.241	1.03	.433		

ejection step directly. Upon comparing the two measurements it was found that the ejection event directly accounted for from 62% to 100% of the time that the flow in the wall region was significantly disturbed. While this information may be of value when considering the relative importance of the ejection event and minor disturbance in heat and mass transfer, it must be recalled that the ejection occurs primarily beyond the sublayer while the other motions, some below the established minimum for measurement, occur throughout the region. In the sublayer even this small disturbance can be very significant.

The deceleration-acceleration sequence and the creation of a high shear layer have been discussed as has interaction of the ejected fluid within this region. It will be recalled that the position of the interaction zone was observed to vary over a rather wide y^+ span depending upon many local factors. In this analysis the location of this zone was carefully noted, and the results appear in Table 8. It can be seen that the zone of interaction has had extremities of from $y^+ \doteq 4$ to $y^+ \doteq 32$. The zone itself has a span of approximately five times the usual sublayer thickness ($y^+ \doteq 5$) and most often occurs in the span of $7 \leq y^+ \leq 30$. Of course, interaction occurs beyond the outer limit of this span, but by then most of the velocity difference between the ejected element and the mean stream has been lost, and the action is more a result of diffusion of turbulence than new creation. The interaction zone is wider than the

TABLE 8

DISTRIBUTION OF INTERACTION ZONE

Run Number	y^+ of Interaction Region
164	8.5-17 7.5-20 7.5-32 7.5-32
165	8.65-20 10-27 5-32 later 10-25
166	10-26 10-29 8.7-26 8.7-23
167	7.5-32 4-26
168	8.7-29 7.5-29 11.5-20 4-20

interface where the maximum shear would occur since the very act of interaction at this position creates a zone.

Top view analysis

Motion pictures of the wall region were also taken from the top view. This particular view was discussed in the section on experimental procedures. Before proceeding with a presentation of the observations, some discussion of the capabilities and limitations of this viewpoint is necessary.

It will be recalled that this position and the depth of focus of the optical system permitted a view through a number of horizontal planes stacked one upon the other for a span of y^+ positions beginning with the wall and extending toward the centerline. Since the photographic system did not provide any depth perception, one could not tell, simply by looking, on which plane or y^+ position the motions were occurring. The use of image quality was of some assistance in establishing the extremes of focus, but that was all. A normal turbulent velocity profile gives the fluid a very steep gradient in the wall area, and this gradient was quite evident in these pictures. It appeared as particles with many different axial velocities superimposed upon one another. By matching the carriage speed of the camera to a particular local mean axial velocity of the flow, one could effectively divide the field into those particles moving faster and those moving slower than the carriage. Those of slower than carriage velocity would appear to be moving in a direction opposite to those of faster than carriage velocity, and moreover, the magnitude of the motion relative to the carriage velocity would be proportional to the distance from the y^+ plane where the carriage velocity matched the fluid velocity. Since one would be examining layers of particles and not individual ones, the possibility of the axial velocity fluctuation causing an error is decreased. This is especially true for those layers whose velocities differ greatly from the

carriage velocity and hence are unmistakably either on one side or the other of the dividing ΘX plane at a particular y^+ position.

At first these films were analyzed in an attempt to observe any regular velocity distribution in the wall area which might be comparable to the spanwise distributions observed by others for flow over flat plates. It was thought that if they existed they would appear as adjacent axial streams at the same y^+ position possessing different local mean axial velocities. This attempt was unsuccessful. The very difficulties described in the beginning of this section precluded any analysis of this type. There is no way of exactly locating the y^+ plane except by the use of the difference in $\overline{U}_x$. Runstadler (50) observed spanwise distributions and determined their spacing. Using his correlation for spacing in the present study, one finds that the best one could hope for would be a single spacing array, i.e., one high and one low velocity stream, in the field of view. Decreasing the magnification to increase field size does not help because the depth of field also increases, and therefore, so does the confusion. With all these limitations it must be stated that the analysis for a spanwise distribution was inconclusive.

These films were also examined for evidence of the ejection process. Since the camera position is completely

different from that used in the wall view, it is necessary to visualize the form in which this process would appear in the top view. If a mass of particles is suddenly ejected outward from the wall region, the radial component of their line of travel as seen in the top view would be parallel to the line of sight. The particles, therefore, would appear to fade out of view if they traveled far enough away from the wall. While this effect is observed, it would be hazardous to assign its cause to the ejection process alone because a similar effect could be caused by other sources, i.e, a change in vertical position of the camera. Earlier, it was described how the matching of the carriage velocity to the velocity at a particular y^+ position divided the field very effectively. The particles in the y^+ plane nearer the wall than the y^+ plane where the speed is matched will have a velocity in a direction opposite to those on the other side of that plane. Thus if these particles suddenly move outward from the wall, they will abruptly change direction when they encounter the higher speed axial velocity layer and are accelerated. Additionally, they should display a somewhat disturbed motion. This sudden change of direction would be very obvious, and it is not likely to be caused by any factor other than the one considered. Of course, not all the ejections will be seen in this fashion since those originating above the y^+ plane of matching will not show this reversal, and any which change more gradually will also be

missed. If the effect is observed it will be support for the ejection event as seen in the wall view, and in addition will present a means of estimating another dimension of the area affected by the ejection process.

The top view can also be used to examine the extent of lateral movement, i.e., movement along a ΘX plane. In the top view these motions will appear as departures from the axial flow. If angular symmetry about the pipe wall is assumed, these motions would correspond to movements along the line of sight for the wall view. It might be of value to refer to Figure 27 for orientation of these various planes.

For analysis, representative films taken at Reynolds numbers from 20,000 to 50,000 were selected. Most had the carriage velocity matched to the mean local velocity which would prevail at $y^+ = 5$ in normal turbulent flow. The exceptions had it matched at $y^+ = 11$ and 8. The field was thus split into two parts, those particles at $y^+ < 5$, and those at $y^+ > 5$. The actual total depth of field depended upon the magnification used. For 2X magnification, the one used most often for the view, the depth of field was 0.041." This corresponded to a y^+ range of 24 to 44 for $N_{Re} = 20,000$ and 50,000 respectively.

Examination of the particle motions for the section at $y^+ < 5$ yielded unmistakable evidence of the ejection process as visualized above. The observed instances where

the particles reversed direction always included a rather large lateral displacement of the particles as well. These events did not occur continuously but at intervals as if each were a separate occurrence. At high Reynolds numbers, the frequency of occurrence was greater. In fact at N_{Re} = 20,000 no event was positively identified. The particles which originally closely approximated the carriage velocity were often the ones which displayed the large lateral motions and were most violent in their reversals. After the reversal, the particles left the field with the higher velocity stream, exhibiting continuing departures from the axial flow. The distance of connected movement for these particles was approximately 0.011 inches laterally by 0.043 inches axially. The events did not occur with great frequency, but since the view was necessarily confined to the region about $y^+ = 5$ this was to be expected.

A second motion was also observed in the region $y^+ < 5$. It was more continuous but also less energetic than the other. The motion was in the form of a small departure from the axial flow, and did not change abruptly. Occasionally they exhibited a slight oscillitory motion, but generally they departed from the axial flow and continued on that trajectory until they passed out of the field. Neither direction of departure from the axis was favored. They are apparently the counterparts of the same type motions observed in the wall view within the same area. In the top view, however,

the deviations are in a plane perpendicular to the plane of the deviations of the wall view.

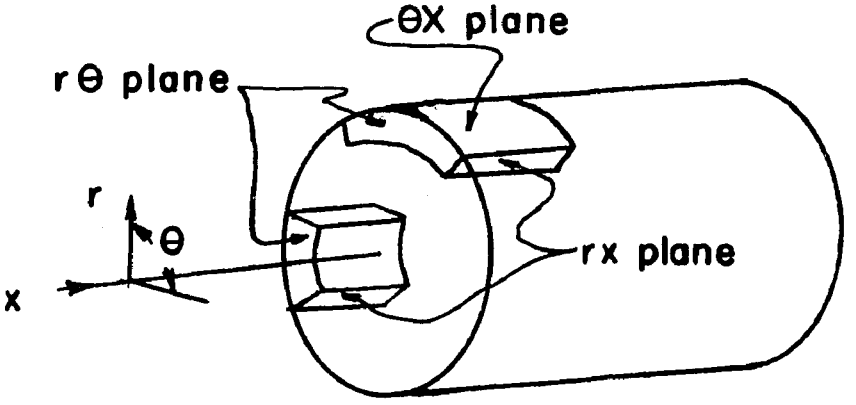

Figure 27.--Orientation of Planes of View.

These deviations usually involved only a small area, i.e., few particles in connected movement, but many deviations were observed to occur simultaneously. There seemed to be an increase in intensity of deviation as the y^+ value increased, but the observation is not conclusive. A definite dependency on Reynolds number was observed for the number and intensity of the deviations. Both increased greatly with increase in Reynolds number from 20,000 to 50,000. Table 9 lists some measured values of the lateral and axial velocities for these deviating particles, and also lists the angle of departure from the axis. The approximate y^+ position was calculated by assuming the normal local mean axial velocity was valid and comparing this value to the measured one. It

may be concluded that in all respects the top view substantiates the wall view observations, and clearly shows the three dimensional character of the fluid motions in the wall region.

TABLE 9

LATERAL DEVIATIONS

Actual velocity	Angle to axis	Lateral velocity	Axial velocity	Approx. y^+ of normal profile	Per cent of axial
.22	9.5°	.036	.217	3.4	16.5
.142	15.5°	.038	.137	2.2	27.7
.183	35°	.105	.150	2.4	70
.134	11.5°	.026	.131	2.1	19.8
.212	11°	.041	.208	3.3	19.7
.095	18.5°	.03	.090	2.3	33.3
.152	19°	.049	.144	3.6	34
.134	11.5°	.026	.131	3.3	19.8
.146	7°	.018	.145	3.6	12.4
.221	17.5°	.067	.211	5.3	31.7

For the region at $y^+ > 5$, the depth of field permitted a view out to a large y^+ position. The particles in the outer reaches of this region appeared to be continually in an agitated state typified by departures from the axial flow. These disturbances moved connectedly as a group of particles encompassing widths (in the θX plane) of 0.043 to 0.065 inches, and appeared as high speed sweeps at an angle to the axis. There appeared to be no preferred direction of approach. The sweeps passed rapidly through the field on a

slightly curved trajectory. As the y^+ position was reduced, the dimensions of the disturbances were also reduced, and eventually even the character changed. At still rather large y^+ positions the area of connected movement was approximately 0.022 to 0.033 inches. There was a definite decrease in the intensity and degree of disturbance with decreasing Reynolds number.

Change in turbulent character with distance from wall

The analysis of the preceding motion pictures indicated that the character of the turbulent motion changed as the distance from the wall region increased. In order to examine this effect more closely, a series of runs were made for flows at a single Reynolds number, N_{Re} = 40,000, in which regions of the flow at successively greater distances from the wall were photographed for analysis. Because the local mean axial velocity changed greatly across this span, it was necessary to adjust both the carriage speed and the filming rate to the particular locale. This necessitate some compensation during the analysis stage when comparisons were made. A magnification of 2X was used for a broad view, and 4.3X was used for details of particularly interesting sections. With the 2X magnification, each region had a width of approximately thirty-one times the sublayer thickness. The total span examined covered an area from the pipe wall to a

$y^+ \doteq 1055$. For 4.3X magnification the single region width was approximately 14 times the sublayer thickness. In all cases, the wall view was used.

The region very near the wall, $y^+ \doteq 72$ showed the now familiar wall region character of the turbulent motions. The ejections originated in this region, and the direction of deviating flow was predominately outward. The fluid motions were intense, abrupt, and of small scale. A great deal of chaotic interaction was present. The infrequent intrusions of wallward flow entering the region from without were usually of a larger scale and were less disturbed within themselves. As the outer boundary of this region was approached, the character of the motions had already undergone a significant change from what they were in the inner regions. Both the broad view of from $y^+ = 0$ to 155 and the narrow view of $y^+ = 72$ to 144 supported this observation. The region of $72 < y^+ \leq 144$ exhibited a few of the traits of the wall region, but they appeared with much less frequency. The trend was toward a larger scaled disturbance. By approximately $y^+ = 150$, the change was complete, and thereafter, at greater y^+ values, the changes which did occur were not a matter of character but of degree. In these regions, the disturbances appeared as increasingly larger aggregations of particles which entered the field through both the wallward and centerline edges, and swept through it with little

interaction. The intensity of activity within these masses was also not very great. The area of connected movement continually increased with increasing y^+, but appeared to level off by $y^+ \doteq 300$. The large, sweeping disturbances usually had an axial velocity component approximately equal to the local mean velocity of the region. These regions, however, were at such large distances from the wall that the velocity gradient is very shallow anyway. These large scaled motions were very difficult to observe properly because they exceeded by a large degree the size of the field of view. Thus only a small segment of a single eddy could be observed at any time, and their interaction with each other or the wall region was not clearly discernible.

Effect of trip wires and obstructions

An investigation into the effect of various tripping obstructions on the fluid motion was made. The purpose was twofold. First, it will be recalled that the glass pipes are joined by flanges, and although care was exercised to eliminate obstructions at the joints, there remained, nonetheless, an unavoidable seam. This seam was located a minimum of twenty-five pipe diameters upstream of the beginning of the test section, and from all considerations should not have contributed anything to the motions in the wall region. To be certain, however, this study was undertaken.

In some other investigations, vibrating ribbons and thin wires have been used to trip the flow or introduce marking elements. In many of these studies a particular pattern at the wall was observed. Therefore, the second purpose of this investigation was to examine the tripped flow in the pipe for evidence of these patterns.

The trip consisted of a wire ring placed axisymmetrically inside the pipe at the beginning of the tested section. The ring diameter was that of the internal pipe diameter, and the wire diameter was 0.0032 inches. The wire was spring steel and was held in the position in contact with the pipe wall by its own spring tension.

The experimental runs covered a range of Reynolds numbers from 2300 to 50,000. In some, the camera carriage was held in one position such that the wire was just visible within the edge of the field. For others, the carriage was moved downstream. In these cases the filming was usually begun while the camera was upstream of the trip. This photographed the flow conditions upstream, at, and downstream of the trip wire, and permitted excellent comparisons. Both the wall view and the top view vantage points were used.

There was no evidence in any of the films of a regular "spanwise" pattern along the wall. As discussed in an earlier section, this result must be inconclusive. A really detailed investigation of this phenomenon would

require a means of circumventing the present limitations of the system to such an analysis.

The films also showed that while the presence of the trip had an effect on the flow locally, its effect was small, and the flow quickly returned to its unaffected state. In order to substantiate this conclusion, a discussion of the observations follows.

At N_{Re} = 2300, comparisons were made of films taken with and without the trip. The camera scanned the flow both upstream and downstream of the wire. No departure from laminar flow was observed at downstream positions. Directly at the wire and in an area approximately 0.2 inches downstream, a pocket of retarded fluid was observed which caused a displacement of fluid and a circulation of minor proportions. However, at adjoining positions downstream, the effect had completely disappeared.

For higher Reynolds numbers and turbulent flow, similar effects were seen. The disturbances were confined to an area near the trip. These quickly faded, and no evidence of their existence could be seen downstream. For N_{Re} = 20,000, the trip induced disturbance was followed downstream and the distance required for it to fade was noted. There was absolutely no question of its disappearance by 0.08 ft. downstream of the trip, and in all probability it was gone by0.04 ft. Thereafter, the flow was no different from those without the trip wire.

One further quite drastic step was taken. In all of the previous runs the trip consisted of a small axisymmetrically placed wire. It was felt that this trip approximated what one might expect from the pipe seam, and also from the ribbons or wires used by others. In order to examine the effect of a very massive obstruction, the collar and scale device used to position the camera for top view studies was inserted into the pipe and located at the joint just upstream of the test section. The collar and scale are described in the equipment section. The scale portion consisting of a brass plate 0.12 inches thick and 1 inch long was placed so that it lay in a horizontal line directly upstream of the position of focus in the test section. The camera was focused at the wall within the test section 25 diameters downstream of the trip position. The Reynolds number was 5270. The films showed no effect at all of the presence of this obstruction. This demonstrated that the length of 25 diameters was sufficient to cause the dissipation of the trip induced disturbance.

Clauser (2) discussed the stability of steady state boundary layers to induced disturbances. He demonstrated that the recovery of such layers at downstream positions from induced disturbances, such as by a trip, was quite rapid, and that the regions nearer to the wall recovered much more rapidly than those further out. As an example he

presented the recovery of a boundary layer, 9.3 inches thick, from a disturbance created by a 1/2 inch rod placed at a y position of 1.5 inches. The decay distance was measured as 19 inches or 2.048δ. Lee (32) also measured the effect of injection apparatus placed near the pipe centerline. For flow at N_{Re} = 41,000, he found that the mean velocity and rms fluctuation values had all recovered by 8D.

These results demonstrate that the pipe seam preceding the test zone by a minimum of 25D is not a factor in producing extraneous motions within this zone.

Dye studies

Since many other researchers have used dye injection techniques to study the motions in the wall region, it was decided to attempt a very elementary investigation in the present system by injecting dye at the wall and photographing its motion. No great care was taken in designing the dye injection system, since the investigation was a preliminary nature only. Consequently, the analysis of the films was made for broad general properties only and no details were examined. In all cases, the dye was injected through a hole drilled into the pipe wall. No injecting device protruded beyond the edge of the hole. With the large hole used, a large quantity of dye could be injected without imparting a significant radial velocity to it. The dye was injected at the wall. The injection process was examined both visually

and photographically at 4.3X magnification. The injected dye remained initially within a very narrow region near the wall, and was accelerated downstream by the fluid. A downstream position within three inches of the injection point the dye was observed to develop a wavy surface, and filaments moved outward from the wall.

In general appearance these dye filaments compared well with those taken at a similar angle by Runstadler (50). The quality of the present motion pictures, however, were much inferior and no extensive comparison was possible.

The lighting technique was quite different from that used for the particle films, so very few particles were visible. If a lighting method could be devised which would permit both dye and particles to appear simultaneously, the resulting motion pictures would be quite valuable for use in interpreting the various dye and particle studies available in the literature.

Summary of observations and composite picture

The preceding sections describing in detail the nature of the turbulent motions in the wall region have, for the sake of clarity and simplicity, been somewhat fragmented. In this section these different observations are compiled to produce a concise description of the nature of this region. The wall region is defined as the region extending approximately from $0 \leq y^+ \leq 30$.

The most important and distinguishing characteristic of the wall region is the ejection of fluid elements outward from the wall. This usually occurs as part of a definite sequence of events.

The first of these events is a deceleration of the axial velocity of the fluid within a local region near the wall. The limited field of view does not permit an estimate of the axial dimension, but the radial dimension involved is of the order of $0 \leq y^+ \leq 30$. The degree of deceleration and the area involved varies randomly. In some instances the entire area is decelerated to approximate plug flow, while for others a velocity gradient is still evident. Deficiencies as great as 50% of the local mean axial velocity are observed.

While the field is thus decelerated, the next step occurs. A mass of fluid from upstream with an axial velocity approximating that of the local mean velocity enters the retarded field and by interaction begins to accelerate the fluid. This stream usually enters above a $y^+ \doteq 15$ position, and as it crosses the field its effect moves wallward. Most often the fluid has a direction nearly parallel to the pipe wall or at a slight angle to it. Occasionally it will enter with a large radial component of velocity, as much as 20% of the axial velocity, and move wallward at angles of from 5°-18°. In both forms, the size of the stream is quite large with widths (in rx plane) of the order of the field dimension

(.068" to .095"), and lengths too great to be measured. The fluid within this stream exhibits some degree of turbulence, but limitations of the photographic technique precluded any detailed analysis. It appears to be a part of a large scale disturbance carried by the mean flow. This stream only succeeds in accelerating the outer portions of the retarded fluid before the ejection event occurs. This partial acceleration imposed upon an already retarded element creates an interface across which a very steep gradient in axial velocity exists.

The ejection event is the abrupt movement outward from the wall area of fluid originally within this region. This event occurs immediately after the acceleration process has begun, and always originates within the mass of fluid constituting the retarded element. The particles which suddenly ejects outward are, just prior to this occurrence, observed to be moving much as the other particles in the region. Other than the accelerating stream described above, no fluid from outside of the region appears to influence them. It may be stated that the ejection event originates within the wall region, and is not a manifestation of some motion occurring outside of this region. The process is of a local nature and random with respect to time and space. It is of small scale and three dimensional. Individual ejected fluid elements involve dimensions of the order of 0.03" to 0.06" measured axially. The angular or θ dimension involved is

difficult to measure but is estimated to be of the order of .01 to .03 inches. Often two or more ejections are observed to occur simultaneously but unconnectedly within the field of view. The region measured in the rX plane where most of the ejections originate is approximately $5 < y^+ \leq 15$ regardless of Reynolds number. There are some ejections which originate outside these limits. There is definite evidence of ejections originating at least as near the wall as $y^+ \doteq 2.5$. Below this position there is often a connected movement of particles which occurs simultaneously with the ejection, but rarely do they possess sufficient radial velocity to escape from the region. Their motion usually consists of a slight outward movement which appears as an axial flow at a slight angle to the wall.

The ejected fluid moves outward from the wall toward the centerline along a slightly curved path directed downstream. The curvature of the path as well as the distance outward which it initially attains depends upon its radial velocity and the position where the velocity interface occurs. This interface does not always occur at the same position, but usually occurs in the zone $4 < y^+ \leq 32$. The exact position in any particular event depends upon the degree of deceleration and acceleration, and magnitude of the radial velocity component. The path of the fluid before it interacts to any extent with the steep gradient is a slightly curved line at a small angle to the wall, and is directed

downstream. The angles of ejection have a wide distribution and reach a maximum value of 21°. They have a most common value of 8.5° measured in the rx plane. The ejection angle is independent of Reynolds number. The instantaneous radial velocity components vary, but some as high as 30% of the axial component are observed. Most, however, fall within the range of 10% to 20%. These, of course, represent the most energetic ejections. The magnitude of the radial velocity increases with Reynolds number, and this factor makes the angle of ejection independent of Reynolds number. The ejection moves not only in the rx plane, but in the θX plane too. These movements show angles as large as 35° and an average angle of 15° measured from the axis. The instantaneous radial velocities within this plane are of the order of 20% to 30% of the axial component.

As the ejected fluid moves outward, it is accelerated axially to a small extent. Because of the retarded nature of the region below the interface, this acceleration is quite small and the fluid is still deficient in axial velocity. Upon reaching the steep gradient at the interface it suddenly encounters a fluid of much greater axial velocity, and a violent interaction occurs. This interaction creates a great deal of turbulent motion and the movements of the fluid elements within it are very intense, abrupt, and chaotic. The entire structure has a very small scale. The intensity of this interaction destroys the identity of the individual

elements. The interaction not only occurs between the mean flow and the ejected element, but the continual ejection of fluid into this chaotic mass by the remainder of the original elements and others which may occur at approximately the same time causes increased interaction and mixing. All this agitation results in some fluid being directed wallward and in all directions. The wallward movement enters the sublayer region and agitates the fluid there. Some elements re-emerge, but many are captured within this region and persist as less violent disturbances. The depth of penetration is random, but generally greater penetration and intensity occur at higher Reynolds numbers. Penetration to the wall is observed.

The position of the zone of interaction changes with the position of the interface. Most commonly the interaction zone occurs over the region $7 \leq y^+ \leq 30$.

Once within the interaction zone, the fluid experiences a rapid acceleration downstream. However, the disturbed motions continue to spread radially outward, so a general diffusion both axially and toward the centerline occurs. This general growth in area is accompanied by a decrease in intensity.

The ejection phase ends with the entry from upstream of a stream of fluid which is directed primarily in an axial direction. This fluid has an axial velocity that corresponds to that which a normal velocity profile would

predict. Usually the ejections have subsided by the time it appears, and it sweeps the field of elements of retarded flow and re-establishes a semblance of a normal velocity profile.

The ejection process has the same basic character for all Reynolds numbers. The frequency of occurrence and intensity of disturbance do, however, exhibit a strong dependence on Reynolds number. The ejections occurred approximately five times more often at N_{Re} = 50,000 than N_{Re} = 20,000. This dichotomy in the nature of this basic event is interesting. In the fundamental structure and form the dependency is independent of mean flow parameter, and seems only dependent upon local conditions. Thus the sequence of events, the ejection angles, the small scale, and the general random behavior are divorced from mean flow dependency. However, the frequency of occurrence, the ejection velocity, and the position of the different zones show a distinct relation to mean flow parameters. It would appear that the mean flow situation operates to provide conditions locally which are conducive to the occurrence of an event, but that the event depends directly only upon the local conditions.

As the distance from the wall increases, the character of the fluid motions changes. In the wall region and out to just beyond the interaction zone, i.e., $y^+ \doteq 50$, the motions are of small scale, intense, and abrupt. By $y^+ \doteq 70$ the

greater part of the change to conditions of the outer region have occurred. By $y^+ \doteq 150$ the change is completed and thereafter the changes occur only in degree but not in character. These outer regions have an increasingly larger scale of disturbance, but the intensity is reduced. The disturbances appear as large sweeps moving across the field of view at a large angle to the axis. The length is always much longer than the width. The motions are so much larger than the field of view that they are difficult to define. They also pass through the field so swiftly that the nature of their internal structure cannot be studied. They appear to be segments of a large structure which exists in the outer region.

The "two layer velocity" is felt to be a result of the local nature of the events in the wall region. It is most often associated with some aspect of the ejection process, and results from the local movements that occur within this process. The higher velocity part of the "two layer velocity" effect has a value which approximates that of the local mean velocity in the area of occurrence. It could be part of a larger structure wherein local events and relatively undisturbed streams are spaced about the tube wall, but no decision for or against this idea can be made from the evidence at hand.

DEDUCTIONS AND HYPOTHESIS

The observations and measurements presented in the previous sections can be supplemented by the measurements of others to permit a hypothesis to be constructed on the character of turbulent pipe flow and the generation and maintenance of turbulence.

It is convenient to divide the radial distance from the wall to the centerline of the pipe into three distinct regions, each of which display fluid motions of a particular character. While the character of the fluid motion is quite distinct, the lines of demarcation between regions is not sharp and a degree of overlapping occurs between adjacent zones.

Sublayer $0 \leq y^+ \leq 5$

This may be called the sublayer region, but the adjective "laminar" is not used because the fluid motions with this region are definitely not laminar. The fluid within it continually exhibits departures from rectilinear flow in the form of excursions of small masses of fluid moving at some angle to the wall and the mean axial flow. The disturbances are three dimensional. The amount of fluid involved in any single movement is quite small, indicating a

rather small scale of disturbance. These disturbed elements rarely leave the region, although a few with particularly strong deviating velocities do escape outward. The fluid motions within this zone which depart from the mean axial motion are, for the most part, produced and sustained by the turbulence generated in the adjacent region, appropriately called the generation region. A small part of the turbulence created in the generation region is transferred to the sublayer region both by viscous transfer and turbulent diffusion. The degree of disturbance within the sublayer is dependent upon the degree of turbulence within the generation zone. Since this latter is dependent on the Reynolds number of the flow, (the range of Reynolds numbers covered was 10,000-50,000), a definite dependency on Reynolds number exists for the disturbed motions within the sublayer. This manifests itself in the form of a greater number of deviations from axial flow with increasing Reynolds number. At higher Reynolds numbers, fluid from the generation region repeatedly penetrates deeply into this region, and occasionally some penetrates to the wall. This penetration indicates that a mixing process is occurring not only within the sublayer region, but between this region and fluid from the generation region. Such a mixing and agitating process is very important in mass and heat transfer considerations. Since the generation region exhibits a nonregular periodicity in time, the sublayer region does too. However, the periodicity

within the sublayer is much less pronounced due to attenuation and averaging effects.

Generation region $5 < y^+ \leq 70$

This is the most important region since within it the major generation and dissipation of turbulence energy occurs. While its limits approximately coincide with the commonly described buffer zone, it cannot in any way be considered such a zone. Instead of a relatively passive transitional zone, this region is the position of origin of the majority of the fluid ejections, and also contains the positions where the maximum interaction of these ejections with the higher axial velocity of the mean stream occurs. It is proposed that these interactions of the ejected fluid with the mean flow, and between the different ejections which may occur nearly simultaneously and interact with one another within the same region is a mechanism whereby energy is extracted from the mean flow and converted into turbulence energy. Furthermore, this region is the source of most of the turbulence created, and from here it diffuses or is otherwise transferred to other regions of the pipe. The nature of the interaction, being of high shear and involving individually small elements of fluid results in a small scale of turbulence and a very disorganized chaotic motion. A large part of the turbulence energy created here is also dissipated here. The small scale, energetic motions create, locally, very high

velocity gradients which cause high rates of shear. The rate of dissipation of the turbulence energy to heat is a function of the local shear rates, so if they are large, the dissipation is large. The turbulence energy which is not dissipated diffuses or is convected away to other regions. A small portion goes to sustain the sublayer disturbances, but the greater amount diffuses outward toward the pipe centerline. The outward diffusion and resulting spread of the turbulence results in an increase in size of the area having connected movements, i.e., the scale of the turbulence increases. The intensity of the disturbance compared to the local mean velocity decreases. The most important feature of this process is the ejection of fluid elements outward from the wall area, $5 < y^+ \leq 15$, to other regions where they interact. The region of most intense interaction is $7 \leq y^+ \leq 30$. The character of these ejections is basically dependent on local conditions. The ejections do, however, exhibit dependency on mean flow parameters with regard to the frequency of occurrence and velocity of ejection. The connection between the mean flow and the local conditions which creates this dependency is not apparent from the data. It may be that some large scale, slow moving eddy within the mean flow influences in a random fashion certain local areas of the wall region and provides conditions conducive to the production of ejection events. The deceleration and wall-ward drift sequences might be a manifestation of this

influence. Both these events occur, but not with the same frequency as the ejection event. Certainly continuity requires that there be a return flow into the wall region, and since it was so infrequently observed it probably was of a large scale, low velocity nature. The ejections might be related to pressure fluctuation which must accompany velocity fluctuation. In fact, the diffusion of pressure energy or flow work, which was calculated by Laufer (31) as the closing term in the turbulence energy equation, does have a maximum in this region, and the direction of diffusion is wallward.

Aside from what has been said above, the data reveal nothing more about how or why the ejection event originates. Other authors, Ferrarri (11) and Grant (13), have attempted to explain similar type occurrences by introducing the effects of pressure fluctuations and gradients, and local instabilities due to vortex stretching. Grant in particular observed jets of fluid emanating from the edges of turbulent wakes and projecting into the main stream. He reasoned that the initial conversion of the mean flow energy to turbulence energy favors certain components, the ones aligned with the direction of stretching of the vortex element. This results in stress being established in the wake which eventually must be relieved. He proposes that the jetting fluid elements represent a secondary flow caused by the stress relieving process. This is, of course, speculative. There simply is

not enough information available to explain the cause of the ejection phenomenon.

Core region $y^+ > 70$

The eddies in this region have all been created in the generation region and have diffused or been convected to this position. This process tends to expand the original eddy so the size increases with increasing distance from the generation region. The intensity of the turbulence decreases with increasing y^+ value. Much of the change in character from the generation region to this region occurs within the approximate limits $50 < y^+ \leq 100$, but the entire zone of $50 < y^+ \leq 150$ may in a sense be considered transitional. Beyond approximately $y^+ = 150$ the changes are less marked and even the growth in eddy size proceeds at a diminished rate. The size and reduced relative motions do not create much turbulence. Nor are these characteristics likely to cause much dissipation, although within the large scale eddies, the small scale will produce some.

This entire region contains eddies which originated within the generation region of various upstream positions. It is more dependent upon what occurred upstream than what is occurring in the wall region at the particular time or axial position at which it is observed. This is a result of the fact that the turbulence requires a finite time to diffuse outward, and the velocity profile which causes the core

region to move much faster axially than the inner regions. The core region, therefore, contains an average sampling of much that has occurred in the inner regions upstream, and as such is a history of these events. This process tends to produce an integral effect on the nature of the motions in this region which eliminates much of the periodicity and local character of the generation zone. It also produces a rather stable character where the fluid motions respond only slowly to local changes which would affect the generation and sublayer regions very quickly. This dependency on preceding events but not to events which are local in space or time could be a factor in the explanation as to how the mean flow affects the local conditions which produce the ejection events. The mean flow since it is an integrated result of past local conditions is somewhat independent of the individual events, but not of the over-all process. Thus local conditions from upstream transmit their combined effect through the mean flow to influence local conditions downstream.

A drawing which shows the position and nature of the different regions superimposed on a turbulent velocity profile appears in Figure 28.

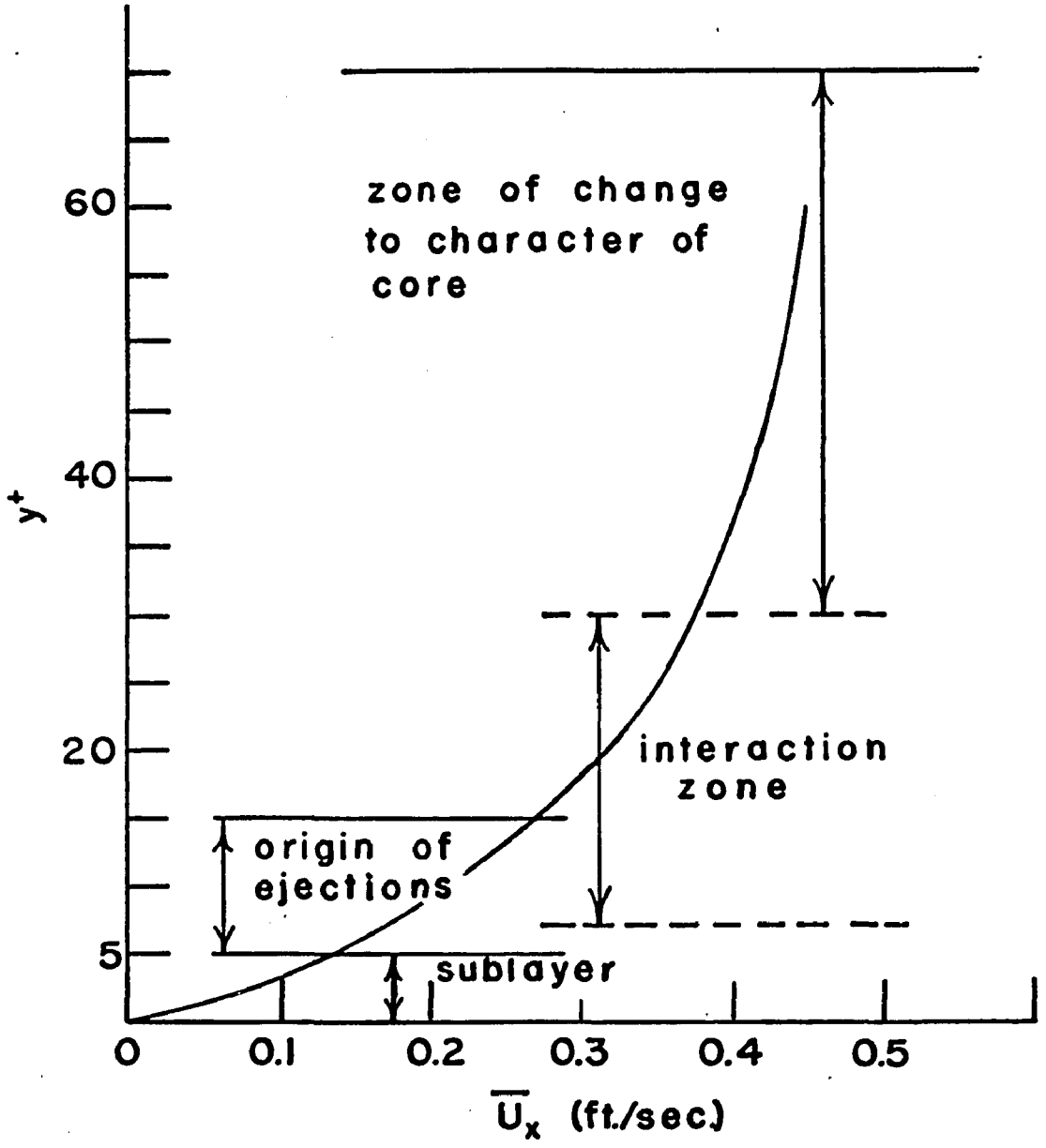

Figure 28. Wall Region Structure

DISCUSSION AND COMPARISON WITH OTHER DATA

The results presented in the preceding sections will now be discussed and compared to the measurements and observations that others have made of the nature of the wall region. These investigators have employed visual-photographic, indirect, and direct quantitative experimental techniques in the various studies. Each of these methods reveals aspects of the nature of this region from a slightly different viewpoint, and they will be considered separately in this section.

Visualization studies

Fage and Townend (10) using an ultramicroscope technique, similar in some respects to the technique employed in the present study, examined visually the character of the fluid motion very near a solid boundary for fully turbulent flow in a square tube. They used a magnification of 200X which gave them a field diameter of 0.03 inches. In the region of $0 \leq y^+ \leq 4$ they noted that the fluid elements continually exhibited departures from truly rectilinear flow. These departures were described as deviations of particles off of the rectilinear path such that their trajectories were at various angles to the wall. These

motions occurred in both the xy and xz planes. The particles were also observed to execute oscillatory movements as they crossed back and forth over a hairline in the microscope eyepiece. They also observed that occasionally two deviating particles separated by a "large distance" moved very similarly, i.e., connected movement in a lateral direction. Since their field of view was only 0.03 inches in diameter, this "large distance" could at most have been of this magnitude. Fage and Townend measured the angles which the deviating particles made with the tube axis at various positions from the wall. In reporting the maximum angles observed, they noted that the angles occurring in the plane parallel to the wall (maximum angle $\doteq 27^{\circ}$), were larger than those occurring in the plane perpendicular to the wall (maximum angle $\doteq 10^{\circ}$). The intensity of turbulence within the region examined was observed to be independent of Reynolds number. However, the frequency of occurrence of disturbed to quiescent periods definitely increased with Reynolds number over the limited range studied.

In most respects the observations of Fage and Townend agree with the results of the present study. The evidence of disturbed motion within the sublayer region, its character and dependence on Reynolds number all agree. The magnitude of the large lateral excursions agrees quite well with the dimensions observed in the corresponding view (top view) in the present study for evidence of ejection events within the

sublayer. This dimension was given as 0.011 x 0.043 inches. The angles of the deviation agree in both magnitude, and in dependency on the plane in which they are occurring, as an examination of Tables 5 and 9 will show.

Fage and Townend did not report any events which correspond directly to the ejection process. The failure to observe this effect was probably due to the limitations of the experimental procedures. They had to rely entirely upon visual examinations, and thus had no way to compare, adequately, different parts of the stream after they had passed the small field of view. Additionally, they concentrated most of the investigation on the sublayer region very near the wall where the ejection process does not occur. When they did examine the regions away from the wall, the rapid passage of the flow through the field of view most likely prohibited any observation of the process. The oscillations they reported for the deviating particles were not observed very often in the present study. At very high magnifications, such as they used, the small movement comprising the oscillation would be visible, but at the much lower magnification of the present study it would probably not be discernible, or at least not as an oscillation.

Fage (9) later performed some similar investigations in a circular pipe and observed much the same motions as in the previous study. He measured the angles of deviation for various radial positions and Reynolds numbers. At any

position, he observed a distribution of angles and reported the maximum angles measured for the xy plane. In the wall region these angles are of the order of 11° to 21°. Interestingly, when the angles for N_{Re} = 13,440 and N_{Re} = 18,340 are compared, one finds that for the same radial position, the angles are approximately the same, i.e., no effect of Reynolds number. The value presented for the intensity of fluctuating velocity, $u_y/\bar{U}_x$, near the wall is of the order of 0.2. An examination of Table 5 at N_{Re} = 20,000 shows that a value for this term in the present study is approximately 0.1 to 0.2.

A great deal of information concerning the nature of the fluid motion in the wall region in turbulent flow has been obtained for boundary layer flow over a flat plate. The reason for this, in addition to the interest in this type of flow, is that in this flow configuration the simple geometry and relatively large dimensions permit measurements to be more readily made than in the other types of flow. If the comparison is restricted to the wall regions, these measurements can, to a degree, be applied to pipe flows as well. This similarity of flow in the wall regions for pipes and boundary layers over flat plates has been considered by Clauser (2), Townsend (66), and Hinze (20), and the measurements of Klebanoff (26) and Laufer (20) support the conclusions. Since this matter is adequately discussed by these

and other authors, it will not be considered any further here.

Kline and Runstadler (28) and Runstadler, Kline, and Reynolds (51) have made extensive visual and photographic studies of the turbulent boundary layer by employing dye and hydrogen bubble injection techniques. These studies permit an excellent comparison with the present work, provided one remembers that there is a basic difference in the two techniques employed. This difference has, in part, been discussed in the section on experimental procedures. In addition to what was said there, there are differences in the photographic techniques of the two studies which warrant some mention. Runstadler et al. did not magnify their images to any extent. They therefore had a rather large field of view, nearly 100 times or greater than the one of the present study, and also an enormous depth of field. Although they at times moved the camera downstream, it was not matched to any particular stream velocity. Also, the filming speed was considerably slower than that used in the present study. All these factors contributed to give them a large, over-all view of the flow, but the higher speed, small scale details could not be observed adequately. The present study permits the more detailed, high speed, fine structure to be examined, but the small field precludes a view of the over-all situation. There are, of course, areas of overlap between the two techniques.

The observations by Runstadler et al., of the general features of the flow, and even some of the detailed structure, show a striking similarity to the observations of the present study. They divided the boundary layer into a number of distinct regions measured from the plate surface. Since only the inner regions near the wall can be compared with pipe flow data, the discussion will be limited to this area. In the region $0 \leq y^+ \leq 10$, they reported the presence of a very regular pattern distributed in a spanwise direction. This pattern consisted of streaks of low $\overline{U}_x$ velocity fluid alternating with high $\overline{U}_x$ velocity fluid. The streaks had a much greater axial dimension than the other two dimensions. While the pattern was quite regular, the streaks were destroyed and re-established with a random distribution so that their existence at any given position was limited. The streak spacing was found to be function of Reynolds number, and was correlated with the mean boundary layer flow parameters by the relation $76.5 = \lambda^+ = (\lambda u^*)/\nu$. These low $\overline{U}_x$ velocity streaks were observed to develop a wavy configuration, and then were observed to be suddenly ejected or lifted outward from the wall in a thin loop-like filament. These filaments moved outward into a region somewhat further removed from the wall where they were broken up by interaction with the flow. The region $0 \leq y^+ \leq 10$ was reported to be the position of origin of all such filaments. The process of ejection appearedto them to be random in both space and

time. The frequency of occurrence, however, was found to be markedly dependent on Reynolds number (for the limited range studied), but no good correlation with mean stream or local parameters was found. The angles which the ejected loops made with the wall were measured, and showed a wide distribution from a maximum angle of approximately 26° downward to 0°. All were directed downstream.

The region of turbulence into which the filaments were ejected, and where they were disrupted was located at $10 < y^{+} \leq 40$. This was reported to be a region of great turbulent activity.

The authors also reported a general increase in the size of the eddies and a decrease in intensity as the distance from the wall increased. This was supported by hot wire traverses which also showed that in the $0 \leq y^{+} \leq 10$ region the pulses caused by fluctuations were positive, but in the $10 < y^{+} \leq 40$ region they were negative.

The agreement of the observations of Runstadler et al. with the present study is excellent. In nearly all respects where the different techniques permit a comparison to be made, the same results were observed. The techniques used in the present study, however, permitted a detailed investigation into the nature of these events, while the dye injection studies could only provide an outline.

Runstadler et al. designated the region of origin of the majority of the ejected loops as $0 \leq y^+ \leq 10$, but noted that even within this region the activity was reduced as the wall was approached. Compare this to the present study, where the region, $0 \leq y^+ \leq 5$ was designated as disturbed, with only infrequent ejections originating there, and the assignment of the region $5 < y^+ \leq 15$ as the position of origin of most ejections. Also, the present study proposes a generation zone of major activity in the region $7 \leq y^+ \leq 30$ which compares quite well with the highly turbulent zone of activity reported by Runstadler et al. as $10 < y^+ \leq 40$. The small differences in reported limits of the zones is more likely due to the somewhat subjective decisions which must be made, than to any real difference in the nature and position of these zones. The interesting result reported by Runstadler et al. concerning the reversal in the polarity of the pulses of fluctuating velocity agree with the observations of the present study that the ejection event originating at a position somewhat removed from the $y^+ < 5$ region penetrates into that region and thus appears as a positive pulse of higher velocity fluid against a lower velocity background. The reverse situation also holds true for the region at $y^+ > 5$.

The frequency of ejection, while dependent upon Reynolds number in a similar fashion for both studies, cannot be compared in absolute terms. The reason is that

Runstadler et al. observed a much larger field, and thereby effectively obtained an average over this area. This eliminated the influence of the random behavior of the ejections upon the value. In the present study, the small field of view and the scanning action of the camera make the observations of occurrence frequency very susceptible to the randomness of the ejection process. Therefore, any extrapolation of these observations to absolute numbers on a basis similar to Runstadler's would be most uncertain and perhaps impossible.

This can be made somewhat more specific as follows. Using u* as a similarity factor, the Reynolds numbers of 1.35×10^6 and 8.4×10^5 for which much of the data of Runstadler et al. was obtained correspond to pipe flow conditions of $N_{Re} = 18,500$ and 13,000 respectively. Since the data of the present study seem to show a much reduced ejection frequency at these Reynolds numbers than do the other data, it might seem that a disagreement exists. This is not so. It has already been demonstrated that the ejection process is a small scaled, locally occurring event. With the small field of view of the present system, only a very small area could be examined for events at any instant. Thus for an event to be seen requires the double coincidence of having it occur and do so in the field of view. Since Runstadler et al. made their frequency count for a large number of streaks which appeared simultaneously within a large area of

view it generally was necessary only for the ejection to occur for it to be seen. Since the process of ejection is random, even an attempt to base the frequency on a unit area will not be successful. Therefore, while the frequency data of the present study are adequate for an internal comparison, they cannot be used to obtain absolute values. The data of Runstadler et al. are probably a more correct representation of these values. Since their data also showed a highly non-linear increase in frequency with increasing Reynolds number, the above reasoning can also explain the infrequent or total lack of delection of ejection events for $N_{Re} < 10,000$.

The agreement between the angles of ejection reported and those measured in this study is excellent. Runstadler reported a distribution of angles about a most favored angle. For the two cases reported ($N_{Re_x} = 1.35 \times 10^6$ and 8.4×10^5) the maximum angle was 26°. The most favored trajectory showed a slight dependency on Reynolds number, i.e., 13° for $N_{Re_x} = 8.4 \times 10^5$ and 10° for $N_{Re_x} = 1.35 \times 10^6$, but, as can be seen, this dependency was quite small. The present study showed no such dependency over the range of $N_{Re} = 2 \times 10^4$ to 5×10^4. The maximum angle observed was 21°, and the average ejection angle was 8.5° for pipe flow.

One might question the fact that the present study did not reveal any "spanwise" structure. In pipe flow this would be distributed about the periphery of the inner wall. This has been discussed in part in the section treating the

top view analysis. If one assumes that Runstadler's correlation for spacing is valid in pipe flow, the spacing for N_{Re} = 20,000 and 50,000 is 0.131 and 0.59 inches respectively. In the top view study, the field width was 0.147 inches. Thus, a maximum of only two streaks might appear in the field. This limited pattern would be impossible to discern against the confusing background of the top view. The wall view has a similar size problem. In this view the depth of field is the limiting dimension for observation of this effect. At 4.3X and 2X magnification this depth is 0.027 and 0.041 inches respectively. The depths are clearly less than the dimension of a single spacing interval, and one cannot hope to see a "spanwise" pattern except when the focus fortuitously coincides with the interface between two streaks of different velocity. With the unsteady nature of the streak structure, this coincidence is highly unlikely to occur very often. In short, one cannot hope to observe an unsteady pattern which in the smallest scale is larger than the field of view.

The "two layer velocity" reported in an earlier section might be an indication of such a "spanwise" pattern. One interesting comparison in this regard can be made between the measured ratio of $\overline{U}_x$ velocities for adjacent high and low velocity streaks measured by Runstadler, and the similar ratio for "two layer velocities." The first gave a value of 1.59/1, while the second had a most common value of 1.5/1.

No conclusion on the existence of a "spanwise" type distribution for pipe flow can be reached. The "two layer velocity" definitely exists, but whether it is a purely local occurrence or part of a large, ordered structure could not be determined.

Runstadler et al. never reported any deceleration-acceleration effect similar to that described in the detailed analysis of the ejection process. This could be due to limitations in their experimental equipment which were discussed earlier. Runstadler et al. also discuss some of these limitations in their paper.

Nedderman (40) by a technique of still photography, and using small air bubbles in water to mark the fluid elements, measured instantaneous velocities in the region of $0 < y^+ \leq 30$ in pipe flow. From these measurements he determined mean velocities which agreed with those obtained by others in air. For $N_{Re} = 1200$, he observed an excellent agreement between the instantaneous velocities and those predicted for a laminar profile. However, at $N_{Re} = 12,000$ and 19,000 he observed a rather wide distribution of these instantaneous values about the mean velocity profile for turbulent flow. This he concludes is clear evidence that the flow is disturbed at least to $y^+ = 1$ and below. The magnitude of the deviation from the mean profile of the measured velocities increased as the y^+ value where they were measured increased. The field of view was 0.196 x 0.196 inches square,

and 0.04 inches in depth. The bubble concentration was quite "dilute" so that in any given photograph only several bubbles were present. Nedderman noted that at no time did any of the few bubbles present appear to be moving in a similar (connected) fashion at the same instantaneous velocity. From this he concluded that the eddy scale must be smaller than the field of view. Finally, he reported that on a few occasions he saw two particles, one directly behind the other (that is, at a different depth along the line of sight), with the one at a greater y^+ position moving more slowly than the one at the smaller y^+ position.

To the extent that a comparison can be made, these results agree with the observations of this present study. The report of a disturbed motion at a $y^+ \doteq 1$ compares with the observed activity at $y^+ \doteq 2$ or less. Additionally, the increasing deviation of the instantaneous velocity distribution with increasing y^+ position over the range $0 < y^+ \leq 30$, corresponds to the increase in turbulent activity in this region observed in the present study. The maximum scale of the eddies within this region, as determined by Nedderman, agree in magnitude with the observed scale of 0.03 to 0.06 inches wide by 0.01 to 0.03 inches deep. Of course, the use of still photography and the "dilute" bubble concentration precluded any measurements by Nedderman of a fine scaled motion or time dependent effects. The unusual behavior of

the two bubbles with inverted instantaneous velocities reported by Nedderman can easily be explained by the "two layer velocity" effect discussed previously.

Although no conclusion regarding the existence of a "spanwise" or peripheral pattern of longitudinal velocity elements could be reached in the present study, some other investigators report results which give support to the concept.

Richardson and Beatty (49) examined the displacement of a uniformly dyed liquid by an undyed liquid in a vertical tube, and found a regular distribution of longitudinal streaks of high and low dye concentration about the periphery of the tube. They estimated that these streaks occurred within a $y^+ = 5$ distance from the wall.

Hopkins, Keating, and Bandettini (21), while studying the supersonic airflow over a flat plate, also obtained indications of a spanwise distribution in the form of longitudinal streaks. They observed these by photographing the surface of the plate in ultraviolet light after it first had been coated with a fluorescent dye. The spacing decreased with increasing Reynolds number, and was generally of the order of 2.5 times the boundary layer thickness.

The preceding are essentially all the visual studies which have a direct relationship to the present investigation. There are, however, a few studies which, while not directly related, are of interest. These are concerned primarily with transition.

Hama, Long, and Hegarty (15) studied the motions of a dye stream which was injected through a slit on the surface of a flat plate which was towed through water. A trip wire attached to the plate was used to produce a disturbance in an otherwise laminar flow. Atfirst only a two-dimensional vortex line was shed from the wire, and it did not develop further. Upon increasing the towing speed, the two-dimensional disturbance was observed to develop a spanwise waviness which intensified as the disturbance moved downstream. At sufficiently high towing speeds, this now three-dimensional vortex line was observed to gradually develop a loop-like structure with the tip of the loop using up off of the plate surface. The loop continued to rise and underwent acceleration and stretching until it was caused to "neck down" just below the tip which by this time extended well into the boundary layer. From the region of the necked down area, bursts of fluid moving outward from the loop occurred which disrupted the loop. Hama (14) furthered the investigation by substituting a vibrating ribbon for the wire. His results were similar to the other study. Since the ribbon vibrated in a vertical plane, two vortex lines were shed, one at each change of direction. Only the one shed into the area of high shear showed the development into the loop structure. Hama devotes a number of articles to a discussion of these matters, but they will not be treated here.

Weske (71) investigated the development of vortex structures similar to the above for pipe flow by using a trip wire and dye injection. In general his observations were in agreement with Hama's.

Indirect studies

The indirect approach to determining the nature of the fluid motion in the wall region was mentioned in the introduction section. At that time the difficulty of deciding which among the many models most nearly represented the physical reality was discussed. The necessity of using information from another source to accomplish this was mentioned. Now that this information is available from the present study, these models may be discussed. The data of this study are not of a nature which presents a quantitative test of the agreement of these models with the rate of transport. This type of data is not what is needed since their agreement with experimental transport data has already been demonstrated by the various authors. Instead, the present data invite a comparison between the physical situation as revealed by it, and the one assumed in the different models. This discussion is not meant to be a critique of the entire field since that is beyond the scope of this work. There are a number of review articles by Sherwood (56), Harriott (17), Perlmutter (43), Johnson et al. (23), which effectively accomplish this aim.

The articles to be discussed can arbitrarily be divided into two groups. One group gives rather detailed physical models from which certain mathematical relations are deduced, which are subsequently tested against experimental data. The other group gives no explicitly stated physical model except that implied by the nature of the mathematical relations, assumed or empirically deduced, regarding the eddy transport coefficient.

Considering these latter first, the analyses by Taylor (11), Van Kármán (70), Summerfield (60), and Deissler and Eian (7) all gave reasonable agreement with experimental data provided the N_{α} value is near unity (N_{α} is either the Schmidt or Prandtl number). If it is not, the relations fail. Nearly all which fail at large values of N_{α} do not allow for any eddy diffusivity in the sublayer region, $y^+ < 5$. They usually assumed the transport here was by purely molecular means, and that eddy diffusivity only was a factor outside of this region. Later analyses, using quite similar approaches as the above but allowing in some fashion for eddy diffusivity in the sublayer region were considerably more successful at predicting experimental data over a wide range of N_{α}. Lin, Moulton, and Putnam (34) introduced an assumed function $\epsilon/\nu = (y^+/14.5)^3$ for the value of the eddy diffusivity in the region of $y^+ < 5$. For the region $5 < y^+ \leq 33$ they differentiated the generalized velocity

profile relation and using the usual techniques, i.e., where $\tau_{wc} = -(\nu + \epsilon)\frac{du}{dy}$, they obtained the relation $\epsilon/\nu = y^+/5 - 0.959$. For the region of $y^+ > 33$, they used Reynolds analogy. The relation they obtained gave results which agreed well for gases with $N_{Sc} = .54 - 1.86$, and for liquids of $N_{Sc} = 320 - 3200$. They measured experimental concentration profiles which also agreed with their predicted profiles.

Deissler (6) used a similar approach and introduced an empirical relation for ϵ in the sublayer, $\epsilon = n^2uy(1-e^{\frac{-n^2uy}{\nu}})$ with $n = 0.124$. His relation gave excellent agreement with experimental data, and at large N_{Sc} is one of the best. Murphree (39) and Rannie (46) also developed expressions which are successful at high values of N_{Sc}.

Johnson, Marangozis, and Trass (23) examined the various relationships proposed, and upon finding that he could not choose among them on the basis of velocity profile data attempted a selection using mass transfer data. He found the best agreement with Deissler's relation for $N_{Sc} > 100$, but noted that other theories based on quite different assumptions also satisfied the data. They remarked that agreement of the relation with mass transfer data was not a satisfactory criteria for selection of the proper relation or model. Part of the difficulty, of course, arises from the fact that the value of ϵ is usually selected to

give good agreement with the data. Vieth, Porter, and Sherwood (68) pointed out that these relations give a value for the transfer coefficient which is dependent on $\sqrt{f}$, whereas the data are dependent upon f.

The most important feature of each of the successful analyses is that they have provided for the presence of an eddy diffusivity or turbulent fluctuation within the sublayer region. For large values of N_{α} , even a very small fluctuation in this region can be very important since molecular diffusivity is low. The results of the present research clearly show that a fluctuation does exist within the sublayer region, and to that extent they agree with the above relations. No estimate of the value or form of ϵ dependency on y^+, except that it decreases as y^+ decreases, can be deduced from the observations.

The second group approaching this problem attempted to avoid the difficulty of evaluating an eddy diffusivity in the wall region by creating rather detailed penetration-mixing models after the fashion of Danckwerts (5) and Higbie (19). All these models greatly simplified the fluid behavior in the wall region in order to obtain relations which were tractable. It should be noted that these models did not purport to exactly represent the actual motions, but were a tool for developing useful relations.

As in the previous cases, the discussion will not treat the individual merits of each model with regard to their ability to predict transport data. This has been done by the authors and in review articles. The intent here is to examine the general features of the motions predicted by the successful models, and compare them to the observations made in the present study. The aim is to decide which, if any, agree, and to suggest modifications which will cause the models to correspond more closely to reality.

The extension by Danckwerts (5) of Higbie's concepts resulted in the surface renewal theory which was the forerunner of many of the present models. In it he proposed that the sublayer of fluid at a boundary, which was usually held to be devoid of turbulent fluctuations was periodically disturbed by the penetration into the boundary of fluid elements originating within the bulk stream and possessing that concentration. Once at the boundary, equilibrium between the boundary and the surface of the element in contact was assumed to occur immediately, and transfer into the element was to proceed by unsteady state molecular diffusion. After a random time of contact, the element was replaced by a new one, and it returned to the bulk stream. The rate of renewal was dependent upon hydrodynamic conditions and geometry, and a distribution function for the rate of element renewal or age was proposed.

Hanratty (16) proceeded along these same lines and tested Danckwerts' model against mass transfer data by evaluating the rate of surface renewal terms using mass transfer data from a different source. He found good agreement with the data of Lin, Putnam, and Moulton (34). He also extended the analysis to momentum transfer by making a large number of simplifying assumptions. Despite this, he found fair agreement for the velocity profile predicted by this method and experimental profiles.

Toor and Marchello (63) extended these concepts to permit a steady state concentration gradient to become established within surface elements of sufficient age. Thus their analysis permitted molecular diffusion to proceed into the element by either the unsteady state or steady state rate depending upon the age distribution of the elements. As before, this distribution was related to the hydrodynamics of the system. For a given geometry, they observed little effect on transport if the surface renewal occurred randomly or at an average age. Using an average age approach, they found for water at N_{Re} = 10,000 and 50,000 a renewal rate of 0.21 sec^{-1} and 3.6 sec^{-1} respectively.

The above proposals all permitted a basically laminar sublayer to be periodically disturbed by fluid elements which entered it from positions further out in the flow, and which penetrated to the wall. At the wall they replaced the

fluid elements already there. These new elements were assumed to have the bulk stream concentration.

These models differ basically from the observed situation in two ways. First, it was observed that the fluid elements did not penetrate to the wall at all times, but penetrated to various depths of the sublayer. Secondly, although the above models permitted the bulk transport of mass by the element replacement mechanism, the transport into and through the fluid elements was considered to be by molecular means only. In the present study it was quite apparent that the fluid elements were highly disturbed within themselves, and that the sublayer fluid itself was somewhat disturbed.

An approximate comparison between the renewal rate reported by Toor and Marchello (63) and the ejection frequency of the present study may be made. At N_{Re} = 50,000 and 20,000, the ejection frequency was 4.3 sec^{-1} and 0.83 sec^{-1} respectively. Harriott (18) felt that Toor and Marchello's contact time of 6.2 seconds was too great and suggested a much higher rate of surface renewal. Since the contact time of 6.2 seconds is directly related to the renewal rate of 0.21 sec^{-1} by the form of the distribution function assumed, the results of the present study tend to support Toor and Marchello's estimate of contact time if both they and Harriott were considering similar models. This is not meant to imply that the model is supported.

Many authors have noted that the above models, while they yield relations which agree with the mass transfer data over a given range, predict for large N_{Sc} values that the over-all transfer coefficient will depend on the molecular diffusivity term, $D\theta$ or Ds, to the 0.5 power. Experimental data have shown this dependency to be to the 0.7 or 0.8 power at large N_{Sc}.

More recent articles have proposed complex models which avoid this difficulty and which in some respects reflect a truer picture of the actual situation.

Marchello and Toor (36) proposed for low turbulence flows that a low order of turbulence existed in the sublayer region which caused local mixing rather than gross displacement of the elements. The frequency and position within the sublayer of the mixing was made dependent upon hydrodynamic conditions. The actual mixing process was considered to occur randomly. The mixing process was confined to the region, and no bulk transport by elements moving out of the region was permitted. This meant that the transport from the wall to the mixing region and from the outer boundary of the mixing region to the main stream was by unsteady state molecular means only. The function of the mixing region was to steepen the concentration gradient locally, and thus enhance the molecular transport. This mixing also prevented a steady-state concentration gradient from forming.

The inclusion of a random mixing zone within the sublayer is an improvement over the other models, but the elimination of the bulk fluid elements from the region, and the assumption that transport is basically by molecular means only is at variance with the present study. At low turbulence levels, the lack of bulk elements is not too serious.

Harriott (18) proposed a model where the fluctuating fluid elements did not penetrate to the wall, but penetrated to varying distances from the wall in the sublayer region. He proposed that these elements swept all the fluid, up to the maximum depth of penetration, out into the main stream, and replaced this fluid by fluid of bulk stream concentration. Thus, the penetrating elements not only caused a bulk transport, but steepened the concentration gradient and therefore enhanced the molecular transport process. The transfer of mass into the elements and during the intervals between elements was by molecular means only for both the wall region and out to infinity. The penetrating elements were thought to originate from various locations beyond $y^+ = 5$, and had uniform concentrations equal to that of the bulk stream.

The order of complexity of this model is great. It not only allows a random distribution of element ages, but by having these elements penetrate to different depths they

cause different, randomly distributed, changes in the local concentration gradient. In final form, the relations were so complex that an analytical solution was not possible. A numerical trial and error procedure using a computer was devised which produced the results for a wide variety of somewhat arbitrarily selected input conditions. The most favorable results gave transfer coefficients which were consistent with experimental data over an N_{Sc} range of 100-3000. For $N_{Sc} \doteq 1$, the predicted values were too high by a factor of two.

In many respects this model agrees best with the observed fluid motions. The random frequency and depth of penetration, the varying position of origin, and the bulk transport of and by the fluid elements all are consistent. The differences arise mainly in the use of molecular diffusion as the sole means of transport within the elements and within the sublayer when there are no elements present. The present study clearly shows that eddy diffusion is occurring within any elements entering the region, and to a lesser extent within the sublayer. The assumption that all fluid elements originating beyond $y^+ = 5$ have bulk stream concentration was based upon Lin, Putnam, and Moulton's (34) data which showed this to be true for liquids (i.e., high N_{Sc}) but not so for gases or low N_{Sc} situations. For these latter, a significant concentration gradient existed at least out to

$y^+ = 10$. The result of such an assumption in Harriott's proposal would be to give too great a transfer coefficient for low N_{Sc}, because the elements originating within $y^+ = 10$ would have a higher concentration than the bulk stream.

Ruckenstein (52) proposed a model where the randomly occurring fluid elements only occasionally penetrated to the wall. At other times the new elements simply stripped off the outer portions of the older elements which remained in contact with the wall. Eventually, a new element penetrated to the wall and removed the old element. As in most of the previous cases, the transport to and through the elements was by molecular processes, and for the old wall element section, a steady-state gradient is permitted to become established.

Einstein and Li (8) proposed a quite different model. They envisioned a periodic growth and decay of the laminar sublayer. They considered that at the beginning of a cycle the turbulent flow extended to the wall, and as a result that a very high shear existed at the wall. This caused the fluid near the wall to be decelerated, and that this constituted the laminar sublayer which continued to grow with time. After some time, due to inherent instabilities and the action of the turbulent outer layers, this sublayer suddenly degenerated into turbulence, and re-established the turbulent flow to the very wall. The cycle then was repeated. They

attempted to measure this periodicity by measuring pressure fluctuations at the wall. They reasoned that these would necessarily accompany any velocity fluctuations, and that the periodicity would be more easily observed in the pressure than in the velocity fluctuations. Their results were not conclusive. They observed a regular periodicity in the auto-correlation curve of pressure fluctuations for one run, but they were not as evident in a second.

There are disagreements between this proposed model and the results of the present study. The model implies that large areas are involved in a connected fashion during the turbulence generation, but the present observations indicate that the generation is basically local and of small scale. Additionally, the model proposes a disintegration of the entire sublayer, but it was observed that the sublayer usually remains intact and is periodically disturbed.

As was stated earlier, one of the purposes of these comparisons was to assist in selecting the existing model which most nearly approximated the physical situation. It would appear that Harriott's (18) is in the best agreement, but even it differs in some basic respects from the observed situation. It is of value therefore to suggest some features that a new model should have. This new model would incorporate many of the better features of Harriott's. In all the previous models, the sublayer was considered to be basically

laminar, and therefore the region of major resistance. This concept is partially true. Since the primary region of turbulence generation, and therefore of extreme mixing, was observed to be approximately in the region $4 \lesssim y^+ \leq 32$, the region below $y^+ = 5$, although somewhat disturbed by this generation, is still one of major resistance to transfer. The difference arises in the fact that the sublayer is not laminar but is disturbed, and therefore some eddy transfer will occur in parallel with the molecular diffusion. Since the resistance here is so great, any contribution which enhances transfer must be important. A point should be made also on the significance of the observation that the region of turbulence generation occurs somewhat removed from the wall. If turbulence were generated at the wall, or to any great extent within the sublayer region, the resistance of this region to transport would be difficult to explain. The new model therefore would retain the sublayer concept, but would introduce a degree of eddy diffusivity, decreasing with y^+, to promote transport in parallel with the unsteady state molecular process. The concept of fluid elements from beyond $y^+ = 5$ penetrating to within random distances from the wall would be retained since it agrees very well with the observations. These elements, however, would cover smaller regions of the sublayer, so that at any time a larger portion of the sublayer would be free of elements than that

covered by them. This is required by the observed small size and local nature of the ejection elements. In this respect they differ from the other surface renewal elements which in toto were required to cover the entire surface. The diffusion through the elements would be by eddy diffusion because of the highly agitated state existing within them. This diffusion would therefore be quite rapid. The elements would not retain their identity for any length of time once they penetrated the sublayer, but would gradually decrease in intensity of motion until they were absorbed by the sublayer. As before, these elements would act to steepen the concentration gradient in the local area by bringing into it fluid of much lower concentration from outer regions. If necessary, the model could even permit a dependency of the concentration of these elements on position of origin. This would be in keeping with the observation that the position varied over the range $5 < y^+ \leq 15$, and for sufficiently low N_{Sc} conditions a concentration gradient might be operative. However, in view of the agitated conditions and the various sweeps that precede the ejection, it may be that such a consideration is unnecessary. The elements which penetrate the sublayer might be looked upon as "short circuits" through the resistant sublayer because of the comparatively rapid transport through them due to eddy diffusivity. Indications are that the frequency of penetration of elements into the sublayer is not very high, and certainly

less than the ejection frequency. The dual transfer paths by eddy and molecular processes through the sublayer coupled with the "short circuits" would tend to increase the transport rate over that of the other models. However, since the elements occupy a smaller area than previously, much more of the total quantity transferred must do so through the sublayer. This could effectively reduce the rate of transfer. Taken together then, it does not seem unreasonable to expect that the transfer rate which such a model would predict could agree with the actual transfer rates. In such a model, the frequency of penetration and not the age of the elements (although, of course, the two can be related in other models) would be the more important variable.

This model would unfortunately include the very thing the previous models sought to avoid, and that is the eddy diffusivity concept. In fact, it requires two eddy diffusivity coefficients, but as a first approximation one could consider the coefficient within the element to be a constant.

Any model attempting to include all the above suggestions would be extremely complex, and in all probability totally intractable. The suggestions, however, are of value because they indicate the nature that any model hoping to reflect the true nature of sublayer region must have.

While most of the discussion has been in terms of mass transfer, heat transfer could readily be substituted. However, the extension of these ideas to momentum transfer

requires special considerations. Hanratty (16) and Hinze (20) discuss some of these considerations.

Reiss and Hanratty (48) and more recently VanShaw and Hanratty (67) measured the fluctuation in concentration at the wall of a pipe in turbulent flow. They used probes buried in the wall surface, and a diffusion controlled electrochemical reaction. The smallest probe was 0.0259 inches in diameter, and was most sensitive to fluctuations perpendicular to the wall. In effect these measurements were designed to permit some deductions concerning velocity fluctuations. The intensity of mass transfer coefficient fluctuation was given as $k^{1/2}/\overline{K}$. They defined k as the fluctuating and $\overline{K}$ is the local mean transfer coefficient. This ratio was found to be approximately 0.47, and nearly independent of Reynolds number. Since in fully turbulent pipe flow there is no local mean velocity perpendicular to the wall, this expression has no exact counterpart in the present study. However, if one assumes that the mass transfer fluctuation is due in large measure to the velocity fluctuation perpendicular to the wall, some comparisons are possible. First, the presence of such a fluctuation at the wall strongly indicates that velocity fluctuations are occurring at the wall. Secondly, there is the independence of this intensity with regard to Reynolds number. Since the local mean rate of transfer must increase with increasing Reynolds

number, the independence of the term $k^{1/2}/\bar{K}$ to this number implies that $k^{1/2}$ is increasing proportionately. Since it has already been assumed by the above authors that the fluctuation in $k^{1/2}$ is a reflection of u_r fluctuations, this then also means that u_r is increasing with Reynolds number. This is exactly the same result that was obtained for the present investigation, and by very similar reasoning.

They also reported that the frequency of fluctuation was quite low, and presented a composite plot of mass transfer coefficient, velocity, and pressure spectra to support this. Of more particular interest were the two oscillograms of the ratio of local instantaneous mass transfer coefficient, K, to $\bar{K}$. One tracing was for N_{Re} = 19,700, and the other for N_{Re} = 43,100. Upon comparing the frequency of positive peaks in the transfer coefficient oscillograms with the frequency of ejection occurrences of the present study, one finds a very good agreement. The oscillograms showed the peaks to be nonregular in occurrence. More important, the frequency of peaking increases with N_{Re}, and at comparable N_{Re} the absolute magnitude of the frequency of peaking agrees rather well with the magnitude of the frequency of ejection and the ratio compares well with that obtained by the timing analysis of the present study. In interpreting this agreement, it must be noted that authors demonstrated a distinct effect on the measurements due to electrode diameter.

The larger the diameter, the lower the resolving power of the system. For the above measurements the electrode diameter was 0.0259 inches. This compares in magnitude to the size of connected movement in an ejection event, but is far greater than the scale of the lesser disturbances in the sublayer. Thus it would appear that the electrode could really "see" only the larger scaled events similar to an ejection.

Li (33) reported wall concentration fluctuations measured with a conductivity probe. Salt solutions were injected at the pipe centerline upstream of the probe. The probe had a working dimension of at least 0.016 inches. He reported concentration fluctuations in the frequency range of 100 sec^{-1}. These results are contrary to the above measurements and to the results of the present study.

Direct studies

It can be seen that as valuable as indirect approaches may be, in the final analysis, the investigation of the nature of the wall region must rely upon direct observation and measurement. The important visual studies have already been discussed. The number of investigations reporting quantitative measurements of turbulent characteristics within the sublayer region is very limited despite the acknowledged important of this region. This is mute testimony to the difficulty of obtaining such measurements.

Ludwieg and Tillman (36) measured local mean velocities into $y^+ \doteq 15$ for flow over a flat plate, and Reichardt (47) did the same for channel flow to $y^+ \doteq 2$. However, the only two measurements for turbulent characteristics within the sublayer were made by Klebanoff (26) in boundary layer flow, and Laufer (31) in pipe flow. Both used air as the fluid, and hot wire probes for the measurements. The similarity of these two flows in the wall region has already been mentioned, and the results of these studies confirms it.

Laufer presented intensities of the turbulent fluctuations as shown in Figures 29 and 30. It is clear from these that fluctuating velocities for all three components occur well within the sublayer. Figure 29 shows that a maximum in the u'_x/u^* distribution occurs at approximately $y^+ = 15$. Even at $y^+ \doteq 1.5$ the reported u'_x value is nearly 50% of the u^* value at $N_{Re} = 50,000$. The other components, while smaller, all have finite values well within $y^+ = 3$ which was the nearest position to the wall reported. Figure 30 shows that the term $u'_r/\bar{U}_x$ has a value of approximately 5% from $y^+ = 10$ outward to $y^+ = 70$. Within $y^+ = 10$, its value decreases toward zero. Since this is the radial component, it may be compared with the instantaneous radial velocity fluctuations observed in the present study. In this case the values are of the order of 10% to 20% of $\bar{U}_x$, and some are considerably larger. Although this may first appear to be in disagreement, it is not necessarily so. The observed

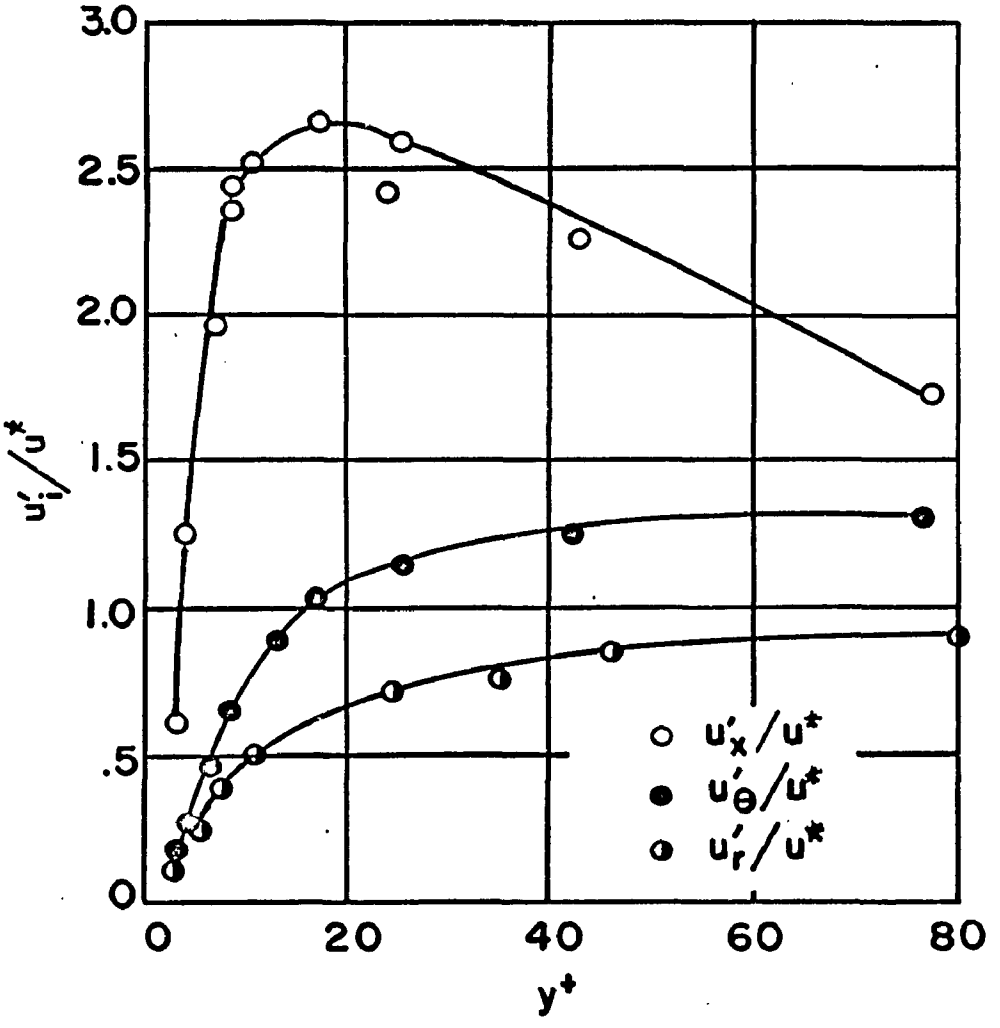

Figure 29. Relative Turbulent Intensities (Laufer, 31 p.17 $N_{Re} = 5 \times 10^4$)

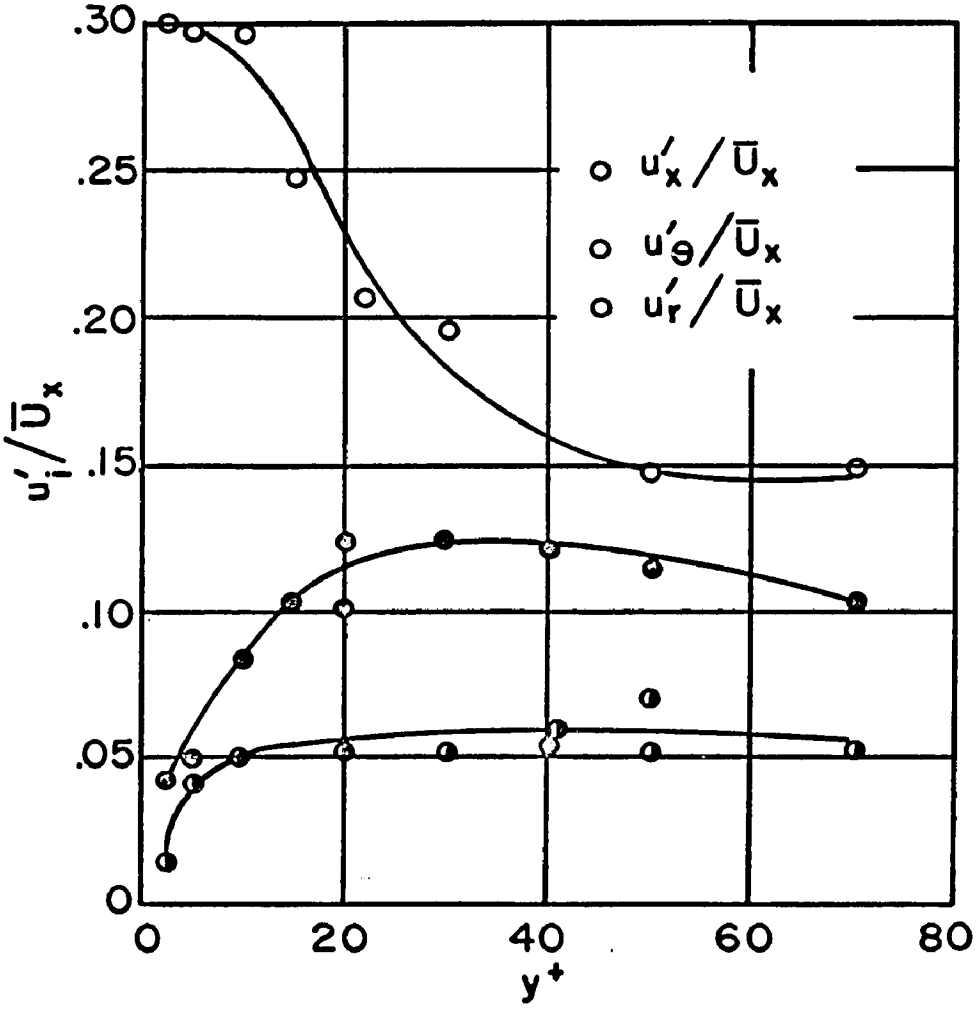

Figure 30. Relative Turbulent Intensities

(Laufer, 31 and Hinze, 20 $N_{Re} = 5 \times 10^5$)

values are instantaneous velocities while the u_r' values are time averaged values, which means they include those periods of low or zero fluctuation averaged with the higher fluctuations.

Klebanoff's data are similar to Laufer's in all important respects.

Although the data support the observed presence of velocity fluctuations within the sublayer, speculation on the significance of the appearance of a maximum in the u_x' intensity at $y^+ = 15$ is inviting. This maximum falls nearly midway in the region presented as the generation zone in the present study, $7 \leq y^+ \leq 30$. The maximum, of course, occurs only in the u_x' term. The other components are decreasing at this point, and show a slight increase with increasing y^+ position. It would not be amiss to suggest that the nature of the interactions within the generation zone might cause the maximum in the u_x' value, and that later as a result of the action of the accompanying pressure fluctuations this turbulence energy is distributed to the other components as well. Hinze (20) considers a simplified case, and suggests that the action of the generation and pressure-velocity gradient correlations might occur in just such a fashion. He did not, of course, consider any particular mechanism for the original generation of turbulence.

Another area where the data of Laufer and Klebanoff and the observations of the present study show good agreement is in the decrease in eddy size with decreasing distance from the wall. Laufer presented an energy spectrum on a wavenumber basis for both the u_x and u_r components. In both cases as the radial position of measurement was moved toward the wall, there was a definite shift in the wavenumber range toward larger values, i.e., smaller eddy sizes. Klebanoff's spectra not only showed this, but showed a decrease in the contribution to turbulent energy by the low wavenumber range as the wall was approached. Additional evidence of the same effect was reported by Hinze (20) who used Laufer's data for pipe flow and calculated the integral and dissipation length scales. Both scales showed an increase with increased distance from the wall.

It might also be noted that the concept of increasing eddy size with distance from the wall is tacitly assumed in Prandtl's mixing length theories.

Laufer also presented a plot of the distribution with distance from the wall of the terms of the turbulent energy equation. The only term he could not measure or estimate was the one for pressure energy, and he calculated it by the difference. Townsend (66) corrected these plots for the effect of the steep velocity gradient near the wall, and the resulting curves for the balance near the wall are presented

in Figure 31. These curves dramatically illustrate the importance of the region $5 \leq y^+ \leq 20$. Within this region, at approximately $y^+ = 11.5$, the production of turbulent energy is a maximum as is the dissipation of this energy. Additionally, the region shows a loss of energy by diffusion of kinetic energy out of it, and a gain caused by the diffusion of pressure energy into it. Also, there is a loss from the region due to the viscous transfer of kinetic energy especially towards the wall in the region $y^+ < 5$. A similar plot for the region removed from the wall shows that the production and dissipation of turbulent energy both decrease rapidly with increasing y^+. These regions also show a consistent loss due to the diffusion of pressure energy, and a consistent gain due to the diffusion into the region of kinetic energy from the wall area. Far out in the core of the pipe, the loss by dissipation is just valanced by the influx of kinetic energy. The above balances all pertain to turbulent energy. Thus the production of turbulence energy while positive in these balances would appear as a negative term in a balance for the mean flow energy. Laufer offered a plot showing how the loss of the mean flow energy is distributed between that which goes directly to viscious dissipation, and that which goes to turbulence production. This is reproduced as Figure 32. The curve for the loss to turbulence production has a maximum at $y^+ = 11.5$, which naturally

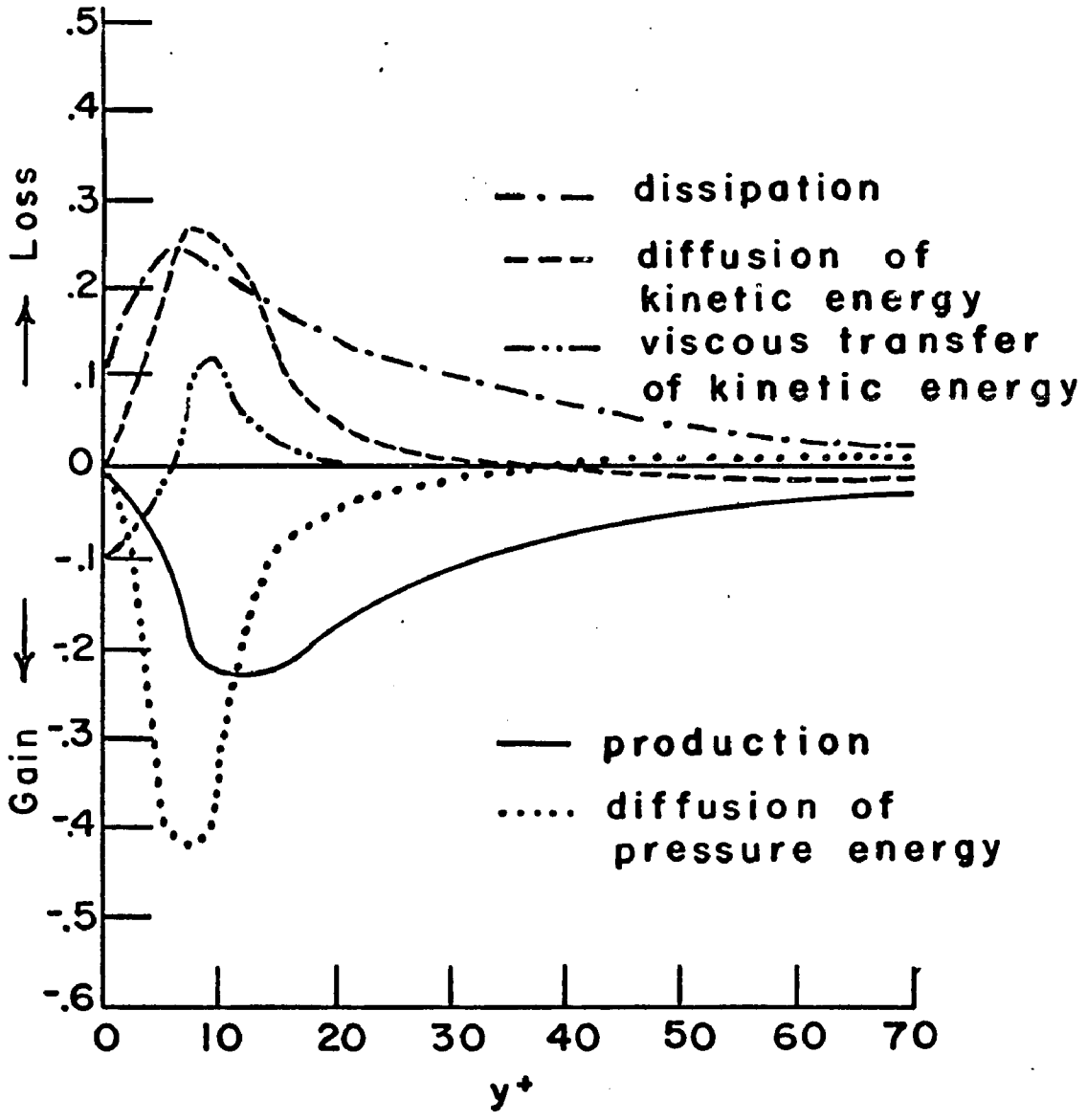

Figure 31. Turbulence Energy Balance in Wall Region
(Laufer, 31 as corrected by Townsend, 66; presented by Hinze, 20 p. 529.)

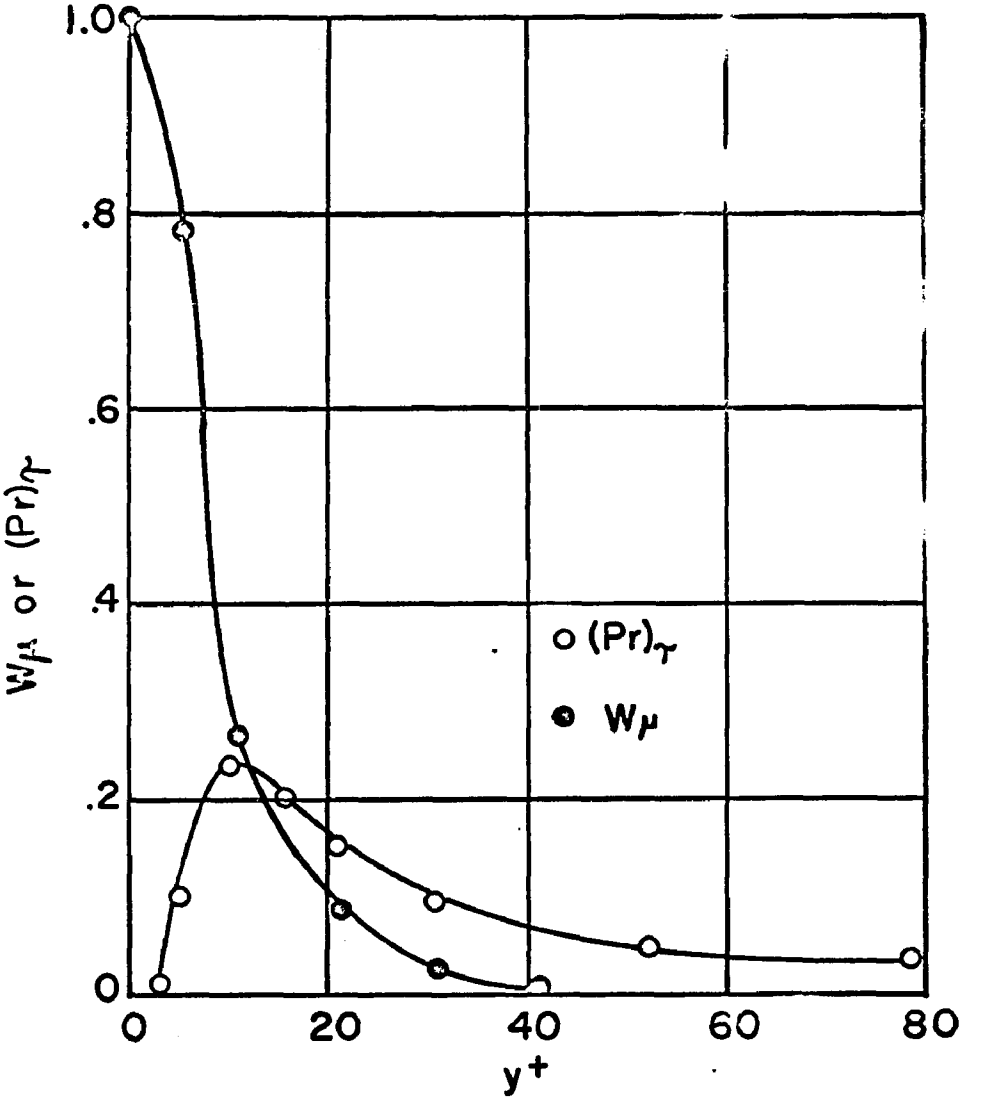

Figure 32. Turbulent Energy Production Rate Compared to Direct Viscous Dissipation

(Laufer, 31 p.13)

must agree with the maximum production position for the turbulent energy balance.

A qualitative comparison of the results of Laufer's investigation and those of the present study show the two to agree very well. The region where Laufer measured the greatest turbulence production by the conversion of mean flow energy to turbulence coincides with the generation zone of the present study. Additionally, it should be noted that the intense, chaotic nature and small scale of the motions within this zone are very likely to cause a high rate of dissipation of the turbulence, and again Laufer's data show this to be the case. The low rate of turbulence production and dissipation as measured by Laufer for the regions away from the wall are clearly in agreement with the nature of these regions as observed in the present study.

Hinze (20) after analyzing Laufer's results, proposed a picture of the structure of turbulent pipe flow. This graphical representation is reproduced as Figure 33. The agreement with nature and contributions to turbulence observed for the different regions in the present study is excellent.

Some mention should be made of Kolmogoroff's proposals concerning the relationship between the wavenumber of turbulence and the energy transfer and dissipation. He suggested that the large sized eddies (small wavenumber) do not lose much energy by viscous dissipation but instead transfer much of their energy to smaller scale eddies by inertial interac-

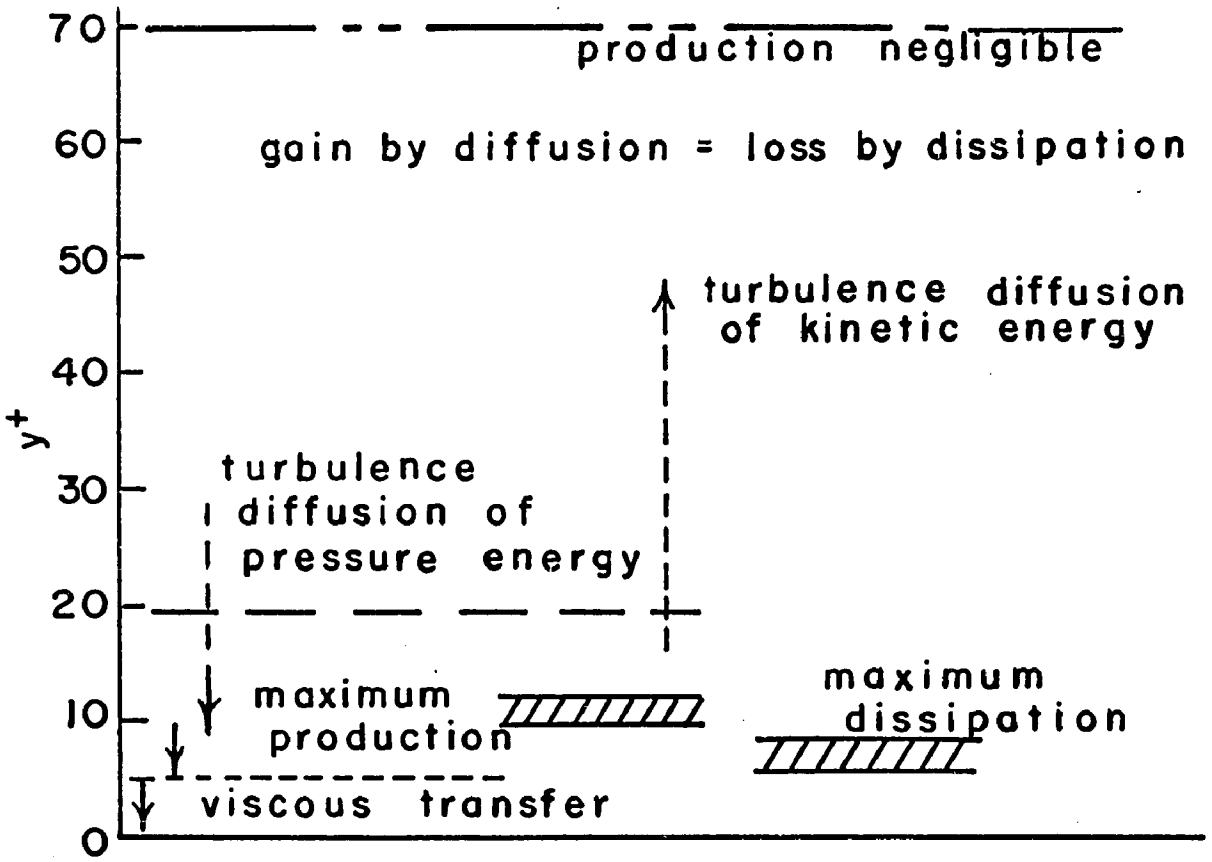

Figure 33. Processes in Turbulent Energy Balance

tion. The transfer of energy proceeds down the scale of turbulence to eddies of increasingly greater wavenumber until eventually a scale is reached where the loss of energy by viscous dissipation becomes significant. Thereafter, as the wavenumber increases, an increasingly greater portion of the turbulent energy is dissipated and less is transferred to the smaller scaled eddies. From these concepts, it is possible to divide the turbulence structure into different wavenumber ranges each of which are dependent upon different parameters. Thus the very low wavenumber ranges is dependent upon the forces and conditions which produce the large scale eddies, while the higher wavenumber ranges are isolated from these influences by the energy transfer chain and are independent of them. This permits the observation that, for sufficiently high N_{Re}, the high wavenumber range of turbulence approaches isotropy even though the actual flow may be anisotropic.

Since a possible relationship between velocity fluctuations and pressure fluctuations has been mentioned, a brief note concerning some measurements in this field is in order.

A number of authors have mentioned pressure fluctuations and correlations at the wall for boundary layer and pipe flow, and suggested that a correlation between fluctuating velocity and pressure should exist. However, until Serafini (55) no measurements of this correlation were made. Using air at Mach 0.6 in boundary layer flow, Serafini

measured the u_x' - P correlation. He commented that the u_r' fluctuation probably contributed most to the wall pressure fluctuation, but due to equipment limitations was unable to measure this. Of most interest all his findings that there were two distinct regions of the boundary layer which correlated best with the wall pressure fluctuations. One of these was the outer limits of the boundary layer where intermittency occurred. This would not be a factor for pipe flow. The other, and best correlated region, was located very near the wall. No conclusion regarding this result can be reached, but it is not contradictory to any proposals of the present study.

Related experiments

There are some experiments treating the transition from laminar to turbulent flow for boundary layer flows which show some very interesting results. These will be mentioned only briefly because their bearing upon the present study cannot be demonstrated, nor is any implied. The differences between the two physical situations are too great. For example, these experiments by Klebanoff, Tidstrom, and Sargent (27) and Kovasznay, Komoda, and Vasudeva (29) examined the early stages of transition by disturbing a basically laminar flow with a vibrating ribbon. Both groups observed the same phenomena, which was the development of a spanwise distribution in the form of high and low $\overline{U}_x$

velocities, and eventual amplification and distruption of this pattern. At the position called the breakdown the wave motion of the disturbance was observed to undergo an abrupt change accompanied by the appearance of a "spike" or sudden negatively directed pulse in the hot wire measurements. The flow at this time was still basically a disturbed laminar. Kovasznay et al., were able to demonstrate that this "spike" was really the intrusion of low velocity flow into the higher velocity shear layer in the form of a bump or kink in the shear layer. Thus the appearance of a negative velocity pulse was only the result of the probe being alternately exposed to a high velocity, a low velocity bump at the same y^+ position, and then high velocity again as the fluid flowed past it. This intruding element was observed to have a very large velocity outward from the plane, and to be rather small in its dimensions. The fluid ahead of and behind the upward moving fluid was observed to be moving toward the plane but much more slowly and over a larger area.

There is obviously a similarity in the description of the above occurrence and the observations of the present study. However, this similarity may very well be only a result of superficial coincidences and may not reflect any deeper relevancy. At present the information about either process is too meager to permit any conclusions, and in view of the vast differences between the two physical situations any further speculation would be most hazardous.

RECAPITULATION

The preceding discussion has demonstrated that the nature of the wall region in turbulent pipe flow as reported in this study is compatible with the results reported by numerous other investigators who used quite diverse methods of study. In many cases where a comparison of specific features or measurements was possible, there was good agreement. It is particularly important to note that the agreement quite often occurred between measurements, for the same feature, that were obtained by very different means. Thus in considering the scale of disturbance, the observed increase in size with increasing distance from the wall agreed quantitatively with the visual studies of Runstadler et al., and Nedderman, qualitatively with the hot wire measurements of Laufer, and with the indirect measurements of Van Shaw and Hanratty. The nature and position of certain distinct zones in the wall region agreed with the visual observations of others, and with the quantitative measurements of Laufer. The position of these regions corresponded approximately to the traditional division of sublayer, transition and core, but the nature of the regions was observed to be quite different from the traditional view.

The very fact that no one has before made visual studies of the wall region which would have revealed the details of the region on a par with the present study, precluded any possible comparison in this regard. The various aspects of such studies as were performed which did relate in some fashion to the present study, were found to be consistent with the present observations. In some cases, certain unexplained effects observed within those studies could be explained by the more detailed knowledge gained from the present study.

Finally, of the various models suggested for the calculation of transport rates, the ones that were considered to be most successful in all aspects for that purpose were found to contain various features of the wall region as revealed by this study. Since none of them were truly representative of the wall region, suggestions were made for a new model. With such a model, the sublayer ($y^+ \leq 5$) would retain its role as the primary source of resistance to transfer. However, the transport through the sublayer would proceed both by unsteady state molecular and eddy diffusion. The latter would decrease in magnitude as the wall was approached. The region $5 < y^+ \leq 15$ would be in a highly agitated state, and would at random send fluid elements into the sublayer. These elements would be small in size relative to the area at the wall, and would penetrate the sublayer to various depths. Transport through the elements would be by

eddy diffusion, and would be very rapid compared to transfer through the sublayer in general. The other function of such elements would be to cause the disturbances within the sublayer which cause the eddy transport, and to disturb the concentration gradient, which determines the rate of molecular transfer. In such a model the frequency of occurrence of the penetrating elements would be an important factor, but the age or contact time would not. Since the spatial distribution of the elements with regard to the peripheral location was apparently random, as a first approximation it might be assumed that they are uniformly distributed. The frequency of occurrence could also be assumed as some function of Reynolds number. The penetration depth into the sublayer is very important, and probably the best first approximation would be to assume a Gaussian type distribution distributed about the the plane $y^+ = 3$. These are suggested, of course, only as possible starting points for the development of a mathematical model.

If one established the mathematical relations for such a model, it would be possible to evaluate all the factors in the model except molecular diffusivity without using mass transfer data. The molecular diffusivity could be measured independently of the important factors under consideration. The other factors such as occurrence frequency and penetration depth could be evaluated from

hydrodynamic data alone. This model then could be checked against experimental mass transfer data with the knowledge that it had been established without any dependence on that data.

CONCLUSIONS

The following conclusions can be drawn from the experimental results of this investigation.

1) In turbulent pipe flow the turbulent motions have a distinctive character which is a function of the distance from the wall. Within the distance of $y^+ \leq 5$ the flow is not laminar, but is disturbed by velocity fluctuations of small magnitude, and by the intrusion of bulk elements of fluid from the adjacent region. The region $5 < y^+ \leq 70$ contains the position of origin of fluid ejections, $5 < y^+ \leq 15$, and the position of interaction of these elements with the main flow, $7 \leq y^+ \leq 30$, to create turbulence. The region beyond $y^+ > 70$ has reduced intensity of velocity fluctuations, and a larger scale of turbulence than the preceding region.

2) The most important feature of the wall region is the ejection of fluid elements which occurs there. These ejections are three dimensional disturbances which occur locally, and randomly with respect to time and axial position. They have a well defined character which is independent of mean flow parameters. The intensity and frequency of occurrence are, however, a measurable function of these parameters. The interaction of these elements with the mean flow creates turbulence.

3) An hypothesis is presented which defines the function and importance of the observed fluid motions in proper context with the known properties of turbulent flow. To the extent that a comparison is possible, the observed character of the wall region is not contradicted by any existing evidence, and in a number of cases is supported by results obtained by quite different means.

4) The role of the wall region with regard to mass and heat transfer processes was explored, and suggestions for a physical model from which a mathematical relation to predict these transfer rates might be derived are presented.

5) The application of a hot film anemometer to a liquid hydrocarbon system was accomplished, and probe stability comparable to that obtained in gases was observed. The radial distribution of u_r' was measured and found to compare in general character to the distribution measured in air.

6) An experimental technique was developed which permitted a detailed qualitative and somewhat quantitative investigation of the fluid motions in the wall region. This technique eliminated the necessity of introducing any measuring or injection device into the flow.

RECOMMENDATIONS

1) A continuing investigation of the wall region and turbulent flow using the established technique should be conducted to

(a) obtain accurate values for the frequency of occurrence of events on a unit area basis.

(b) Obtain further information which might reveal the underlying cause of the ejection events, and how the event which is local in character is connected to mean flow parameters. This might be undertaken in pipe flow or flow over a flat plate. The latter geometry would provide a larger wall region which could permit observations and measurements to be more easily made. It would be necessary to determine if the detailed fluid motions in the two geometries were the same.

2) Simultaneous hot film and photographic investigations of the entire turbulent flow field would be valuable in formulating a detailed, quantitative physical picture of the structure, and an aid in resolving some of the question posed in (1) above and in interpreting hot film signals.

3) The excellent stability of the hot film probe in trichloroethylene can be used to obtain a complete survey of

the statistical structure of turbulent shear flow in liquids similar to Laufer's study in air. By using trichloroethylene as the liquid, the stability problems which have plagued such measurements in water would be eliminated. This survey would permit a comparison between the measurements in air and liquids to resolve the question of similarity.

4) A new transport model which incorporates the suggestions presented in this study should be formulated mathematically. With this model, an attempt should be made to evaluate all parameters from hydrodynamic data only. This would eliminate the present common usage of heat and mass transfer data for this purpose. Comparing the predictions of this model with experimental transfer data would then provide an independent test.

5) A modified form of the experimental technique and simultaneous hot film measurements would make it possible to study the problems of dilute solid-liquid flows and to consider experimentally the particle-wall interaction problem (Appendix 1 and Soo and Tiens (58)). Particles of different dimensions could be used and the results compared.

APPENDIX I

Hinze (20) presents and discusses Tchen's (62) theoretical treatment for a small particle suspended in a turbulent fluid. The assumptions made by Tchen are that

1) The turbulence of the fluid is homogeneous and steady.

2) The domain of the turbulence is infinite in extent.

3) The particle is spherical and so small that its motion relative to the ambient fluid follows Stokes' law of resistance.

4) The particle is small compared with the smallest wavelength present in the turbulence.

5) During the motion of the particle the neighborhood will be formed by the same fluid particles.

6) Any external force acting on the particles originates from a potential field, such as gravity.

For the present case of pipe flow, neither assumption (1) nor (2) are valid because the flow is definitely confined, and the presence of the shear due to the confining boundaries does not permit homogeneous turbulence. Number (3) applies rather well although the particles are not spherical, they have a significant three dimensional structure and are

certainly small enough that the relative motion between them and the fluid, if any, would obey Stokes' law. Assumption (4) is also quite valid, as is assumption (6). As to assumption (5), as Hinze points out, since the fluid elements are deformed and stretched due to the turbulent motions, it is not likely that the same elements of fluid will remain with the particles for long periods of time. However, in the present case the particles are extremely small, much smaller than the scale imposed on the fluid elements by the shearing and stretching process. Thus it is not unreasonable to expect that the particles will remain in the vicinity of local fluid elements for relatively long periods of time. This would not be so for particles of larger dimensions. As stated before, the treatment is for a single particle which means that if other particles are present they do not cause any effect on the particle considered or the fluid surrounding it. To be valid for a fluid suspension, it requires that the volume concentration is very dilute. This is certainly true in the present case. Thus the only demands not reasonably met are those which the presence of confining walls prevents. The effect of the presence of walls was considered in the text when the work by Soo and Tiens (58) was discussed.

An outline of the development leading to the equation presented in the text will now be presented as given by

Hinze.[1] The starting point is the equation for slow motion of a spherical particle in a fluid moving with variable velocity. The coordinate system is assumed to move with the particle, and the external force field is neglected.

$$\underset{\text{I}}{\frac{\pi}{6} d^3 \rho_p \frac{Dv_p}{Dt}} = \underset{\text{II}}{3\pi\mu d(v_f - v_p)} + \underset{\text{III}}{\frac{\pi}{6} d^3 \rho_f \frac{Dv_f}{Dt}} + \underset{\text{IV}}{\frac{1}{2}\frac{\pi}{6} d^3 \rho_f \left(\frac{Dv_f}{Dt} - \frac{Dv_p}{Dt}\right)}$$

$$+ \frac{3}{2} d^2 \sqrt{\pi \rho_f \mu} \underset{\text{V}}{\int_{t_0}^{t}} \left(dt' \frac{Dv_f}{Dt'} - \frac{Dv_p}{Dt'} \Big/ \sqrt{t - t'}\right) \qquad \text{A-1}$$

In this equation the operator $\frac{D}{Dt}$ is the substantial derivative written for the coordinate system moving with the particle, i.e.,

$$\frac{D}{Dt} = \frac{\partial}{\partial t} + (v_P)_k \frac{\partial}{\partial X_k}$$

subscripts i, j, k are used for different components and coordinates.

where the rectangular coordinates are $X_k = X_1, X_2, X_3$. Subscript f refers to the fluid and P to the particle.

Term I is the force required to accelerate the particle, or the particle mass times acceleration. Term II is the force on the particle due to its movement relative to the fluid and is Stoke's law of resistance. Term III is the force exerted on the particle by the surrounding pressure field which is created by the acceleration of the ambient fluid past the particle. Term IV is the force needed to

[1] Hinze (20), pp. 354-361.

accelerate relative to the ambient fluid the mass of fluid displaced by the particle. Term V accounts for the effect of the deviation of the flow pattern from steady state. Corrsin and Lumley (4) pointed out that Term III must be modified when the equation is applied to turbulent flow where the velocity is a function of space and time. This is true in the present case for the fluid, although the moving coordinates make the particle velocity a function of time only. They argued that since the force in Term III is due to the pressure field, it can be modified by writing the Navier-Stokes equation for the flow over the particle. This is in general terms

$$\frac{\partial P}{\partial X_i} = \rho_f \left[\frac{(\partial v_f)_i}{\partial t} + (v_f)_k \frac{\partial (v_f)_i}{\partial X_k}\right] - \mu \frac{\partial^2 (v_f)_i}{\partial X_j \, X_j} \qquad \text{A-2}$$

Substituting this for the pressure term in A-1 gives for the i^{th} component of the particle velocity

$$\frac{\pi}{6} d^3 \rho_p \frac{D(v_p)_i}{Dt} = 3\pi\mu d\left[(v_f)_i - (v_p)_i\right] + \frac{\pi}{6} d^3 \rho_f \left[\frac{\partial}{\partial t}(v_f)_i + (v_f)_k \frac{\partial (v_f)_i}{\partial X_k}\right]$$

$$- \frac{\pi}{6} d^3 \mu \frac{\partial^2 (v_f)_i}{\partial X_j \, X_j} + \frac{1}{2} \frac{\pi}{6} d^3 \rho_f \frac{D}{Dt}\left[(v_f)_i - (v_p)_i\right]$$

$$+ \frac{3}{2} d^2 \sqrt{\pi \rho_f \mu} \int_{t_o}^{t} dt' \left[\frac{D}{Dt'}\left[(v_f)_i - (v_p)_i\right]\right] \Big/ \sqrt{t - t'} \qquad \text{A-3}$$

However, the equation A-2 was written for the fluid without regard to the particle coordinate system, so it can be

modified by the identity

$$\frac{\partial}{\partial t}(v_f)_i + (v_f)_k \frac{\partial (v_f)_i}{\partial X_k} = \frac{D}{Dt}(v_f)_i + [(v_f)_k - (v_P)_k] \frac{\partial (v_f)_i}{\partial X_k}$$

to yield

$$\frac{D}{Dt}(v_P)_i = \frac{3\rho_f}{2\rho_P + \rho_f}\left[\frac{D}{Dt}(v_f)_i - \frac{2}{3}\nu \frac{\partial^2 (v_f)_i}{\partial X_j \partial X_j}\right]$$

$$+ \frac{2}{2\rho_P + \rho_f}\left\{\frac{18\mu}{d^2}[(v_f)_i - (v_P)_i] + \rho_f[(v_f)_k - (v_P)_k]\frac{\partial (v_f)_i}{\partial X_k}\right.$$

$$\left. + \frac{18}{(2\rho_P + \rho_f)d}\sqrt{\rho_f \mu/\pi}\int_{t_0}^{t} dt' \left[\frac{D}{Dt'}[(v_f)_i - (v_P)_i]\right] \Big/ \sqrt{t - t'}\right\} \qquad \text{A-4}$$

At this point a number of additional assumptions are necessary in order to proceed. These are

(1) $\rho_f \frac{\partial v_f}{\partial X} \ll \frac{\mu}{d^2}$

(2) $v_P \frac{\partial v_f}{\partial X} \gg \nu \frac{\partial^2 v_f}{\partial X^2}$

(3) That the last term in A-4 is negligible

(4) That the particle and fluid velocity may be represented by a Fourier integral

$$v_f = \int_0^\infty d\omega\,(\alpha \cos \omega t + \beta \sin \omega t)$$

$$v_P = \int_0^\infty d\omega\,(\gamma \cos \omega t + \delta \sin \omega t)$$

(5) A form of the Lagrangian correlation coefficient is assumed for the fluid, and the energy distribution function E_{fL} calculated from it and (4)

and Equation A-4 to yield

$$E_{fL}(n) = 4\,\overline{v_f^2}\,\Gamma_{fL} / (1 + \omega^2\,\Gamma_{fL}^2)$$

$$E_{PL}(n) = 4\,\overline{v_f^2}\,\frac{a^2+b^2\omega^2}{a^2+\omega^2}\,\frac{\Gamma_{fL}}{1+\omega^2\,\Gamma_{FL}^2}$$

where $a = \dfrac{36\,\mu}{(2\rho_p+\rho_f)d^2}$, $b = \dfrac{3\rho_f}{2\,\rho_p+\rho_f}$

and Γ_{fL} = Lagrangian integral time scale

Assumption (1) is valid for very small particles. Number (2) cannot be commented on one way or another. Assumption (3) is thought to be acceptable since Item V of equation A-1 was stated to be substantial when the external force field creates large accelerations of the particle which does not occur in the present case. Assumptions (4) and (5) are based on a homogeneous turbulent field.

The resulting equation is

$$\overline{v_P^2} = \frac{a\,\Gamma_{fL} + b^2}{a\,\Gamma_{fL} + 1}\;\overline{v_f^2} \qquad \text{A-5}$$

for the i^{th} component.

APPENDIX II

The individual particle velocities were calculated by dividing the distance they traveled by a measured period of time. The distance traveled was measured directly from the projected image by projecting the films at a known magnification onto a rectangular grid with spacings drawn to the scale of the magnified image. Thus the grid distances corresponded to the actual distances within the peipe. By recording the coordinates of the particle at the beginning and end of the flight, and counting electrically the elapsed frames the distance traveled and time of flight are obtained. From the timing marks on the film, and the elapsed frame count the real time can be calculated. This will be made clearer by an example. In what follows, it is essential to remember that the camera was moving axially relative to the fluid, so the motions observed on the film are those of an observer moving with the camera. These motions are called "apparent" in the discussion. Later the real values are calculated. In the example, the wall view is considered. All calculations are the same for the top view except the plane of motion is the θX plane instead of the rX plane below.

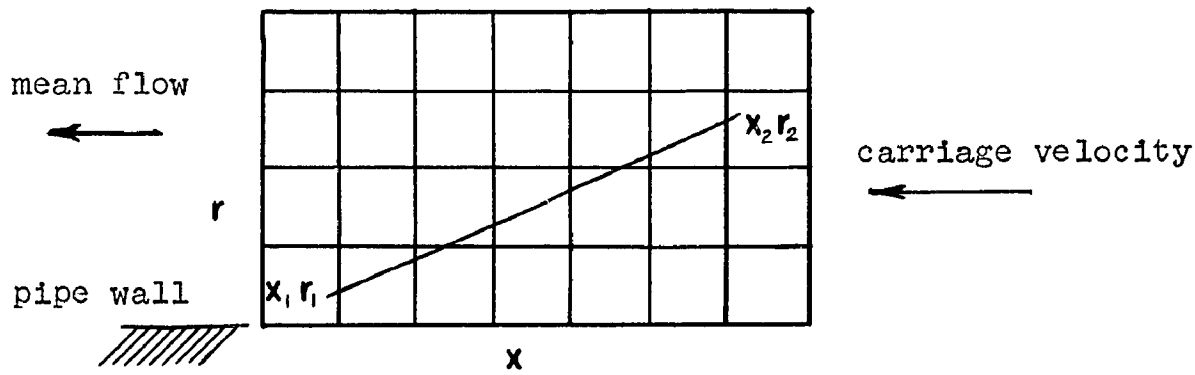

Fig. 34.-- Analysis Grid.

The line marked $(X_1 r_1)$, $(X_2 r_2)$ represents the observed or apparent particle trajectory. The measurements taken are

X_1 = .045" r_1 = .011"

X_2 = .005" r_2 = .030"

frames elapsed = 24

timing mark length = 52 mm.

carriage speed 0.332 ft/sec.

α = apparent angle of ejection measured from wall

e = apparent length of travel of particle

t = time of travel

g = apparent ejection velocity

c = magnitude of carriage velocity, opposite direction

b = actual ejection velocity

γ = actual ejection angle

u_r = actual radial velocity

From the measurements

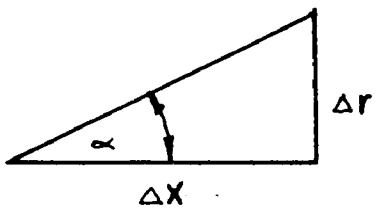

$$\tan \alpha = \frac{\Delta r}{\Delta X} = \frac{.019}{.04} = 0.475 \qquad = 25^\circ\ 25'$$

$\cos \alpha = 0.903$

$\sin \alpha = 0.429$

$$e \quad \frac{\Delta X}{\cos \alpha} = \frac{.04}{.903} = 0.0444"$$

$$t = \frac{\text{frames elapsed}}{\text{frames/sec}}$$

Since 120 timing marks per second are printed on the film, by dividing the number of frames enclosed by a streak by .00833 seconds, the frames/second can be calculated. Each frame is 7.6 mm. wide. Therefore,

$$\frac{\text{timing mark length}}{(7.6)(.00833)} = \text{frames/sec} = \frac{(52)}{(7.6)(.00833)} = 822$$

$\therefore t = \frac{24}{822} = .0292$ seconds.

$$g = e/12t = \frac{(.0444)}{(12)(.0292)} = .126 \text{ ft./sec.}$$

In order to determine the actual velocities and ejection angles, the motion of the camera must be accounted for. Consider the figure below.

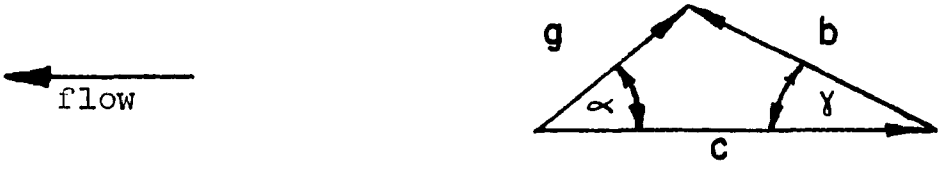

From trigonometry, $b^2 = c^2 + g^2 - 2gc \cos \alpha$

$b^2 = (.332)^2+(.126)^2-2(.126)(.332)(.903) = .0504$

$b = .224$ ft/sec.

$$\sin \gamma = g \frac{\sin}{b} = \frac{(.126)(.429)}{.224} = .241$$

$$\gamma = 13^{\circ}57'$$

$$u_r = b \sin \gamma = .054 \text{ ft/sec.}$$

Note that the apparent angle was nearly twice the value of the real angle of ejection. The enhancement of the observed angle by the use of a moving camera permitted small deviations to be observed and accurately measured.

The preceding calculation was based on the assumption that the particle trajectory was a straight line, and that its motion was all in a single plane. The first assumption is reasonable because the section of the trajectory selected for measurement was usually only slightly curved. The second assumption is quite wrong. Both the wall and top views clearly showed that the trajectories were three dimensional. An estimate of the possible error can be made. It will be recalled that the average ejection angle in the rX plane was 8.5° and the average angle for the θX plane was 15°. When the calculation in the rX plane are made, the movement in the θX plane are the ones which cannot be seen but which cause the error. This is clear from the figure below which is drawn for the apparent angles and trajectories.

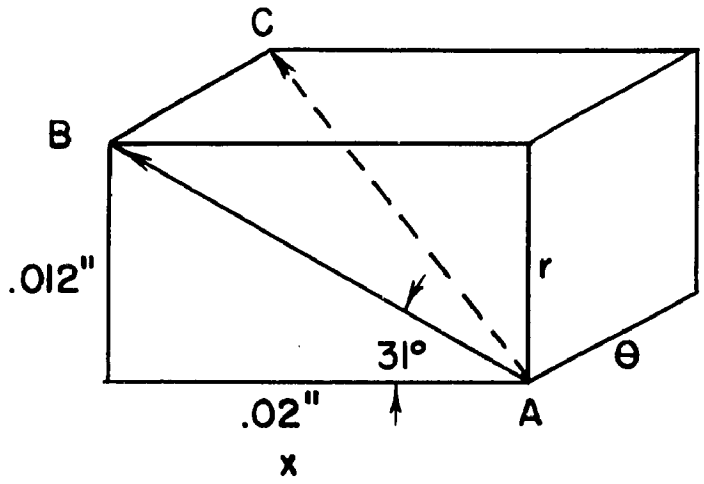

Fig. 35.--Apparent Ejection Trajectory.

Line AB is the observed or apparent trajectory as seen in the top view, but line AC is the trajectory which would be observed by the moving camera if three dimensional vision were possible. At first the error due to movement in the θX plane would seem to be quite large, but it must be recalled that this is only the apparent motion. In actuality, the true X dimension is many times greater than the other dimensions becau e it includes the carriage velocity which is accurately known. Since the carriage motion is purely axial, neither the r nor the θ movements are affected by it. The carriage velocity for the case shown is 0.113 ft./sec. By calculations such as were given previously, it is found that the actual ejection angle is 9°. If this is so, then the real X dimension is .076 inches, while the r and θ dimension

remain the same. Thus the actual picture is

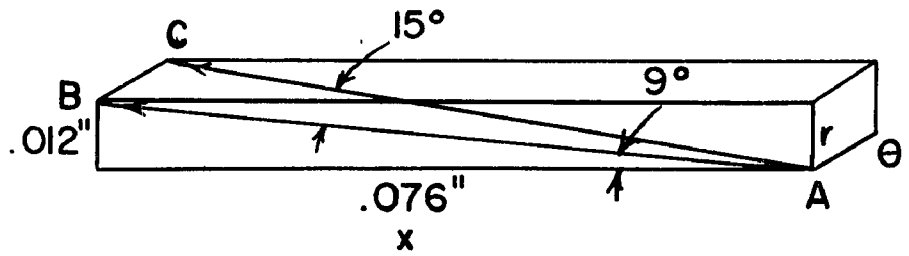

Fig. 36.--Actual Ejection Trajectory.

The angle for the deviation in the θX plane was selected as 15° because this was the average observed. Now the measured length of travel is $\frac{.076}{\cos 9^{\circ}} = 0.077"$

The measured velocity is 0.141 ft./sec.

The actual length of travel is $\frac{.077"}{\cos 15^{\circ}} = .079"$

the actual velocity is 0.146 ft./sec. The error is 3.42% of the actual velocity. For this example the case of rather low carriage velocity was selected. This will give a larger error in the calculation than the higher carriage velocity because it does not extend the X dimension as such. The carriage velocity used is representative of those used for $N_{Re} = 20,000$. For higher N_{Re}, larger values were used.

The error caused by the slight arcing of the trajectory is also diminished for the same reasons as those given above.

While the error in absolute velocity is small, the values where a difference between absolute velocities is

taken are subject to greater error. For these cases the procedures used to eliminate the effect of the error on the results were discussed at the time the results were presented.

APPENDIX III

Calculation of Velocity Difference Due to Depth of Field

The observed presence of "two layer velocity" in wall view films raised the question as to whether the observed velocity difference might not be due to the finite depth of field and the curvature of the pipe wall. Referring to the drawing below, consider that BD represents the depth of

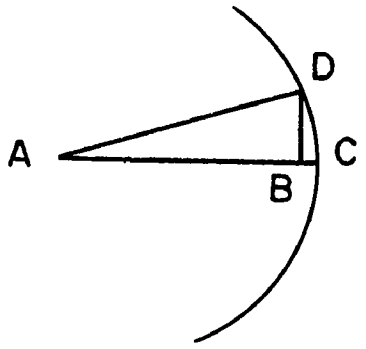

Fig. 37.--Depth of Field at Wall.

field, and that AC is the plane of focus. It is clear that in the wall view all the particles will appear to be in a single plane parallel to AB. However, a particle at B and one at D while they will appear to be in the same plane and at the same radial position are in fact in different planes and at different distances from the wall. Since a steep velocity gradient exists in the wall region, the question posed is whether the distance BC is greater enough to cause

the two layer velocity effect. In order to give the greatest possible dimension to BC, the depth of field is assumed to occur totally on one side of the plane of focus. In actuality it is distributed equally on both sides of the plane so is effectively only one-half of the value used. At 4.3X the depth of field was 0.0274". By simple geometry,

$$\overline{AB^2} + \overline{DC^2} = \overline{AD^2}$$

$$\overline{AB^2} = 1.00000 - .000751 = .99925$$

$$AB = .999598$$

and $\overline{BC}$ = 0.000402" which is the maximum radial displacement. Considering the value of $\frac{d\overline{U}_x}{dy}$ in the wall area as calculated from Pai's equation for N_{Re} = 20,000 one finds that the velocity difference due to this displacement is

$$\frac{(4.02 \times 10^{-4})}{12} (.939) = 3.12 \times 10^{-5}$$

This difference is insignificant, and cannot account for the "two layer velocity" differences observed.

BIBLIOGRAPHY

1. Brodkey, R. S., A. I. Ch. E. Jour., 448, 9 (1963).
2. Clauser, F. H., Adv. in App. Mech., I, IV (1956).
3. Cohen, M. F., M.S. thesis, Chemical Engineering, The Ohio State University 1962).
4. Corrsin, S., and J. Lumley, App. Sci. Res., 114, 6A (1956).
5. Danckwerts, P. V., Ind. and Eng. Chem., 1450, 43 (1951).
6. Deissler, R. C., NACA Tech. Rept., 1210 (1955).
7. Deissler, R. C., and C. S. Eian, NACA Tech. Note 2629 (1952).
8. Einstein, H. A., and H. Li, Proc. ASCE, paper 945, 82 (1956).
9. Fage, A., Phil. Mag., 80, 21 (1936).
10. Fage, A., and H. C. H. Townsend, Proc. Roy. Soc. London, 656, 135A (1932).
11. Ferrari, C., NASA Republication RE 2-8-59W (1959).
12. Friedlander, S. K., A.I.Ch.E. Jour., 381, 3 (1957).
13. Grant, H. L., Jour. Fluid Mech., 149, 4 (1958).
14. Hama, F. R., Tech Note BV-195, AFOSR-TN-60-290, Feb. (1960).
15. Hama, F. R., J. D. Long, and J. C. Hegarty, Jour. Appl. Phys., 388, 28 (1957).
16. Hanratty, T. J., A.I.Ch. E. Jour., 359, 2 (1956).
17. Harriott, P. Can. Jour. Chm. Engr., 60, 40 (1962).
18. Harriott, P. Chem. Eng. Sci., 149, 17 (1962).
19. Higbie, R. Trans. A.I.Ch. E., 365, 31 (1935).

20. Hinze, J. D., Turbulence, McGraw Hill (1959).

21. Hopkins, E. J., S. J. Keating, Jr., and A. Bandettini, NASA Tech. Note D-328 (1960).

22. Hubbard, P. G., Bulletin No. 37, Studies in Engr., State Univ. of Iowa (1957).

23. Johnson, A. E., J. Marangozis, and O. Trass, Can. Jour. Chem. Engr., 195, 41 (1963).

24. Kada, H., and T. J. Hanratty, A.I.Ch.E. Jour., 624, 6 (1960).

25. Kirsten, H., Ph.D. thesis, University of Leipzig (1927).

26. Klebanoff, P. S., NACA Tech. Notes 3178 (1954).

27. Klebanoff, P. S., K. D. Tidstrom, and L. M. Sargent, Jour. Fluid Mech., 1, 12 (1962).

28. Kline, S. J., and P. W. Runstadler, Jour. App. Mech., 166, 26 (1959).

29. Kovasznay, L. G., H. Komoda, and B. R. Vasudeva, Proc. Heat Transfer and Fluid Mech. Inst., Stanford University Press (1962).

30. Latzko, H., Z. angew, Math. u. Mech., 277, 1 (1929).

31. Laufer, J., NACA Report 1174 (1954).

32. Lee, J., Ph.D. dissertation, Chemical Engineering, The Ohio State Univ. (1962).

33. Li, C., Ph.D. thesis, Cornell Univ. (1960).

34. Lin, C. S., R. W. Moulton, and G. L. Putnam, Ind. Eng. Chem., 636, 45 (1953).

35. Ludwieg, H., and W. Tillmann, Ingr. Arch., 288, 18 (1949).

36. Marchello, J. M., and H. L. Toor, Ind. Eng. Chem. Fund., 8, 2 (1963).

37. Mickelsen, W. R., NACA Tech. Note 3570 (1955).

38. Munk, M. M., Proc. Second Midwestern Conf. on Fluid Mech., 19 (1952).

39. Murphree, E. V., Ind. Eng. Chem., 726, 24 (1932).

40. Nedderman, R. M., Chem. Eng. Sci., 113, 16 (1961).

41. Nikuradse, J., VDI-Forschungsheft No. 361 (1933).

42. Pai, S. I., Viscous Flow Theory, II--Turbulent Flow, Van Nostrand, Princeton, New Jersey (1957).

43. Perlmutter, D. D., Chem. Eng. Sci., 287, 16 (1961).

44. Prandtl, L., Proc. 3rd Intern'l. Math. Congr., Heidelberg (1904). Reprint NACA Tm-452 (1928).

45. Prandtl, L., Proc. 2nd Intern'l. Congr. App. Mech. Zürich (1926).

46. Rannie, W. D., J. Aero. Sci., 485, 23 (1956).

47. Reichardt, H. Z., angew. Math. u. Mech., 208, 1 (1951).

48. Reiss, L. P., and T. J. Hanratty, A.I.Ch.E. Jour., 154, 9 (1963).

49. Richardson, F. M., and K. O. Beatty, Phys. of Fluids, 718, 2 (1959).

50. Runstadler, P. W., Ph.D. thesis, Thermosciences Div., Stanford Univ. (1962).

51. Runstadler, P. W., S. J. Kline, and W. C. Reynolds, Report MD-8, Thermosciences Div., Stanford Univ., AFOSR-TN-5241 (1963).

52. Ruckenstein, F., Chem. Eng. Sci., 233, 18 (1963).

53. Schlichting, H., Boundary Layer Theory, McGraw Hill, New York (1960).

54. Sears, F. N., Principles of Physics, Addison Wesley, Cambridge, Mass. (1946).

55. Serafini, J. S., NASA Tech. Report R-165 (1963).

56. Sherwood, T. K., Chem. Eng. Prog. Symp. Series 55, 71, No. 25 (1959).

57. Soo, S. L., Ind. Eng. Chem. Fund., 33, 1 (1962).

58. Soo, S. L., and C. L. Tien, Trans. ASME, 5, E-82 (1960).

59. Sternberg, J., Jour. Fluid Mech., 241, 13 (1962).

60. Summerfield, M., Heat Transfer Pymp., 151, Univ. of Michigan (1952).

61. Taylor, G. L., Advisory Comm. Aero. (Gt. Br.), Tech. Report 272 (1916).

62. Tchen, Ph.D. thesis, Delft (1947).

63. Toor, H. L., and J. M. Marchello, A.I.Ch.E. Jour., 97, 4 (1958).

64. Townsend, A. A., Boundary Layer Symp., Int. Union of Theo. and App. Phys., Berlin (1958).

65. Townsend, A. A., Proc. Cambridge Soc., 375, 47 (1951).

66. Townsend, A. A., The Structure of Turbulent Shear Flow, Cambridge Univ. Press (1956).

67. Van Shaw, P., and T. J. Hanratty, A.I.Ch.E. Jour., 475, 10 (1964).

68. Vieth, W. R., J. H. Porter, and T. K. Sherwood, Ind. Engr. Chem. Fund., 1, 2 (1963).

69. Von Kármán, T., Proc. 3rd Intern'l. Congr. of App. Mech. 85, Stockholm (1930), Reprint NACA TM-611 (1931).

70. Von Kármán, T., Trans. A.S.M.E., 705, 61 (1939).

71. Weske, J. R., Tech. Note BN-47, Univ. of Maryland (1955).

AUTOBIOGRAPHY

I, Edward Robert Corino, was born in Belleville, New Jersey, on September 20, 1936. I received my primary and secondary education in the Belleville public school system. As an undergraduate I attended Newark College of Engineering and was granted a Bachelor of Science degree in 1958. I was subsequently employed in industry for one year. I entered the Graduate School of The Ohio State University, and in 1961 received a Master of Science degree. While earning this degree, I held a graduate assistantship in the Chemical Engineering Department and the Dow Chemical Fellowship. I continued my studies toward the Doctor of Philosophy degree at the Ohio State University. During this time I received financial support from the National Science Foundation.